

**Steady and Transient Analysis of Flow and Heat Transfer in SPND
Assembly**

Jose Tijiboy

**Thesis submitted to the faculty of the Virginia Polytechnic Institute and
State University in partial fulfillment of the requirements for the degree of**

**Master of Science
In
Mechanical Engineering**

**Danesh Tafti – Chair
Mark Paul
Eugene Brown**

December 3, 2008

Blacksburg, Virginia

Keywords: Nuclear, SPND, Heat Transfer

Steady and Transient Analysis of Flow and Heat Transfer in SPND Assembly

Jose Tijiboy

Abstract

This thesis presents the analysis of flow and heat transfer for the SPND (Self-Powered Neutron Detector) system used within the nuclear reactor core in the U.S. Evolutionary Power Reactor developed by AREVA. The SPND system is composed of six individual detectors which are used for in-core measurement of thermal neutron flux. The study of the SPND system is important since this system provides information and signals necessary for safe reactor operation and control. The main goal of the project was to determine the maximum temperature for the SPND detectors under three different operating scenarios. The maximum temperature of the detectors is of special interest, since if it exceeds a limiting temperature of 622 K then the accuracy of the information provided by the system is reduced. All of the flow and heat transfer simulations were performed using the commercial software Fluent.

The first scenario that was studied was for the system under normal operating conditions. For this case, the maximum temperature for a detector was determined to be 603.4 K, which is within the proper range of operation. It was also important to determine the maximum temperature of the fluid within the SPND assembly in order to ascertain that boiling does not occur within the system during normal operation. The maximum fluid temperature was found to be 613.7 K, which is below the boiling temperature of water (618.05 K) at an operating pressure of 2250 psi.

The second scenario involved an increase in the power of the reactor's core by a factor of 17% in a 30 second period. The results of the unsteady calculation indicated that the maximum temperature for a detector was 608.5 K. The results also indicate that no boiling occurs inside of the SPND system.

The third scenario involved a loss of coolant flow in the SPND system. This reduction in flow rate caused the maximum temperature of the detectors to reach 619.6 K. For this case, boiling occurs within the guide tube and protection tube.

Acknowledgments

The successful completion of this work would have never been possible without the valuable help of many people that in one way or another helped me to overcome all of the difficulties I encountered along the way. First, I would like to thank my advisor Dr. Danesh Tafti. I will be always thankful for his help, teachings, and guidance throughout the entire time I worked in this thesis. I would like to thank my committee members, Dr. Mark Paul and Dr. Eugene Brown for reviewing my thesis and providing suggestions.

I would also like to thank the Center for Advanced Engineering and Research (CAER) for providing the funding for this project. Without their support, I would have never had the opportunity to work on this project and to learn as much as I did. Also, I would like to give very special thanks to AREVA NP, especially to Chris Lewis, Jonathan Witter, and Bernie Copsey. I really appreciate the time they took to provide detailed information about the project.

I am also very grateful for the help of my HPCFD lab mates: Mohammad Elyyan, Pradeep Gopalakrishnan, Sai Shrinivas, Naresh Coimbatore, Kohei Takamuku, Sunil Patil, Amit Amritkar , Nagendra Krishnamurthy, and Jonathan Cowan. Finally, I would like to thank my parents and my sisters for their encouragement and support.

Table of Contents

Chapter 1 Introduction	1
Chapter 2 Problem Description and Mesh Generation Process	8
2.1 Description of Physical Problem	8
2.1.1 Geometry Overview	8
2.1.2 Internal Heat Generation	9
2.1.3 Flow Paths	12
2.1.4 Problem Review	14
2.2 Computational Model	15
2.2.1 Geometry Description	15
2.2.2 Zones	17
2.3 Mesh Generation	19
2.3.1 Geometry Simplifications	19
2.3.2 Mesh Model	21
Chapter 3 Flow and Heat Transfer Analysis for SPND under Normal Operation.....	26
3.1 Problem Description	26
3.2 Objective	27
3.3 Boundary Conditions	27
3.4 Solver Settings	30
3.5 Calculation of External Heat Transfer Coefficient	31
3.6 Verification	32
3.6.1 Evaluation of Effect of the Grid Element Shape on the Accuracy of the Discretization Scheme	32
3.6.1.1 Problem Description.....	32
3.6.1.2 Mesh Configurations.....	33
3.6.1.3 Boundary Conditions.....	34
3.6.1.4 Calculation of Truncation Error.....	35
3.6.2 Sensitivity of Results to Near Wall.....	37
3.6.3 Global Energy Balance	39
3.6.4 Estimation of Friction Factor in Guide Tube (Annulus).....	40
3.6.5 Friction Factor Protection Tube	41
3.6.6 Calculation of Heat Transfer Coefficients for Guide Tube (Annular Duct)....	45
3.7 Results.....	49
3.7.1 Velocity Contours	49
3.7.2 Temperature Contours	52
3.7.3 SPND Temperatures	56
3.7.4 Location of Maximum SPND Temperatures	56
3.7.5 Fluid Temperatures	57
3.8 Summary and Conclusion	59

Chapter 4 Overpower Transient Case	60
4.1 Description of Overpower Transient	60
4.2 Objective	64
4.3 Solver Settings	65
4.4 Establishing Validity of Results.....	66
4.4.1 Revision of Boundary Conditions.....	66
4.4.2 Sensitivity of Results based on Time Step (Δt)	67
4.4.3 Steady State Calculation	68
4.5 Results.....	69
4.5.1 Temperature Profiles.....	69
4.5.2 Temperature Contours	71
4.5.3 Final Maximum Temperatures.....	73
4.5.4 SPND Detector Final Maximum Temperatures.....	73
4.6 Conclusion	74
Chapter 5 Partial Loss of Flow Transient	75
5.1 Description of Partial Loss of Flow Transient.....	75
5.1.1 Inlet and Outlet Pressure and Temperature Conditions	77
5.2 Objective	79
5.3 Solver Settings	79
5.4 Sensitivity to Time Step.....	80
5.5 Results.....	81
5.5.1 Mass Flow Rate.....	81
5.5.2 SPND Detector Temperature Profiles.....	83
5.5.3 Maximum Temperature of SPND Components.....	85
5.5.4 Boiling in the Guide Tube and Protection Tube Channels	85
5.5.5 Temperature of Free Stream and GT Wall	89
5.5.6 Maximum Temperature of SPND Detectors.....	91
5.6 Conclusion	92
References.....	93
Appendix A Governing Equations and Solver Settings.....	94
A.1 Governing Equations.....	94
A.1.1 Conservation of Mass.....	94
A.1.2 Momentum Equation.....	94
A.1.3 Energy Equation.....	95
A.2 Second Order Upwind (SOU)	96
A.3 Green-Gauss Cell Based Gradient Evaluation	98
A.4 Discretization in Time.....	99
A.5 Under - Relaxation Factors	100
A.6 Turbulence Modeling.....	101
A.6.1 Reynolds Averaged Equations	101

A.6.2 K-Epsilon Model.....	102
A.6.3 Wall Functions	103
Appendix B User Defined Functions	106
B.1 UDF for Steady State Case (DEFINE_SOURCE).....	107
B.2 UDF for Steady State Case (DEFINE PROFILE)	109
B.3 UDFs for Transient Cases	110
Appendix C Material Properties	112
Appendix D Normal Operation Data	115
Appendix E Overpower Transient Data.....	122
Appendix F Partial Loss of Flow Transient Data	127

List of Figures

Figure 1-1 Nuclear Complex Main Buildings.....	1
Figure 1-2 Primary and Secondary Systems in Areva’s EPR [1]	2
Figure 1-3 (a) In-core Instrumentation; (b) Instrumentation Layout	3
Figure 1-4 Fuel Assembly.....	4
Figure 1-5 Illustration of Typical Cross-section of the SPND Detector.....	5
Figure 1-6 Rod Cluster Control Assembly [1].....	6
Figure 2-1 Components of SPND system	9
Figure 2-2 Fuel Rod Active Region.....	10
Figure 2-3 Graphs for Heat Generation Data and Curve Fits	11
Figure 2-4 SPND System Schematic	13
Figure 2-5 a) Guide Tube; b) Guide Tube with Protection Tube and Detectors	16
Figure 2-6 Protection Tube Slice at 147”	18
Figure 2-7 Simplification of Original Geometry for Cables.....	19
Figure 2-8 SPND Geometry with Simplifications	21
Figure 2-9 Mesh Cross-section at 50.57”	22
Figure 2-10 Mesh Cross-sections at Different Heights along Protection Tube	23
Figure 2-11 Three-dimensional mesh from 146.8” to 147.7”	24
Figure 2-12 Three-dimensional mesh from 50.57” to 70.57”	25
Figure 3-1 Pressure and Temperature Boundary Conditions.....	28
Figure 3-2 Pipe Dimensions.....	33
Figure 3-3 Cartesian Mesh.....	34
Figure 3-4 Unstructured Mesh.....	34
Figure 3-5 Domain Dimensions and Boundary Conditions.....	34
Figure 3-6 Energy Balance on SPND Assembly	39
Figure 3-7 Guide Tube (Annular Cross-section)	40
Figure 3-8 Protection Tube Geometry. The two sections to be studied are highlighted..	42
Figure 3-9 Cross-sections of the PT at (a) 80” and (c) 160”	42
Figure 3-10 Velocity Profiles at (a) 80” and (b) 109.8”	43
Figure 3-11 Velocity Profiles at (c) 160” and (d) 184”	43
Figure 3-12 Annulus Dimensions	45
Figure 3-13 Velocity Field through Guide Tube and Protection Tube at 34	50
Figure 3-14 Guide Tube Bottom Insert.....	50
Figure 3-15 Pressure Variation at Inlet Region	51
Figure 3-16 Velocity Profiles for Guide Tube and Protection Tube at 123”	52
Figure 3-17 Temperature Contours at Different Heights along the Core	53
Figure 3-18 GT Outer Wall Temperature and Free Stream Temperature vs Height	54
Figure 3-19 Radial Temperature Distribution at Different Heights.....	55
Figure 3-20 Temperature Contours.....	57
Figure 3-21 Temperature Contours at 184”	58
Figure 4-1 Increase in Power with Respect to Time	61
Figure 4-2 Overpower Transient Schematic	62
Figure 4-3 (a) SPND Pressure Boundary Conditions ; (b) Free Stream Temperature Profiles	63

Figure 4-4 Core’s Operating Pressure with Respect to Time	64
Figure 4-5 Comparison of Pressures Reported by Fluent and Pressures Specified by Areva.....	66
Figure 4-6 Maximum Temperature History for SPND Detectors.....	70
Figure 4-7 (a) Guide Tube Wall Temperature Profiles with Respect to Time;	71
(b) Temperature Profiles at the GT Outer Wall and Free Stream.....	71
Figure 4-8 Temperature Contours at 151”	72
Figure 5-1 Reduction in Flow Rate through SPND Assembly	75
Figure 5-2 Core Power vs Time.....	76
Figure 5-3 Operating Pressure with Respect to Time	77
Figure 5-4 Pressure Boundary Conditions	78
Figure 5-5 Temperature vs. Time at (a) 0”, (b) 34”, and (c) 184”	78
Figure 5-6 Comparison of Guide Tube Flow Rate	82
Figure 5-7 Comparison of Protection Tube Flow Rate.....	82
Figure 5-8 Maximum Temperature History for SPND Detectors.....	83
Figure 5-9 Temperature Contours at 151”	84
Figure 5-10 Maximum Temperature of the GT Water	87
Figure 5-11 Maximum Temperature of the PT Water	88
Figure 5-12 SPND D6 Cross-section at 151”	89
Figure 5-13 Temperature Profiles for the GT Wall and Free Stream at t=0 sec.....	90
Figure 5-14 Temperature Profiles at (a) 8 sec; (b) 12 sec.....	91
Figure A1 Domain Discretization	97
Figure A2 Domain Discretization	98
Figure D1 Guide Tube in which the SPNDs are inserted in the fuel rod section.	116
Figure D2 Part 1- Protection Tube Detailed View.....	117
Figure D2 Part 2- Protection Tube Detailed View.....	118

List of Tables

Table 2-1 Radii for Grouped Cables	20
Table 3-1 Boundary Conditions at Inlets and Outlets	27
Table 3-2 Convective Heat Transfer Coefficient	31
Table 3-3 Comparison of ϵ_{avg} for Cartesian and triangular mesh.....	36
Table 3-4 Values of n for the Triangular and Cartesian Meshes	36
Table 3-5 Mass Flow Rates for Three y+ ranges	38
Table 3-6 Energy Values Reported by Fluent.....	39
Table 3-7 Friction Factor Calculation	41
Table 3-8 Friction Factor Calculation for Section A.....	44
Table 3-9 Friction Factor Calculation for Section B.....	45
Table 3-10 Average Heat Flux Values.....	47
Table 3-11 Interpolated Heat Flux Calculation Parameters	47
Table 3-12 Comparison of Heat Transfer Coefficients	48
Table 3-13 Heat Transfer Coefficients.....	48
Table 3-14 Average Temperature SPND Detectors.....	56
Table 3-15 Maximum Temperatures SPND Detectors	56
Table 3-16 Maximum and Average Temperatures for Components of Assembly	58
Table 4-1 SPND Maximum Temperature after t=7 sec.	67
Table 4-2 SPND Maximum Temperature after t=15 sec	67
Table 4-3 Guide Tube Flow Rates after t= 15 sec.....	67
Table 4-4 Comparison for Detector Temperature between Transient and Steady Fluent simulations	68
Table 4-5 Maximum Temperatures for SPND Components at 30 seconds	73
Table 4-6 Maximum SPND temperatures after 30 seconds with $\Delta t=0.2$ sec.....	73
Table 5-1 SPND Maximum Temperature after t=6 sec.	80
Table 5-2 Guide Tube Flow Rates after t= 6 sec.....	81
Table 5-3 Maximum Temperature for SPND Components at 12 seconds.....	85
Table 5-4 Boiling Temperatures with Respect to Time	86
Table 5-5 Boiling temperatures for SPND.....	87
Table 5-6 Maximum SPND temperatures after 30 seconds.....	91
Table B-1 DEFINE_SOURCE Arguments (Fluent UDF Manual).....	108
Table B-2 DEFINE_PROFILE Arguments (Fluent UDF Manual)	109
Table C-1 Properties for Water.....	112
Table C-2 Guide Tube (Zirconium alloy Zr-2.5Nb, Nuclear Grade) [10].....	112
Table C-3 Protection Tube (Austenitic Stainless Steel AISI 321) [10]	112
Table C-4 Cables (Inconel 600) [10]	112
Table C-5 SPND (Cobalt, Al ₂ O ₃ , Inconel).....	113
Table C-6 Radii for SPND Components.....	113
Table C-7 Thermal Conductivity for SPND Components	114
Table D-1 Thermal-Hydraulic Data Surrounding the Guide Tube	119
Table D-2 Heat Generation Rates(W/cm ³).....	120
Table E-1 Delta-P Variation [psi]	123

Table E-2 Free Steam Temperature Variation [K].....	125
Table F-1 Delta-P Variation [psi]	128
Table F-2 Free Stream Temperature Variation [K]	129

Nomenclature

A	Area
Dh	hydraulic diameter
\bar{h}	heat transfer coefficient
Pr	Prandtl number
Re	Reynolds number
V	velocity
k	thermal conductivity
ρ	density
Cp	specific heat capacity at constant pressure
μ	dynamic viscosity
ν	kinematic viscosity
t	time
T	temperature
L	length
\overline{Nu}	averaged Nusselt Number
f	Darcy friction factor
Δp	pressure drop
S	source term
ε	error vector
ε_{avg}	L2 norm of error vector
P_w	wetted perimeter
R	radius

SPND	Self-Powered Neutron Detector
SIMPLE	Semi-Implicit Linked Equations
UDF	User-Defined Functions
GT	Guide Tube
PT	Protection Tube
EPR	Evolutionary Power Reactor
PWR	Pressurized Water Reactor

Chapter 1 Introduction

This chapter presents an introduction to the analysis of the flow and heat transfer in the Self Powered Neutron Detector (SPND) system. The SPND system is installed within the U.S. Evolutionary Power Reactor designed by Areva.

A layout of the main buildings that compose a nuclear power plant is shown in Figure 1-1. The SPND system is located within the reactor building which is located at the center of the nuclear complex. The functions of this building are to house the power plant's main equipment and to guarantee the protection of the environment against internal and external hazards [1].

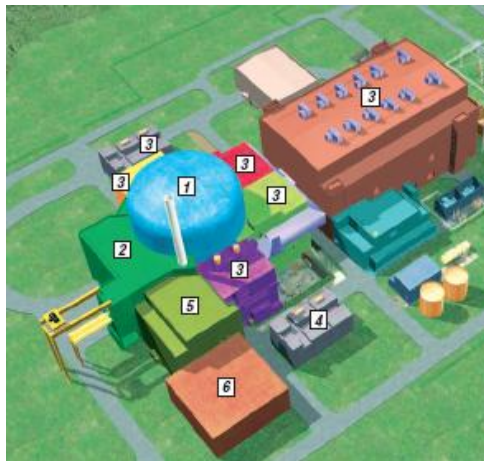


Figure 1-1 Nuclear Complex Main Buildings: (1) Reactor (2) Fuel (3) Safeguard (4) Diesel (5) Nuclear Auxiliary (6) Waste (7) Turbine (Figure Courtesy of Areva) [1]

A layout of the systems used in the U.S. EPR is shown in Figure 1-2. As seen in the figure, the primary system is contained within the reactor building. The components of the primary system are the following: reactor core, pressure vessel, primary pump, pressurizer, control rod drive mechanism, and steam generator. The EPR primary system

is a 4-loop design. This means that there are four “flow loops” as the one highlighted in red in Figure 1-2. Therefore, there are a total of four coolant pumps and four steam generators. In the EPR, ordinary water is used as the primary fluid to remove the heat from the reactor core generated by the nuclear fission process. The flow path that is followed by the water is indicated by arrows in Figure 1-2. In this path, water leaves the reactor pressure vessel and goes to a steam generator. In the steam generator, heat is transferred to a secondary circuit. After that, the water goes to a reactor coolant pump and then re-enters the reactor pressure vessel. Once inside the vessel, the water first flows downwards and then upwards flowing through the core (shown in orange in Figure 1-2) in order to cool the system [1].

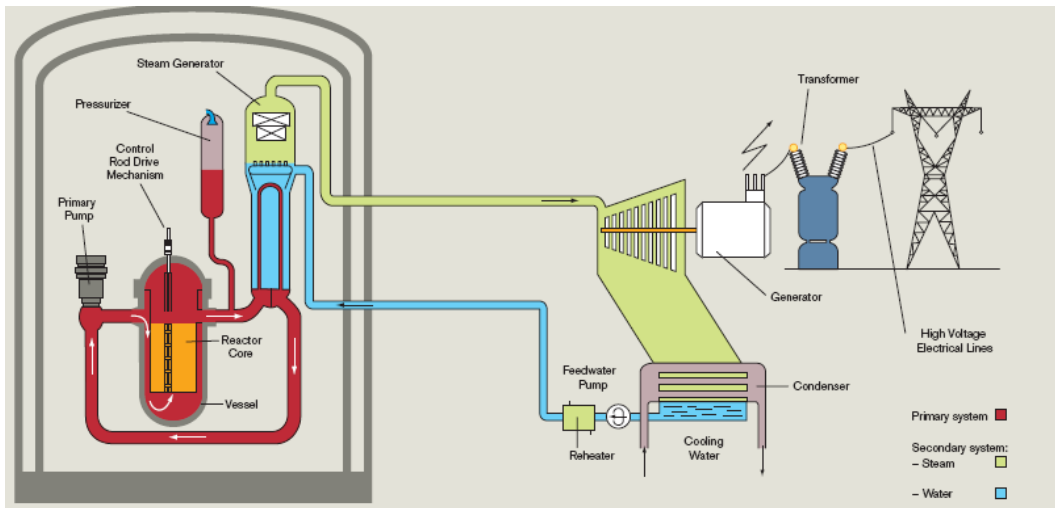


Figure 1-2 Primary and Secondary Systems in Areva’s EPR [1]

The reactor core is the part of the nuclear power plant in which the fuel is located. Also, inside the reactor core, the heat used to produce steam is generated by fission. Due to its importance, it is obvious that the behavior of the reactor core has to be closely monitored. The operation of the nuclear power plant is monitored and controlled by the Instrumentation and Control (I&C) system.

The part of the I&C system that monitors the operation within the reactor core is composed of movable and fixed in-core instrumentation. The SPND system, studied in this project, is part of the fixed in-core instrumentation, and is positioned within the reactor core as shown in Figure 1-3a. The SPND assembly serves as a surveillance system that measures the thermal neutron flux, and monitors the three-dimensional power density distribution in the U.S. EPR core. The information provided by this system is key for determining if the reactor is operating in the expected manner.

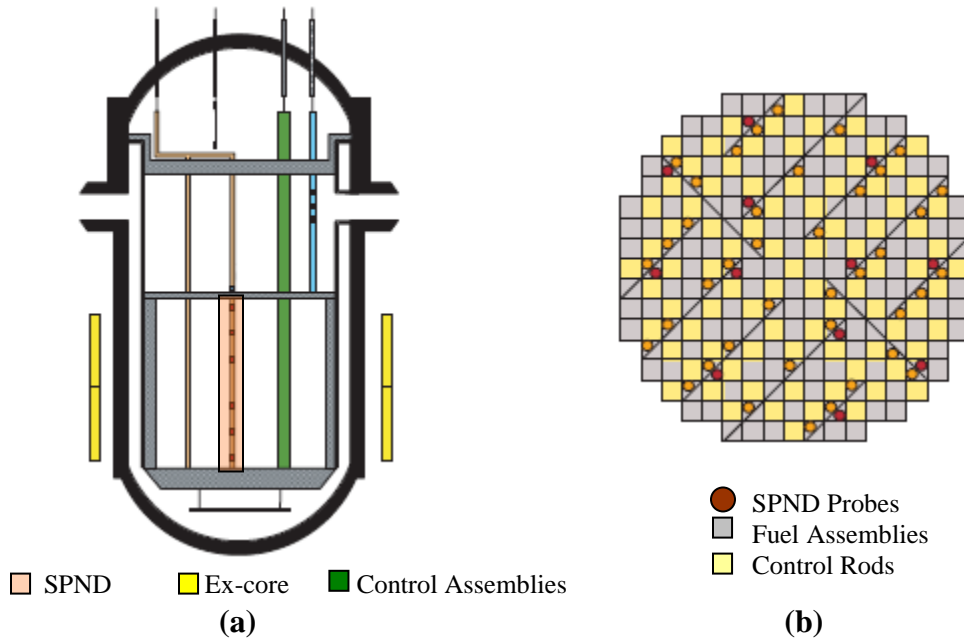


Figure 1-3 (a) In-core Instrumentation; (b) Instrumentation Layout [1]

The SPND system is contained within a thin stainless steel tube, referred to as the Protection Tube. The protection tube is introduced into a guide tube that is located within a fuel assembly. There are a total of 241 fuel assemblies distributed in the reactor core as shown in Figure 1-3b. Each fuel assembly is composed of a bundle of fuel rods that contain the nuclear fuel (Figure 1-4). As seen in Figure 1-4 the fuel rods are vertically

arranged in a square lattice with a 17X17 array [1]. Most of the tubes in this array are fuel rods, but there are some empty spaces in the array that are used to insert control or instrumentation devices, such as the SPND protection tube. The protection tube contains a total of six individual detectors which measure the neutron flux. More information on the specifics of the SPND components will be given in the following chapter.

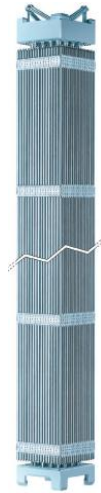
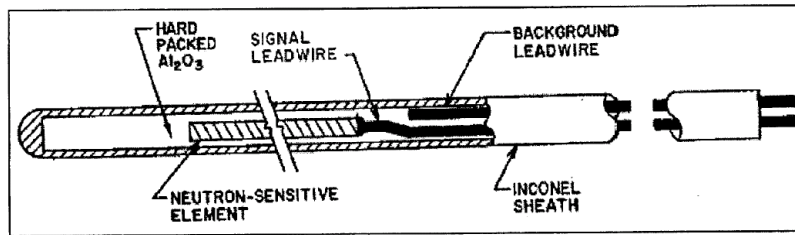


Figure 1-4 Fuel Assembly (17 X 17 array) [1]

The SPND detectors consist of three main parts: emitter, insulator, and collector (Figure 1-5). The thermal neutron flux interaction with the cobalt emitter results in the generation of a current that is directly proportional to the neutron flux. This information is used to ensure safe reactor operation. The emitter is surrounded by an insulator, hard-packed Al_2O_3 . The outermost layer of the detector, the collector, is made from Inconel.

In order to be able to measure the neutron flux at several locations, there are a total of 12 SPND probes (protection tubes) distributed azimuthally in the core cross-section (Figure 1-3b), and each probe contains six detectors for a total of 72 SPND detectors within the reactor core.



**Figure 1-5 Illustration of Typical Cross-section of the SPND Detector
(Figure Courtesy of Areva)**

In addition to the SPND system, there are two other relevant systems that are located within the reactor core. The first one, which was already discussed, is composed of the fuel assemblies (Figure 1-4). Neutron and gamma flux from the fuel rods fission process acts on all components of the SPND assembly and produces internal heat. This internal heat generation will increase the temperature of the SPND detector system. Monitoring the temperature increase of the detectors is the main objective of this project. As mentioned earlier, the SPND detectors generate a signal proportional to the neutron flux, but once the temperature of the detector exceeds a limiting value of 622 K, the accuracy of the information provided by the system decreases. Therefore, it is important to find out the maximum temperature of the detectors in order to discover if it exceeds the permitted level.

The other important system is the Rod Cluster Control Assembly (RCCA) which is shown in Figure 1-6. RCCAs are inserted into the core through the top. There are a total of 89 RCCAs located as shown in Figure 1-3b. The purpose of the RCCAs is to help control the average coolant temperature, and they also serve to shut the reactor down when a reactor trip (or scram) is called for by the protection system. Each RCCA consists of 24 rods fastened to a common head assembly (Figure 1-6) [1].



Figure 1-6 Rod Cluster Control Assembly [1]

The control rods may be removed from the reactor core by means of control drive mechanisms located on the top part of the reactor pressure vessel as seen in Figure 1-2. Removing these control rods from the reactor core sets off a reactivity imbalance such that the neutron population, and hence the power level, increases. The effect that the increase in power level has on the detectors will be discussed later in this thesis.

Three different operating scenarios are studied in this thesis. The scenarios are the following: normal operation, overpower transient, and partial loss of flow transient. In order to obtain a license to construct the US EPR, Areva has to submit extensive information about their design to the United States Nuclear Regulatory Commission (NRC). Part of that information is the Final Safety Analysis Report. This report contains information about the three scenarios studied in this thesis, and many other safety related events that have been analyzed by Areva. Information specific to each of the scenarios will be given in later chapters and can also be found in the NRC website [5].

The main objectives for this research project are the following:

1. Use the data provided by Areva to set up the problem and obtain a steady state solution of the temperature distribution during normal operation.

2. Investigate the temperature response of the SPND system to the Overpower Transient scenario. In this scenario the core's power increases by 17 % in a period of 30 seconds. Specific details of this scenario will be given in Chapter 4.
3. Investigate the temperature response of the SPND system to the Partial Loss of Flow Transient scenario. This scenario simulates a loss in the flow of coolant through the reactor core. Specific details of this scenario will be given in Chapter 5.
4. Determine the maximum temperature reached by the SPND detectors during normal operation, and during the two transient cases. The SPND detectors generate a signal proportional to the neutron flux, but if the temperature of the detector exceeds a limiting temperature of 622 K, then the accuracy of the information provided by the system is reduced. Therefore, it is important to find the maximum temperature of the detectors in order to discover if it exceeds the permitted level for any of the three cases that will be studied.
5. Investigate if boiling occurs inside of the SPND system for any of the three scenarios, and consider the impact that boiling could have on the temperature of the detectors.

The flow and heat transfer studies for the three cases (normal operation, overpower, and loss of flow) were performed using the commercial software Fluent. The geometry was meshed using the grid generation software Gambit. A detailed description of the SPND geometry and the mesh generation process is given in Chapter 2. Chapter 3 presents the first SPND study, which analyzes the normal steady state operation of the system. The overpower and partial loss of flow transients are presented in Chapter 4 and 5 respectively.

Chapter 2 Problem Description and Mesh Generation Process

The first sections of this chapter provide a description of the physical problem being analyzed. This includes a description of the SPND geometry, internal heat generation rates, and flow paths inside of the SPND system. Descriptions of the mesh generation process and the computational model are also given in this chapter.

2.1 Description of Physical Problem

2.1.1 Geometry Overview

A schematic of the SPND system is shown in Figure 2-1. The five main components in the SPND system are the following: guide tube (GT), protection tube (PT), cables, detectors, and support. The outermost component of the assembly is a zirconium tube known as the guide tube. A second tube, of smaller diameter, is located inside the guide tube. This stainless steel tube is known as the protection tube (PT). Six SPND detectors are distributed axially along the height of the PT. As seen in Figure 2-1, each detector hangs from a cable giving a total of six cables contained within the PT. Each detector is also attached to a support plate that runs through the center of the PT.

The entire SPND system is contained within the guide tube. The guide tube is located in the fuel assembly as part of the 17X17 square array shown in Figure 1-4. Rods containing the nuclear fuel (fuel rods) are also contained in this array, and run parallel to the guide tube as seen in Figure 2-1. The fuel rods are composed of enriched Uranium dioxide pellets encased in a zirconium alloy cladding tube.

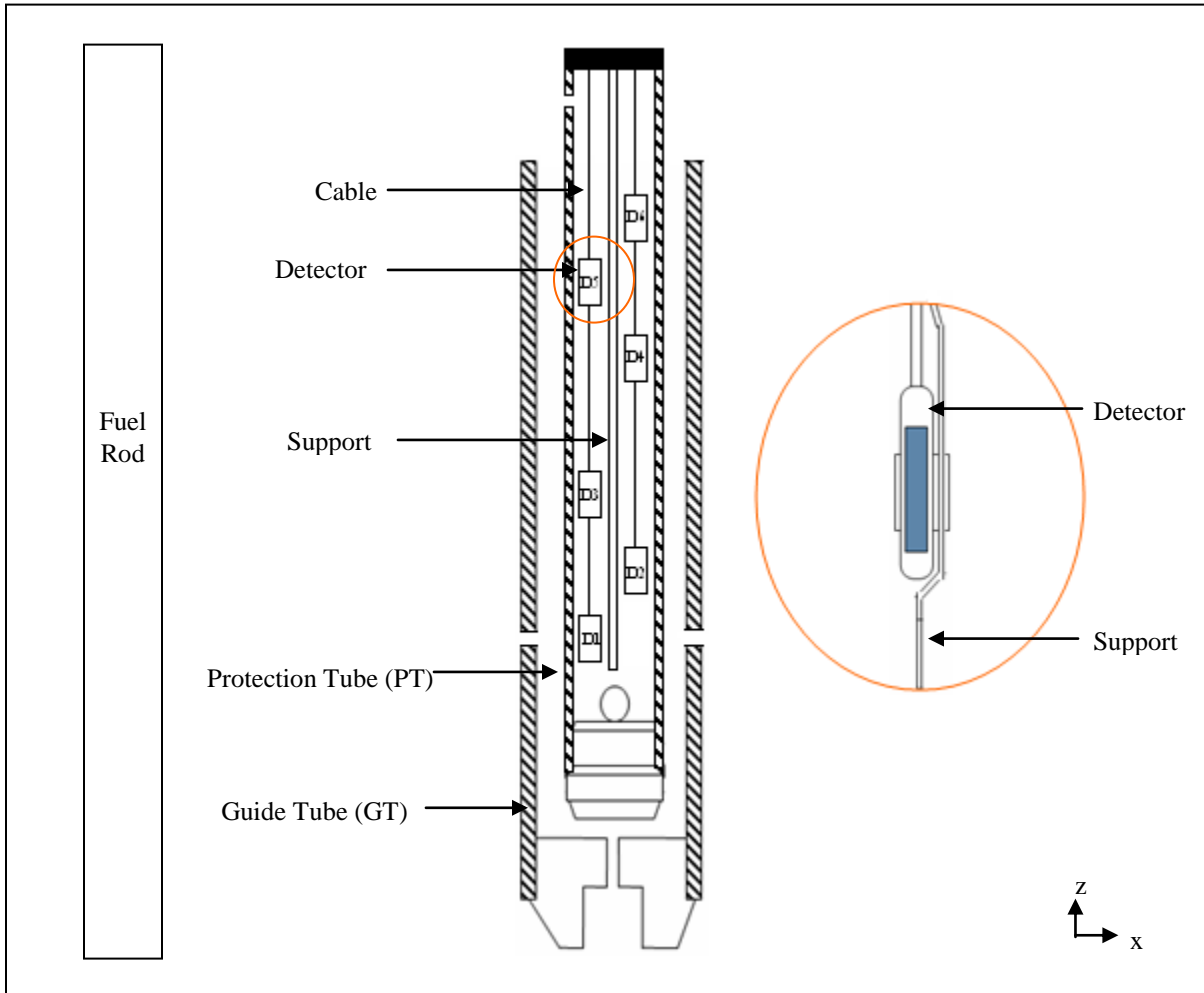


Figure 2-1 Components of SPND system

2.1.2 Internal Heat Generation

The thermal neutron flux in the fuel rod active region (Figure 2-2), acts on all of the components of the SPND assembly and produces internal heat which has to be dissipated by the bypass flow of reactor coolant. Data for the heat generation rates for each of the components in the assembly was provided by Areva (Table D2). The magnitude of the heat generation rates is different for each of the components, but all of them follow the same trend. The internal heat generation rates are small in the upper and lower regions of

the SPND system, and high near the center (Figure 2-2). The components for which the heat generation terms are given are the following: cobalt emitter, SPND insulator, SPND collector, guide tube, guide tube water, protection tube, protection tube water, support, and cables. Curves for the heat generation rates for some of the components may be seen in Figure 2-3.

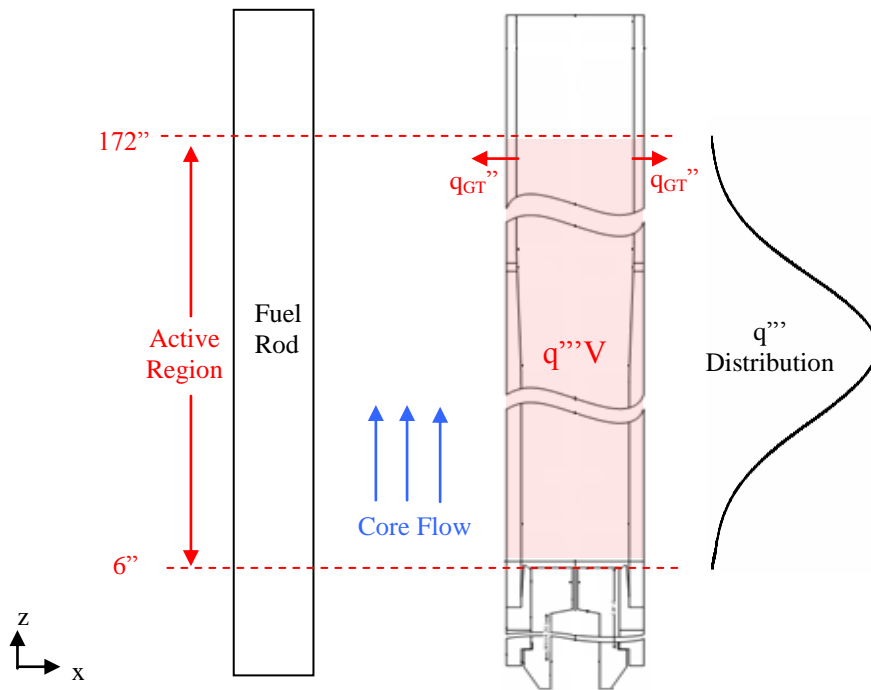


Figure 2-2 Fuel Rod Active Region

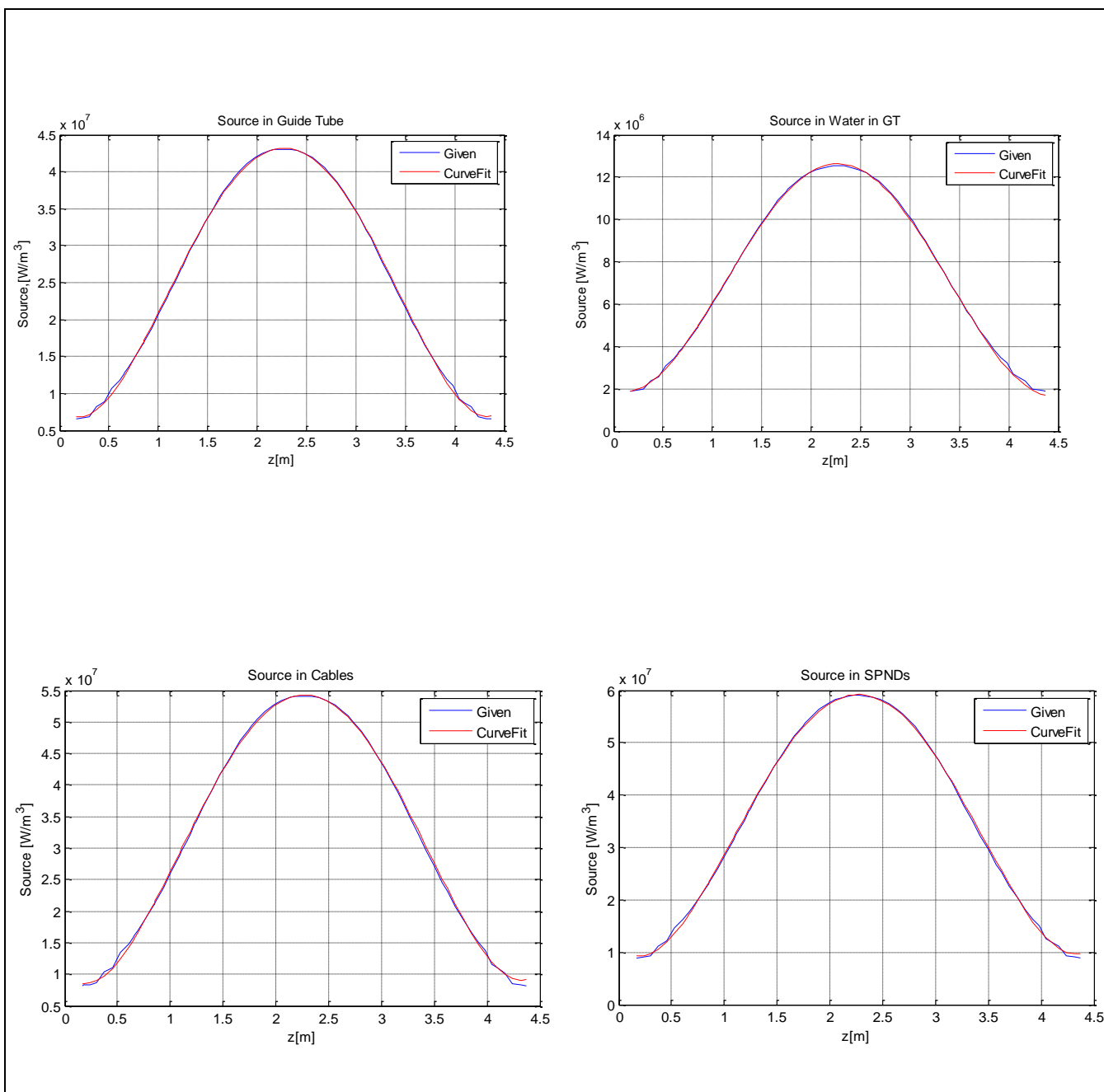


Figure 2-3 Graphs for Heat Generation Data and Curve Fits

A curve fit was generated for the data provided for each of the components in the system. Curve fits for the cables, GT, GT water, and SPND detectors may be seen in Figure 2-3. The equations obtained from the curve fits were utilized to generate user defined functions in Fluent to account for the variable source terms in each component. A user-defined function (UDF) is a function that is programmed and may be dynamically loaded into Fluent to expand the default capabilities of the code [3]. These functions are especially useful when the case being modeled contains varying properties or sources. Detailed information about the UDFs used in this project may be found in Appendix B.

In order to simplify the geometry and the mesh generation process, the three components of the detectors (emitter, insulator, and collector) were combined into an effective volume or zone. Since the computations do not differentiate between emitter, insulator, and collector, but lump all three into the “detector zone”, an effective volume weighted source term was calculated as follows:

$$S_{effective} = \frac{S_{emitter} \cdot V_{emitter} + S_{insulator} \cdot V_{insulator} + S_{collector} \cdot V_{collector}}{V_{effective}} \quad (2.1.1)$$

In equation 2.1.1, S represents the source term and V the volume of each component. $V_{effective}$ is the total volume of the SPND detector.

2.1.3 Flow Paths

The internal heat produced by each of the components has to be dissipated by the coolant flowing within the reactor core. In the U.S. EPR, ordinary water is utilized as the reactor coolant. Water from the primary system (see Figure 1-2) enters the core, and flows in an upward direction. Most of this water flows outside of the guide tube, but some enters the

system through the GT inlets located on the surface of the guide tube (GT inlets 1-5 in Figure 2-4). This water continues to flow through the remaining components of the system as shown in Figure 2-4.

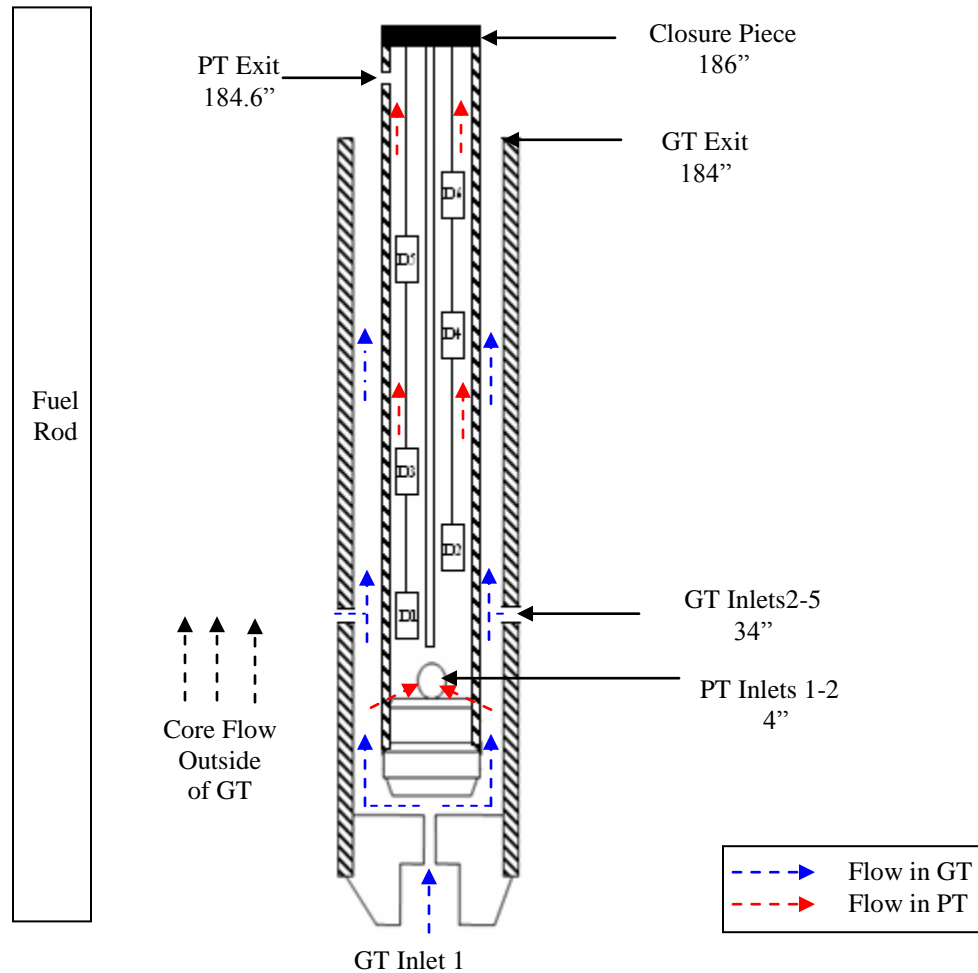


Figure 2-4 SPND System Schematic

Core flow from the reactor enters the guide tube at an inlet located at 0", (GT Inlet 1 Figure 2-4) and also through four circular inlets located at 34" (GT Inlets 2-5). Water flows upwards, and exits the guide tube at a height of 184" (GT exit). This path is indicated by the blue dotted arrows in Figure 2-4.

The red path is for water flowing within the protection tube. Water enters the PT through two inlets located at a height of 4'' (PT Inlets 1-2 Figure 2-4). Both inlets are at the same height and are 180 degrees apart from each other. Water exits through three holes located at 184.6'' (PT exits 1-3). At a height of 186.6'' there is an end piece which impedes the flow of water further up the protection tube.

2.1.4 Problem Review

The two main aspects of the problem have been shown in Figures 2-2 and 2-4. Basically, due to the thermal neutron flux, each component in the assembly generates heat, and the water flowing through the system (as shown in Figure 2-4) acts as a coolant, so there is heat transfer between the solid and fluid regions. The SPND problem involves conjugate heat transfer analysis, and therefore we need to account for conduction heat transfer within the solids, and convective heat transfer between the solid and liquid regions. In the solver, the conditions at the solid-fluid interfaces have to be set in a proper way as to allow for conjugate heat transfer.

The temperature of the SPND system is not only influenced by the internal heat generation rates, but also by the water flowing outside of the guide tube (free stream). In order to account for the heat transfer between the guide tube and the surrounding fluid (q''_{GT} in Figure 2-2), the heat transfer coefficient (h) is calculated in section 3.5.

So, in summary, we need to account for the heat transfer between the SPND components and the coolant, heat transfer between the GT and the free stream flow, and the internal heat generation rates in each of the SPND components.

The description of the problem given in this chapter is the basis for the three distinct scenarios studied in chapters 3-5. Each of the three cases studied has its own special considerations which will be described in detail in the corresponding chapter.

2.2 Computational Model

For computational purposes, the SPND assembly was divided into zones. Each zone corresponds to a component of the SPND assembly. This section contains a detailed description about the geometry of the SPND components and the corresponding zones.

2.2.1 Geometry Description

A detailed view of the components and dimensions of the SPND system is shown in Figure 2-5. The figure on the left shows the dimensions for the guide tube (GT). The GT is the outermost tube, which is very long and thin. The total length is 184", and the outer diameter of the tube is 0.49". From Figure 2-5 it is seen that the aspect ratio of the SPND assembly is very high ($184"/0.49"$). The guide tube is made from zirconium. The properties of this and other materials are given in Appendix C.

Figure 2-5b shows the protection tube (PT) which is inserted into the guide tube creating a channel in between the two tubes. Water flows within the channel acting as a coolant for the SPND system. This channel will be referred to as guide tube channel. Within the protection tube, there are a total of six SPND detectors distributed axially. The detectors are composed of three materials: cobalt, Al_2O_3 , and Inconel. Each detector hangs from a cable and is attached to a support. Each of the components of the SPND

assembly was assigned to specific zone in the computational model. The seven zones are described in the next section.

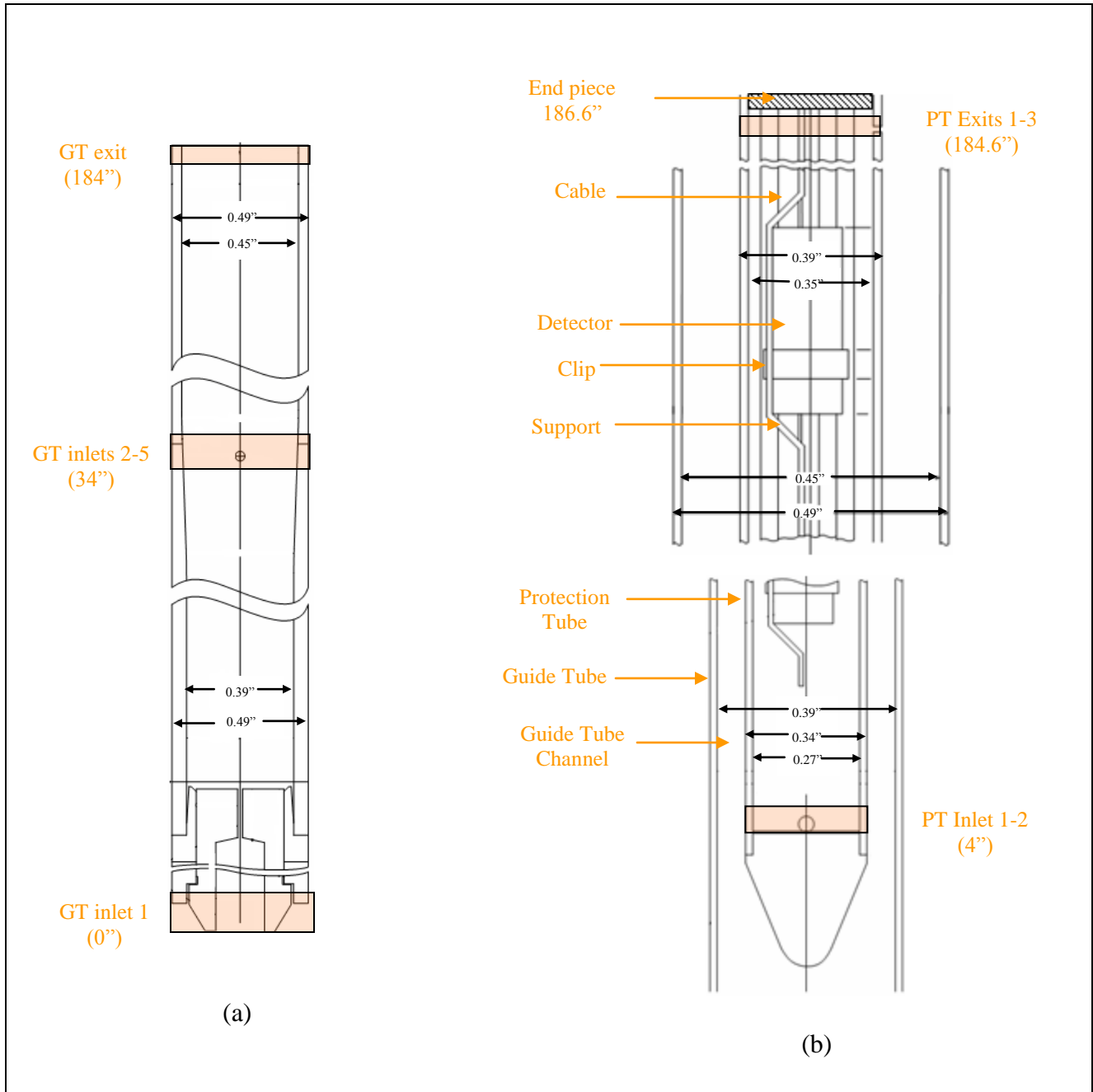


Figure 2-5 a) Guide Tube; b) Guide Tube inserted with Protection Tube and Detectors
(Figures Courtesy of Areva)

2.2.2 Zones

For computational purposes, the SPND assembly was divided into seven zones. This section contains a description of each of the zones.

Zone 1: Guide Tube: The outermost component of the assembly, the guide tube, spans from 0" to 184". The guide tube has an entry port located at 0" and four other circular inlets located at a height of 34". A detailed view of the guide tube and its dimensions is given in Figure 2-5a and Figure D1 (Appendix D).

Zone 2: Protection Tube: It consists of the probe containing the 6 SPND detectors. It has two entry ports at 4", which are 180 degrees apart from each other. The probe spans from 3.4" to 306". At a height of 186.6" there is an end piece which impedes the flow of water further up the protection tube. Therefore the computational domain for the PT extends only from 3.4" to 186.6". Water exits the probe through three outlets located at a height of 184.6" which are 120 degrees apart from each other. For a detailed drawing of the protection tube see Figure D2.

Zone 3: Detectors: SPND detectors are composed of three main parts: emitter, insulator, and collector (Figure 1-5). For simplicity, the SPND zone was modeled as an effective volume consisting of the three aforementioned parts. The radius of the detectors is 0.0748". The three lower SPND detectors (D1 through D3) have a length of 8.27". The remaining three detectors (D4 through D6) are 9.17" in length.

Zone 4: Cables: Consists of the cables from which the SPND detectors hang from. There are a total of six cables (1 cable connected to each detector) within the protection tube. At a height of 147", the cables are positioned as shown in the cross-sectional view in Figure 2-6. In order to reach their respective detector, the cables have to shift from

their original position, therefore the geometry within the protection tube becomes very complex. The cables are labeled C1 through C6. In Figure 2-6, C6 is not shown since it is attached to the detector D6.

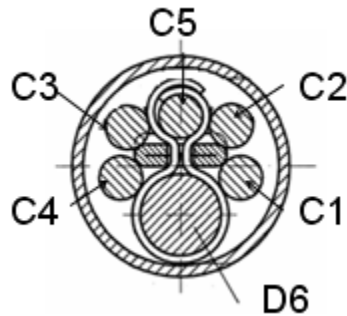


**Figure 2-6 Protection Tube Slice at 147”
(Figure Courtesy of Areva)**

Zone 5: Support: Consists of a plate that runs parallel to the SPND detectors (see Figure 2-5b). The detectors are attached to the support by means of a clip that surrounds the detector and goes through a slot in the support.

Zone 6: Water in Guide Tube: Consists of the flow path formed between the guide tube and the protection tube.

Zone 7: Water in Protection Tube: Consists of water flowing inside the protection tube which serves to cool the detectors.

2.3 Mesh Generation

The grid generation software GAMBIT was used to generate the mesh for the geometry.

Both hexahedral and triangular prism elements were used as described in section 2.3.2.

2.3.1 Geometry Simplifications

Due to the complexity of the geometry within the protection tube, the following simplifications were done to the original geometry in order to successfully generate the mesh.

- The six cables (1 cable for each detector) were arranged into two groups of three cables each (G1 and G2 Figure 2-7). Group 1 contains cables C1, C3, C5. Group 2 contains cables C2, C4, C6. The diameter of G1 and G2 will be reduced along the height of the system after each SPND detector is reached since there is one less cable after each detector. Table 2-1 shows the values for the three different radii of sections G1 and G2.

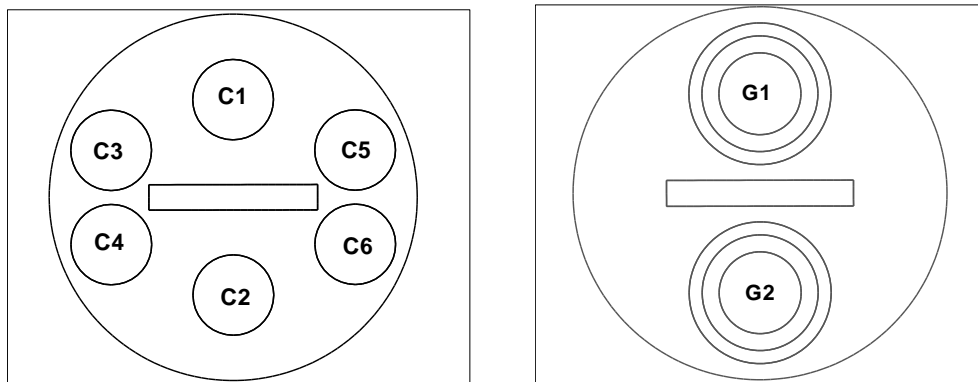


Figure 2-7 Simplification of Original Geometry for Cables

Table 2-1 Radii for Grouped Cables

Number of Cables Grouped	Radius (in)
1	0.0395
2	0.0558
3	0.0684

- The inlets GT 2-5, PT 1-2 and the exits PT 1-3 are circular (Figure 2-5), but were modeled as squares of equivalent area in order to simplify the meshing process.
- The inlets located at a height of 34", GT inlets 2-5, were assumed to be in-line rather than offset by 0.197" (the offset is in the direction along the height).
- The support was modeled as a straight plate.
- The component that attaches the detectors to the support was not modeled since heat generation data was not provided for it.

With the simplifications described above, the geometry was created in Gambit. Figure 2-8 shows a small section of the three dimensional geometry of the SPND assembly. This section extends from a height of 50.57" to 70.57". The two outer cylinders are the guide tube and the protection tube. Inside the protection tube, we can see the implementation of the previously mentioned geometry simplifications. The support is modeled as a straight plate though the center of the tube and the cables are lumped into two groups (G1 and G2).

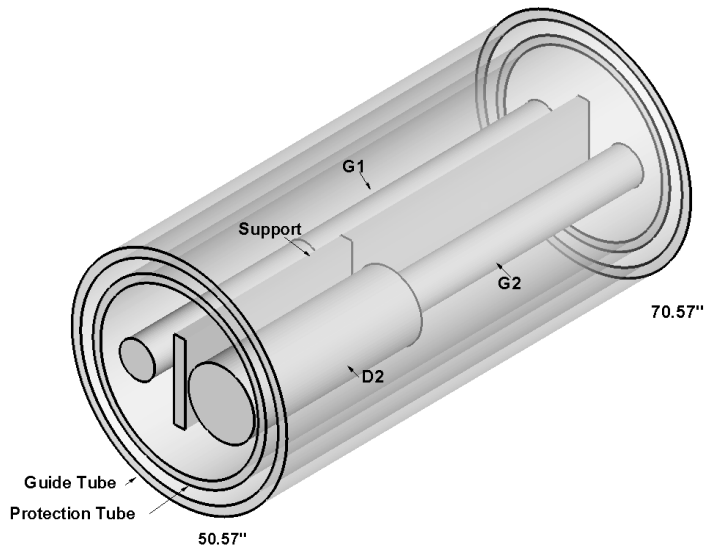


Figure 2-8 SPND Geometry with Simplifications

2.3.2 Mesh Model

The number of cells for the entire model is 4580720 elements. The mesh for the guide tube, pressure tube, and guide tube channel zones consists of hexahedral elements aligned with the flow direction. The zone for the water within the protection tube consists of triangular prism elements.

Figure 2-9 shows a cross-section of the mesh at 50.57". This same mesh is maintained from a height of 50.57" up to a height of 184". The two circular zones within the protection tube are of special interest since they may be either fluid or solid depending on the location along the height of the core. Figure 2-10a shows the final distribution of the SPND detectors in the protection tube. In this figure it is seen how after each detector, the diameter of the zones G1 and G2 is reduced. Mesh cross-sections at different heights may also be seen in Figure 2-10b. The solid zones at each slice are

shown in black. Slice 1 is at a height of 31” (going through D1). This same mesh cross-section extends from 3.8” to 38.84” along the height of the protection tube.

Slice 2 is at a height of 50.57” (going through D2). This same mesh cross-section extends from a height of 50.57” to 184”. For the section of the domain from 38.84” to 50.57”, an unstructured, tetrahedral mesh was used to transition between the mesh cross-sections shown at slice 1 and slice 2.

Slice 3 is located at 147” and goes through D6. Comparing slices 2 and 3, it is seen that the diameter of section G1 is reduced from slice 3 to slice 2 since the number of cables in G1 has been reduced from three cables to one.

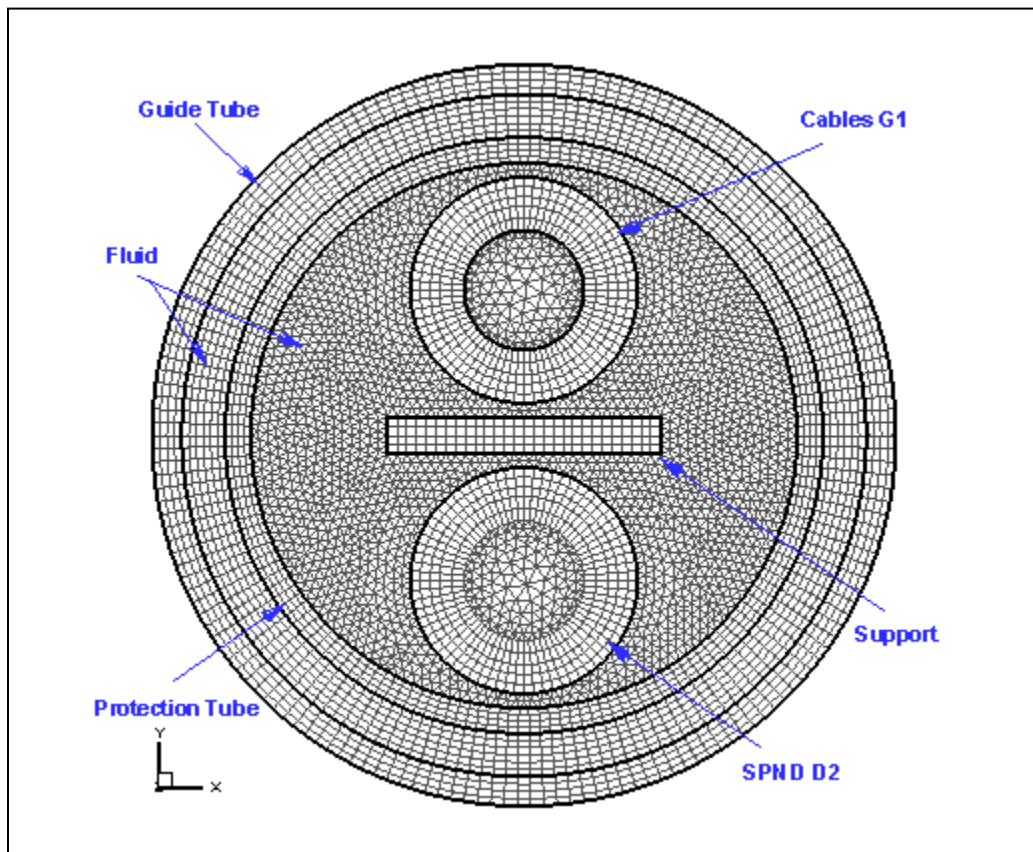


Figure 2-9 Mesh Cross-section at 50.57”

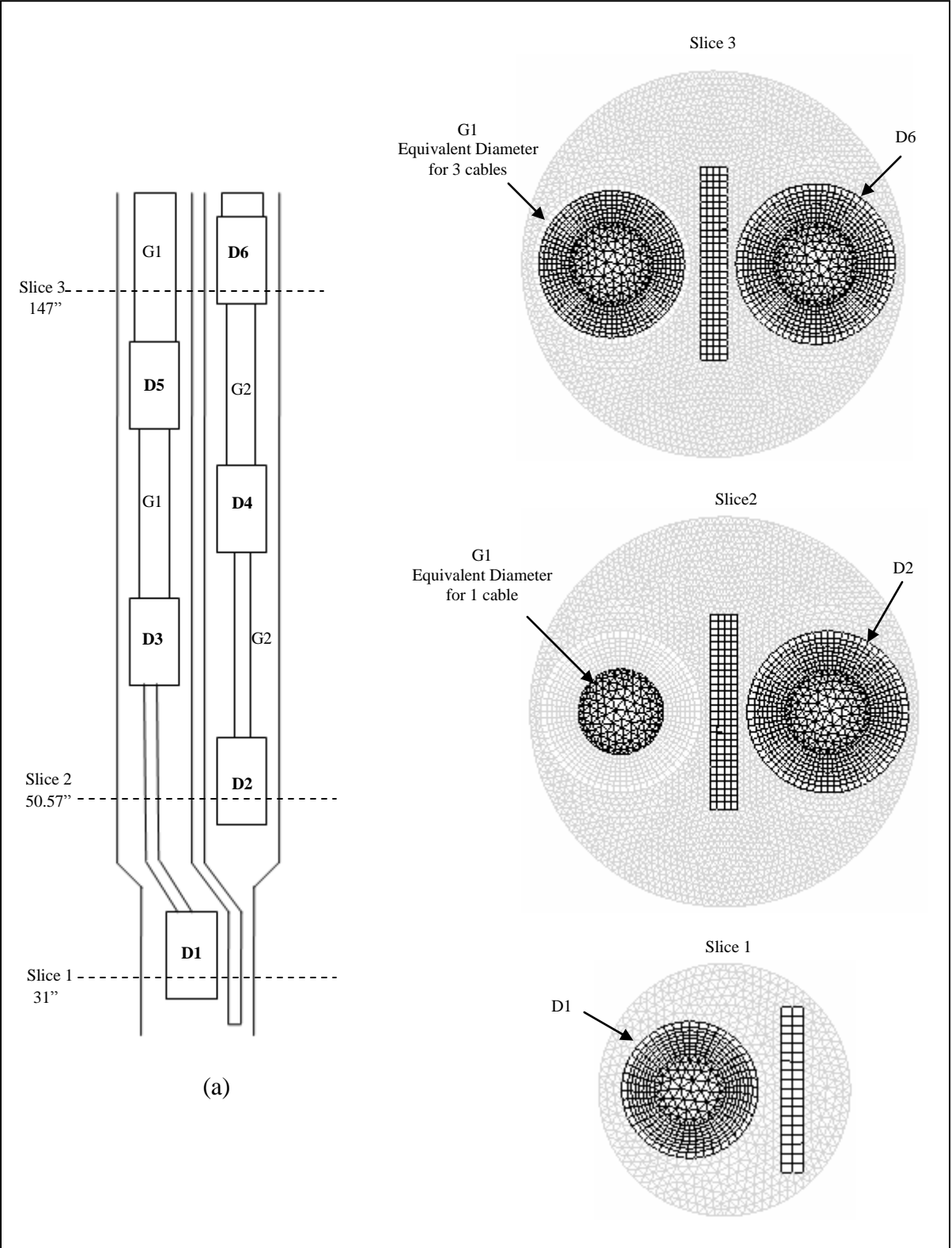
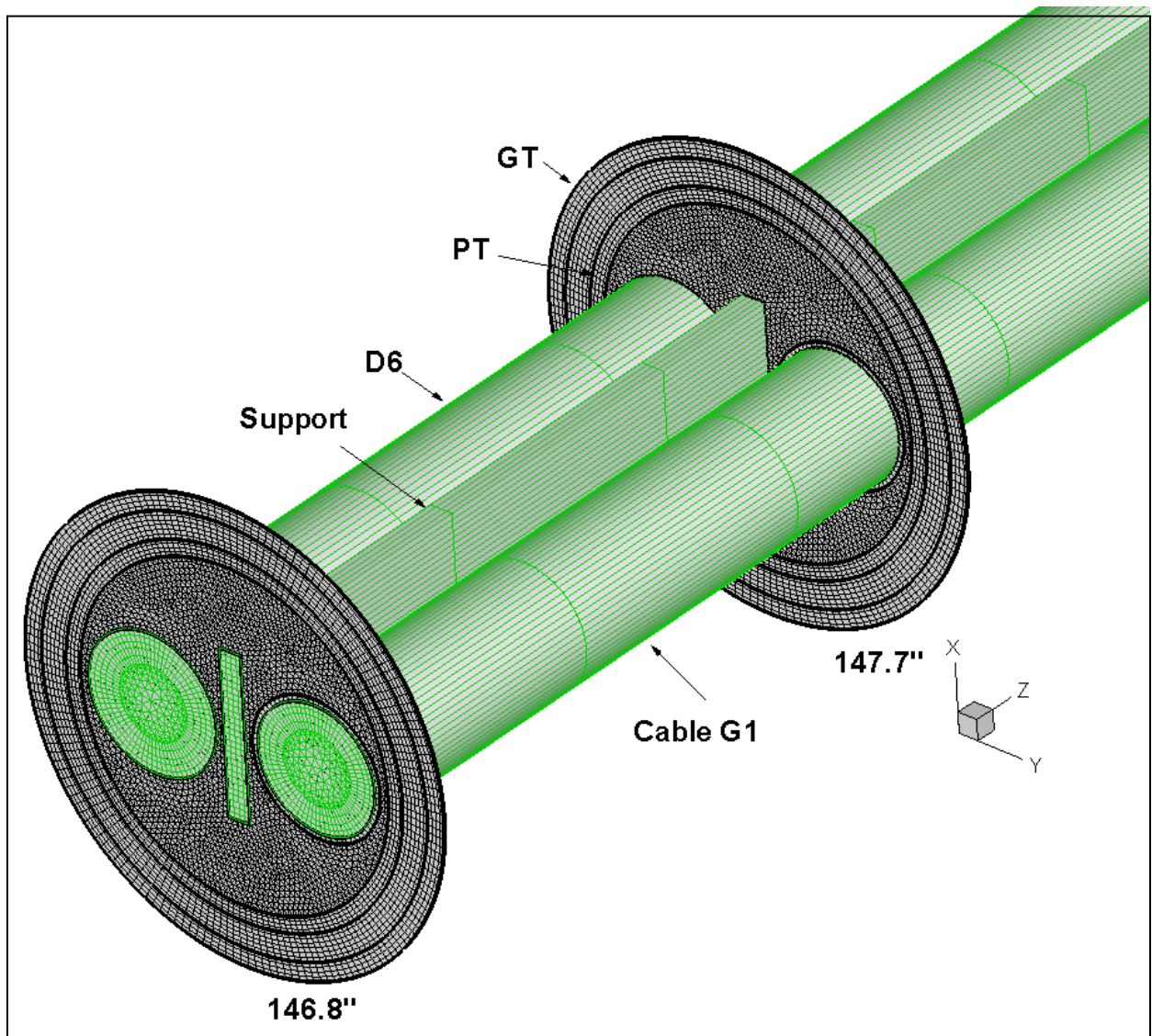


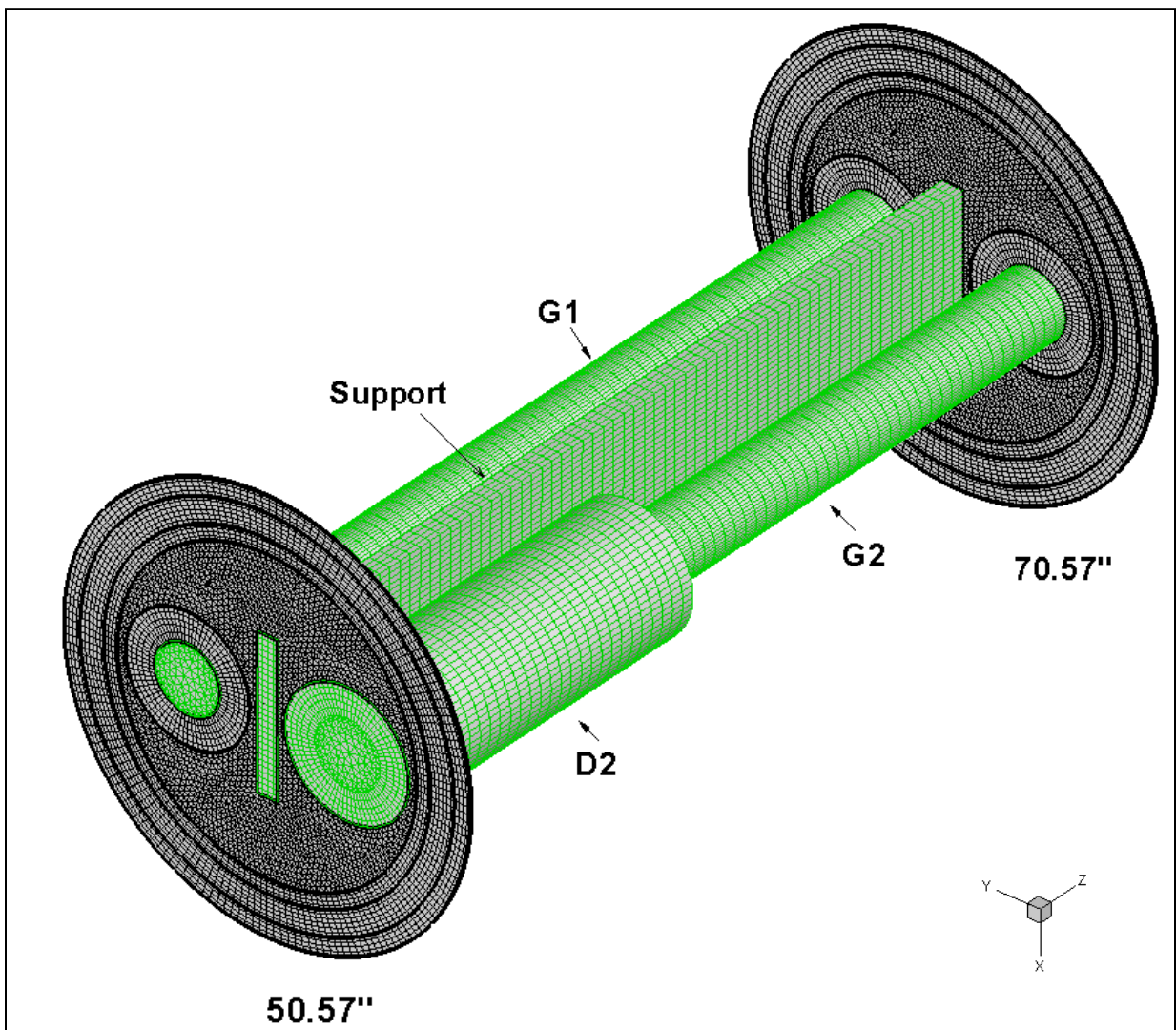
Figure 2-10 Mesh Cross-sections at Different Heights along Protection Tube

Figure 2-11 shows a three dimensional section of the mesh that extends from 146.8" to 147.7". The solid components within the protection tube are shown in green. As seen from Figure 2-11, at this height in the SPND assembly, G1 represents the equivalent diameter of 3 cables, which is close to the SPND diameter. Also, from the figure it is seen how the same mesh cross-section is extruded along the height of the assembly.



**Figure 2-11 Three-dimensional mesh from 146.8" to 147.7"
(Solid zones shown in green)**

Figure 2-12 shows the mesh of a section extending from 50.57" to 70.57". In this figure it can be seen how a detector is attached to a cable (in this case D2 to G2). The diameter of G2 at this height is representative of a single cable. Also, Figure 2-12 shows that even though the diameter of the solid zones is not constant (diameter is reduced in going from D2 to G2), the same mesh cross-section is maintained from 50.57" to 70.57" and throughout the remaining of the height of the SPND geometry.



**Figure 2-12 Three-dimensional mesh from 50.57" to 70.57"
(Solid zones shown in green)**

Chapter 3 Flow and Heat Transfer Analysis for SPND under Normal Operation

This chapter presents the steady state flow and heat transfer analysis for the SPND system under normal operation. In the first sections of this chapter, the boundary conditions and solver settings will be described. Then a series of verification studies will be presented, followed by a section presenting the results.

3.1 Problem Description

As described in Chapter 2, the SPND analysis involves conjugate heat transfer between the SPND solid components and the water flowing through the GT and PT channels. Since the analysis presented in this chapter is for the SPND system under normal operation, the problem description (heat generation, flow paths) is exactly the same as that given in Chapter 2. Each SPND component has internal heat generation which is produced by the neutron flux in the active region of the fuel rods. This heat has to be dissipated by water flowing through the SPND assembly in the paths described in section 2.1.3. Also, there is heat transfer between the guide tube and the core free stream flow. The value of the heat transfer coefficient (h) for the free stream region is calculated later in the chapter.

3.2 Objective

The main objective of this study is to monitor the temperature of the SPND detectors and verify that it does not exceed a limiting value of 622 K. If the temperature of any of the detectors exceeds this value, then the information provided by the SPND system will become less accurate. It is also important to ascertain that no boiling occurs within the SPND system.

3.3 Boundary Conditions

The data for the thermal-hydraulic conditions surrounding the guide tube during normal operation was provided by Areva and is tabulated in Table D1 in Appendix D. The data given was for the hottest quadrant of the reactor core. All four quadrants were assumed to be identical, thus providing a conservative approach with regard to heat transfer.

The flow within the SPND assembly is driven by the pressure difference between the inlets and outlets of the system. In the SPND system, there are a total of five inlets (GT inlets 1-5) and four outlets (GT exit 1, PT exits 1-3). Figure 3-1 shows the location of the inlets and outlets. As seen from the figure, there are only three heights of interest where the inlets and outlets are located. Pressure and temperature data at these three heights was provided by Areva and is shown in Table 3-1 and Figure 3-1. The values for ΔP are with respect to the reactor's operating pressure (2250 psi).

Table 3-1 Boundary Conditions at Inlets and Outlets

	Type	Location [in]	ΔP [psi]	Temperature [K]
GT inlet 1	Pressure Inlet	0	-3.51	570.79
GT inlet 2-5	Pressure Inlet	34	-8.63	575.3
GT exit	Pressure Outlet	184	-33.89	618.12
PT exits 1-3	Pressure Outlet	184.6	-33.89	618.12

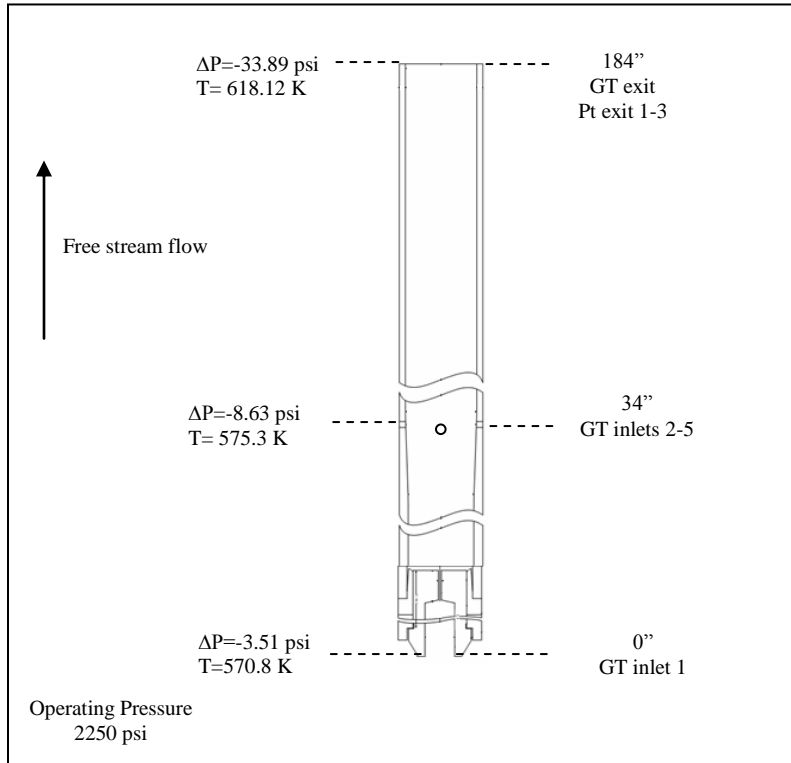


Figure 3-1 Pressure and Temperature Boundary Conditions

In Fluent, the values shown in Table 3-1 were assigned to the corresponding inlet or outlet. Since this is a pressure driven flow, the inlets (GT inlets 1-5 in Figure 3-1) were defined as pressure inlets and the outlets (GT exit 1, PT exits 1-3 in Figure 3-1) as pressure outlets. For the pressure inlets, Fluent requires the total pressure (sum of static and dynamic pressure) to be specified. The total pressure is given by:

$$P_{Total} = P_{static} + \frac{\rho V^2}{2} \quad (3.3.1) \quad [3]$$

Therefore the static pressure and the velocity at the inlets had to be specified. The static pressure is known from the given data (Table 3-1). On the other hand, the velocity at the inlets is unknown, thus an iterative procedure was followed. First, the calculation was conducted in Fluent for a number of iterations. Then the value of the current velocity

at the inlets was obtained and used to compute the dynamic pressure. The process was continued until the difference between the total and dynamic pressure matched the desired static pressure.

In addition to the previously mentioned conditions, convective boundary conditions were applied on the outside wall of the guide tube in order to allow for heat transfer between the guide tube and the surrounding fluid. The heat transfer coefficient was assumed to be uniform and was calculated using the average velocity and temperature of the free stream as described in section 3.5. The temperature of the free stream also varies along the height as seen in Table D1 in Appendix D. In order to be able to specify this varying temperature in the solver, a curve fit was done on the data shown in Table D1. The equation obtained from the curve fit was used to define a User Defined Function (UDF) for the variable free stream temperature. Finally, in order to allow for conjugate heat transfer, coupled wall conditions were enabled at all of the solid-fluid interfaces.

3.4 Solver Settings

The k-epsilon model with standard wall functions was selected in the solver as the turbulence model. The k- ϵ model is a two equation model since it requires the simultaneous solution of the equation for the turbulent kinetic energy (k), and the equation for the dissipation rate (ϵ), in addition to the momentum and continuity equations. More details about these equations are given in Appendix A. The k- ϵ model with standard wall functions requires the values of the non-dimensional length y^+ to be within the range $30 < y^+ < 300$ [3]. An adaptation of the grid was performed so that the y^+ values fell within the proper range. This process is described in section 3.6.2.

The mass, momentum, and energy conservation equations along with the transport equations for turbulent kinetic energy (k) and dissipation rate (ϵ), were solved for turbulent flow. The flow was assumed to be incompressible, and the constant material properties shown in Appendix C were used. For the pressure velocity coupling the SIMPLE algorithm was enabled, and the convection terms were differentiated by using a second order upwind scheme. At convergence, the residuals for the velocity quantities are of at least $O(10^{-4})$, for turbulence quantities of $O(10^{-4})$, and for energy is of $O(10^{-7})$.

3.5 Calculation of External Heat Transfer Coefficient

The external heat transfer coefficient was calculated in order to account for the heat transfer between the guide tube and the surrounding fluid. An average value of the heat transfer coefficient was computed based on average values for the free stream temperature and velocity.

By assuming zero pressure gradient and a flat plate boundary layer on the outside of the guide tube, the following correlation was used to calculate the average Nusselt number (Nu) based on the Prandtl number (Pr) and the Reynolds number (Re_L) [4].

$$\overline{Nu}_L = (0.037 Re_L^{4/5} - 871) Pr^{1/3} \quad (3.5.1)$$

The Reynolds number based on the height of the tube is defined as:

$$Re_L = \frac{\rho VL}{\mu} \quad (3.5.2)$$

L represents the height of the guide tube (184 in). The values for the density (ρ) and dynamic viscosity (μ) of water are defined in Appendix C. The average heat transfer coefficient was obtained from 3.5.3:

$$\overline{h} = \frac{\overline{Nu} * k}{L} \quad (3.5.3)$$

The results obtained for Re_L and Nu_L, and the value for the convective heat transfer coefficient are summarized in Table 3-2.

Table 3-2 Convective Heat Transfer Coefficient

Effective Length [m]	4.64
Average Velocity [m/s]	5.37
Re _L	211x10 ⁶
Nu _L	164364.3
h [W/m ² K]	18709

3.6 Verification

This section presents a series of tests that were performed to verify certain aspects of the calculation procedure.

3.6.1 Evaluation of Effect of the Grid Element Shape on the Accuracy of the Discretization Scheme

In section 2.3.2 a description of the mesh generated for the SPND system was given. As described in that section, both hexahedral and triangular prism elements were used to mesh the geometry. Specifically, triangular prism elements were used to mesh the interior of the protection tube. This type of element was used in order to facilitate the mesh generation process since the geometry contained within the protection tube is complex. This section of the report intends to demonstrate that the use of these triangular elements does not affect the accuracy of the scheme being used to discretize the momentum equation.

In order to demonstrate that the accuracy of the scheme is not affected by the shape of the grid elements, the value of n , the truncation error $(\Delta x)^n$, is calculated for both a structured and an unstructured mesh. The following sections contain descriptions of the problem setup, boundary conditions, mesh configurations used, and the method used to calculate the accuracy of the discretization scheme.

3.6.1.1 Problem Description

Since there is no analytical solution available for the flow within the protection tube, the results obtained from Fluent cannot be compared to any known results. Therefore, the simple case of fully developed flow inside a pipe is considered. Flow within a pipe may

be modeled as axis-symmetric, and therefore a two dimensional mesh is used to solve the problem in Fluent. The flow considered is laminar and fully developed. The dimensions of the pipe are shown in Figure 3-2. The area shown in red is the two dimensional plane that will be meshed in order to model the flow.

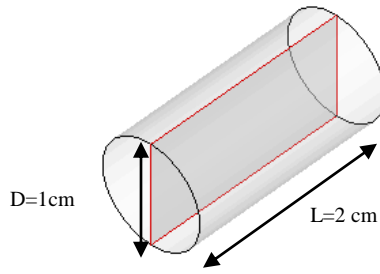


Figure 3-2 Pipe Dimensions

3.6.1.2 Mesh Configurations

Two mesh configurations were used in this study. One of the meshes was structured and the other unstructured. A simple definition for a structured mesh is one that has a set connectivity between its elements. Also in 2-D meshes, each interior cell must have a total of four neighbors. On the contrary, the elements in an unstructured mesh have no set connectivity. The triangular prism elements that were used to mesh the inside of the SPND protection tube fall within the category of an unstructured mesh. Again, the purpose of this study is to determine if the use of such type of mesh affects the accuracy of the scheme used to discretize the momentum equation.

For the simplified 2-D pipe-flow case, the structured mesh to be used is the Cartesian grid shown in Figure 3-3. From Figure 3-3 it can be seen that each cell has four neighboring cells, and they have a set connectivity between them. The unstructured mesh will be composed of triangular elements as shown in Figure 3-4. From the figure, it is

seen that each cell has only three neighbors, and that the set connectivity among the cells is lost.

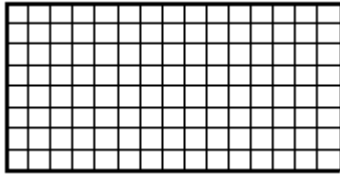


Figure 3-3 Cartesian Mesh

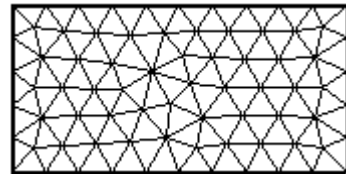


Figure 3-4 Unstructured Mesh

3.6.1.3 Boundary Conditions

The boundary conditions for the domain are shown in Figure 3-5. The top boundary (1) represents the outside of the pipe, therefore that edge is a wall boundary. Boundary (2), located at the center of the pipe is the symmetry boundary condition. For the remaining two boundaries (3 and 4), periodic conditions were utilized. This is because since the flow is fully developed, the velocity in the x-direction will not change as we move along the x direction. Therefore the values of the x- velocity at boundary 3 will be the same as for boundary 4. For periodic conditions, Fluent allows the user to define the value of the pressure gradient (dP/dx). It is important to remember that for laminar internal flow the Reynolds number should be less than 2300. In order to have an idea of what would be a reasonable value for dP/dx , the average velocity was calculated using equation 3.6.1.

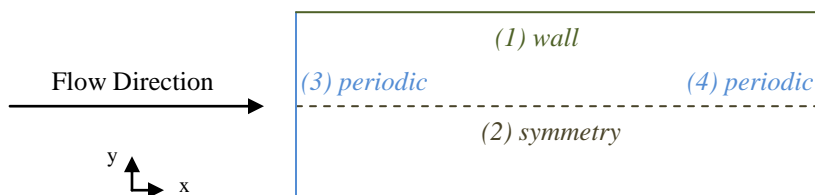


Figure 3-5 Domain Dimensions and Boundary Conditions

$$V_{avg} = \frac{-R^2}{8\mu} \left(\frac{\partial p}{\partial x} \right) \quad (3.6.1) \quad [7]$$

The value for dP/dx was set to -30 Pa/m. With $R=0.005$ m, viscosity (μ) = 0.001003 kg/m-s, and density (ρ) = 998.2 kg/m³, the average velocity was found to be 0.0934 m/s and the Reynolds number is 930 .

3.6.1.4 Calculation of Truncation Error

The commercial software Fluent was used as the solver for the flow. The convective term in the momentum equation was discretized by using a second order upwind approximation. The expected value of n for this approximation is 2 . The momentum equation in cylindrical coordinates for laminar fully developed flow in a pipe is reduced to the following form:

$$\frac{1}{r} \frac{d}{dr} \left(r \frac{du}{dr} \right) = \frac{1}{\mu} \frac{\partial p}{\partial x} \quad (3.6.2)$$

The analytical solution for this equation is:

$$u = \frac{-R^2}{4\mu} \left(\frac{\partial p}{\partial x} \right) \left[1 - \left(\frac{r}{R} \right)^2 \right] \quad (3.6.3) \quad [7]$$

The values of the computed (Fluent) and analytical x-velocities were compared to find the truncation error. The first step in this process was to obtain the values for the velocities along a line in the domain ($x=1$ cm) from Fluent. The error vector (ϵ) was calculated as the difference between the analytical and the computed solution at the nodal points along the selected line.

The L2 norm of the error vector is defined as:

$$\varepsilon_{avg} = \left(\frac{1}{N} \cdot \sum_{i=1}^N \varepsilon_i^2 \right)^{1/2} \quad (3.6.4)$$

where N is the total number of interior nodes.

Three sets of Cartesian and triangular meshes with the same number of elements were created. The number of elements for the mesh configurations used are: 122, 244, and 488. Using the value of ε_{avg} from 3.6.4, the value of n can be calculated using equation 3.6.5.

$$n = \frac{\ln\left(\frac{\varepsilon_{avg\Delta}}{\varepsilon_{avg2\Delta}}\right)}{\ln(1/2)} \quad (3.6.5)$$

The obtained values for ε_{avg} and n are presented in Tables 3-3 and 3-4.

Table 3-3 Comparison of ε_{avg} for Cartesian and triangular mesh

Number of Elements	ε_{avg} for Triangular Mesh	ε_{avg} for Cartesian Mesh
Mesh 1 = 122	2.98E-04	2.57E-04
Mesh 2 = 244	6.22E-05	5.98E-05
Mesh 3 = 488	1.48E-05	1.38E-05

Table 3-4 Values of n for the Triangular and Cartesian Meshes

Meshes Used	n for Triangular	n for Cartesian
Mesh 1 and 2	2.2	2.1
Mesh 2 and 3	2.1	2.1

The value of n should be equal to 2 since the second order upwind scheme was used to discretize the momentum equation. From Table 3-4 it is seen that for both types of meshes, the value of n is close to the expected value of 2. Therefore, we may conclude that the shape of the elements in the mesh does not affect the magnitude of the truncation error for a second order upwind discretization. Although this conclusion has been

obtained by analyzing a very simple laminar flow case, it gives some assurance that utilizing unstructured meshes will not affect the accuracy of the results to a great extent.

In addition to determining the value of n , it was desired to compare the values of ϵ_{avg} between square and triangular meshes with the same number of elements.

From Table 3-3 it is seen that the values for ϵ_{avg} for Cartesian and triangular grids with the same number of elements are close to each other, but as expected the values of ϵ_{avg} for the Cartesian mesh are slightly smaller than for the triangular mesh.

3.6.2 Sensitivity of Results to Near Wall

The study described in this section was performed on the actual SPND geometry in order to verify that the resolution of the grid had no considerable effect on the results. The idea of this sensitivity study is to monitor a relevant parameter and verify that it does not vary significantly as the mesh is refined. In that way, it is verified that the solution has become independent of the mesh. The adaptation of the grid was done with respect to the non-dimensional length y^+ , which is defined as:

$$y^+ = \frac{u_\tau y}{\nu} \quad (3.6.6)$$

where y is the distance from the surface to the midpoint of the first cell, and u_τ is defined as:

$$u_\tau = \sqrt{\frac{\tau_w}{\rho}} \quad (3.6.7)$$

First, the range of y^+ values was maintained between 30 and 500. The mass flow rates for this range of y^+ values are shown in the first column of Table 3-5. Next, the grid was adapted as to only allow y^+ values between 30 and 300 and finally between 30 and

90. Table 3-5 also shows the mass flow rates for these two cases and the corresponding number of total cells for each case.

It is important to mention that for the k-epsilon turbulence model with standard wall functions the values of y^+ should be in the range of $30 < y^+ < 300$, but as close to 30 as possible [3]. The last grid adaptation with y^+ between 30 and 90 was the one used to obtain the final results because its values of y^+ fall within the proper range.

Table 3-5 Mass Flow Rates for Three y^+ ranges

	$30 \leq y^+ \leq 500$	$30 \leq y^+ \leq 300$	$30 \leq y^+ \leq 90$
Inlet GT 1	0.001871	0.001903	0.001904
Inlet GT 2-5	0.087254	0.088380	0.088743
GT Exit	0.046602	0.047247	0.047140
PT Exit 1-3	0.041540	0.043096	0.043021
Number of elements	4457944	4495730	4580720

From Table 3-5 it is seen that the mass flow rates do not vary by more than 3.6% for any of the cases, thus the results obtained are independent of the grid resolution as desired. It is important to mention that this sensitivity test does not guarantee that the obtained solution is physically correct, but it only verifies that the mathematical model is accurate. Therefore it was necessary to find another way to verify the obtained results. A series of studies presented in the following sections intend to provide a greater level of confidence in the results.

3.6.3 Global Energy Balance

In order to verify that Fluent was correctly interpreting the analytical form of the source terms in the UDF (see Appendix B), an energy balance was performed on the SPND assembly (Figure 3-6).

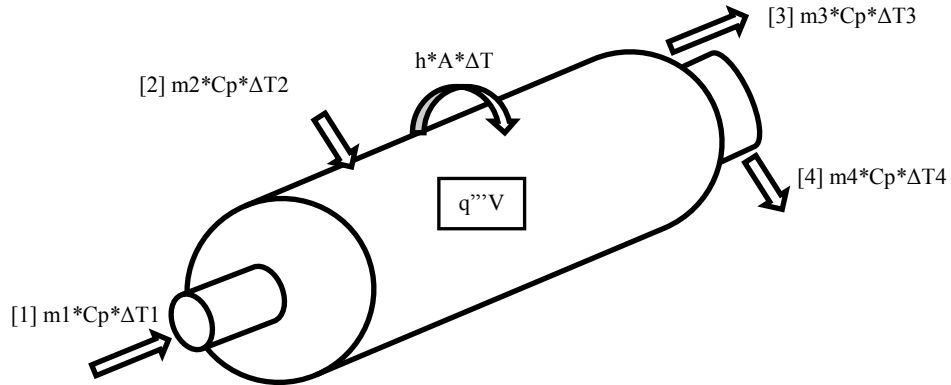


Figure 3-6 Energy Balance on SPND Assembly

The values reported by Fluent at each of the locations shown in Figure 3-6 were obtained and are summarized in Table 3-6. The volumetric source term obtained from the Fluent energy balance was 8423 W. Then, by utilizing the internal heat generation rates provided by Areva, and integrating over each of the components, the total volumetric source term was calculated to be 8230 W. The difference between the volumetric source term value obtained from Fluent and the calculated (Areva) value is 2.3%.

Table 3-6 Energy Values Reported by Fluent

[1] GT inlet 1 (0")	3320.2 W
[2] GT inlets 2-5 (34")	154283.9 W
[3] GT exit (184")	-91712.2 W
[4] PT outlets 1-3 (184")	-84099.6 W
Guide Tube Convection	9785 W
Volumetric Source Term	8422.7 W

3.6.4 Estimation of Friction Factor in Guide Tube (Annulus)

The next section presents the calculation of the friction factor for the guide tube channel. The inner wall of the guide tube and the outer wall of the protection tube form an annulus as shown in Figure 3-7.

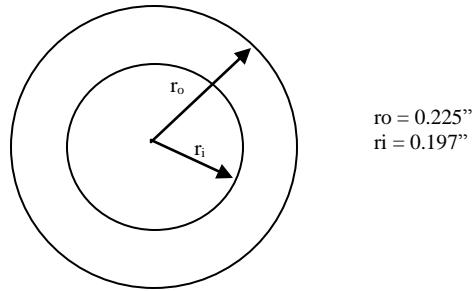


Figure 3-7 Guide Tube (Annular Cross-section)

The purpose of this calculation is to compare the friction factor obtained from data from Fluent, with a theoretical friction factor for an annulus obtained from the Moody chart. The goal of this process is to gain assurance that the grid resolution and turbulence model used are appropriate to correctly model the flow within the guide tube channel.

The friction factor calculation was done for a section where the flow is fully developed. The region considered was for a length between 114'' to 184''. The friction factor is defined as:

$$f = 2 \frac{\Delta P D_h}{L V^2 \rho} \quad (3.6.8) \quad [7]$$

The values for the pressure gradient (ΔP) and average velocity (V) were obtained from Fluent and are shown in Table 3-7. D_h is the hydraulic diameter of the annulus, L is the length of the section, and ρ is the density of water.

A theoretical value for the friction factor (f_{theor}) is obtained from the Moody chart and it is shown in Table 3-7.

Table 3-7 Friction Factor Calculation

Average Velocity	2.85 m/s
D_h	0.0014478 m
Re based on Hydraulic Diameter (D_h)	35050
$\Delta P/L$	44766 Pa/m
f_{theor}	0.0225
f_{fluent}	0.0235

The difference between the friction factor obtained using Fluent reported values (f_{fluent}) and the friction factor obtained from the Moody chart (f_{theor}) is 4.4%.

3.6.5 Friction Factor Protection Tube

A calculation similar to the one shown in the previous section was performed for the protection tube. The main goal of this study is to provide a greater level of confidence that the mesh resolution and turbulence model ($k-\epsilon$) used are appropriate to model the flow within the protection tube. It is not the intent of this study to provide a thorough validation of the flow conditions within the protection tube. A thorough validation would be very hard to achieve because of the non-canonical geometry of the components within the protection tube.

In the following calculation, the friction factor obtained from the Blasius correlation is compared with the friction factor reported by Fluent. As seen in Figure 3-8, the shape of the cross-sectional area of the protection tube changes continuously due to changes in thickness of the cables attached to the SPND detectors. Therefore the friction factor could not be calculated for the entire protection tube, but only for areas where the Blasius correlation (3.6.10) could be applied. In order to be able to calculate the friction

factor using the Blasius correlation the flow must be fully developed and the cross-sectional area must be constant.

The friction factor at two sections of the protection tube was calculated. The sections are highlighted in red in Figure 3-8. These two sections were selected since they have constant cross-sectional areas which are shown in Figure 3-9. Section A extends from point (a) at 80'' to (b) at 109.8'', and section B extends from point (c) at 160'' to (d) at 184''.

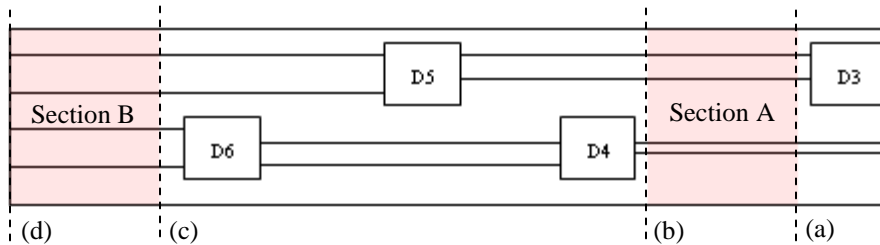


Figure 3-8 Protection Tube Geometry. The two sections to be studied are highlighted.

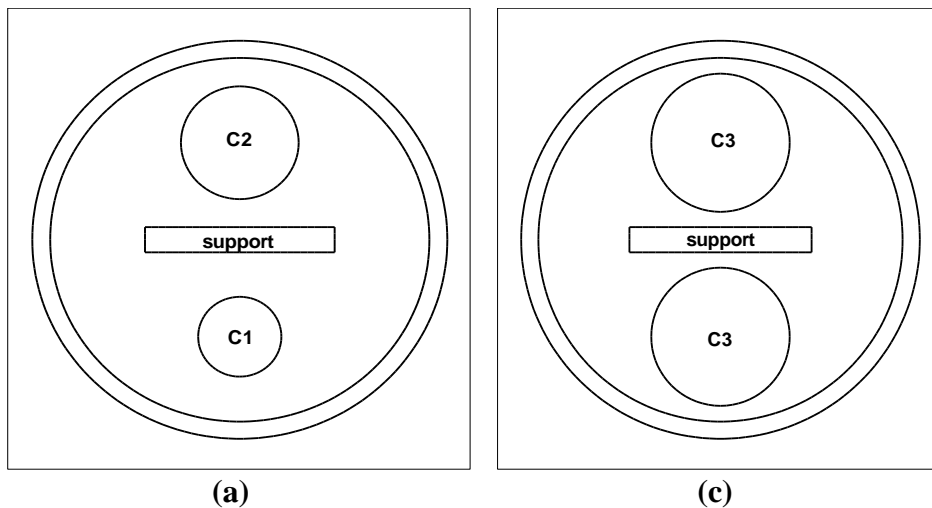
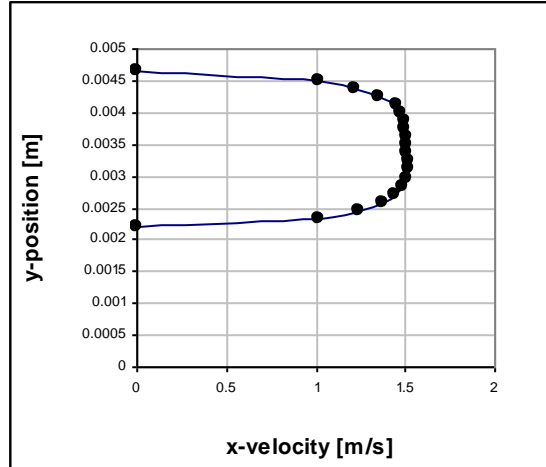
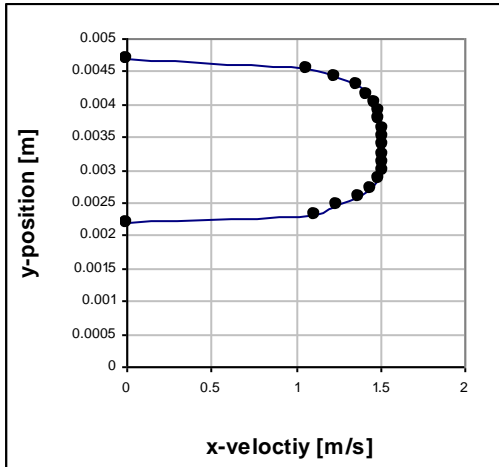


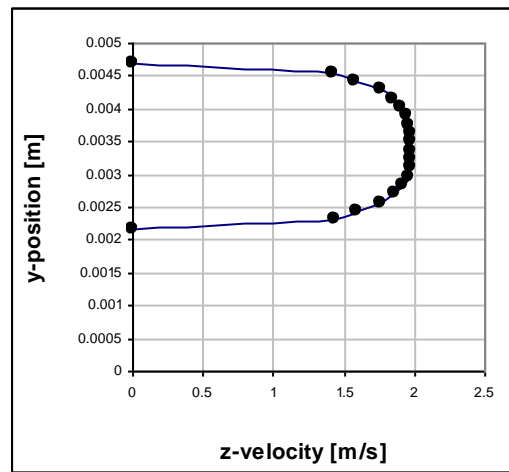
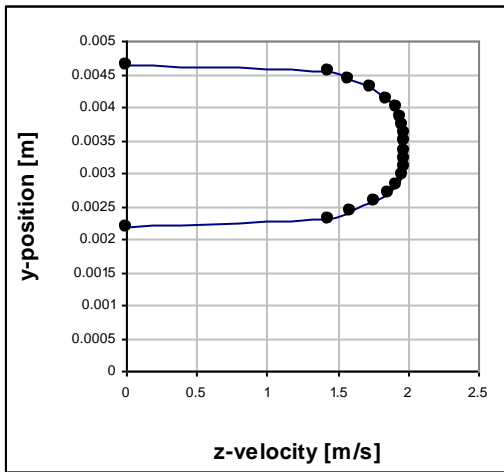
Figure 3-9 Cross-sections of the PT at (a) 80'' and (c) 160''

It was also necessary to make sure that the flow is fully developed in both of the sections. Figure 3-10 shows a comparison of the velocity profiles at the entrance (80'') and exit (109.8'') of section A.



(a) (b)
Figure 3-10 Velocity Profiles at (a) 80” and (b) 109.8”

As seen from Figure 3-10 the velocity profiles are the same at both locations, and the flow is fully developed in section A. The same study was done for section B. From the profiles shown in Figure 3-11 it is seen that the flow is also fully developed in this region.



(c) (d)
Figure 3-11 Velocity Profiles at (c) 160” and (d) 184”

The friction factor for section A was calculated first. An equation for the friction factor (f) was defined in section 3.6.4. The values for the pressure gradient (ΔP) and

average velocity (V) were obtained from Fluent and are shown in Table 3-8. Since the cross-sectional area of the protection tube is non-circular, the equivalent hydraulic diameter (D_h) was used in equation 3.6.8. D_h is defined as:

$$D_h = \frac{4A}{P_w} \quad (3.6.9)$$

where A is the cross-sectional area, and P_w is the wetted perimeter, which is the measure of the wall in contact with the flowing fluid at the cross-section shown in Figure 3-9.

Using equation 3.6.8 and the values shown in Table 3-8, the calculated friction factor was found to be 0.0221.

Table 3-8 Friction Factor Calculation for Section A

Average Velocity	1.19 m/s
Dh	0.00392 m
$\Delta P/L$	2713 Pa/m
f_{fluent}	0.0221

The friction factor may also be calculated using the Blasius correlation which is shown below:

$$f = \frac{0.3164}{\text{Re}^{0.25}} \quad (3.6.10)$$

The Reynolds number in 3.6.10 is based on the hydraulic diameter. The Blasius correlation is valid only for turbulent flows with $\text{Re} < 50,000$ [7]. For section A the Reynolds number was found to be 39625, and the friction factor was equal to 0.0224. The difference between the Fluent (f_{fluent}) and theoretical friction factor is 1.3%.

The same procedure was followed in order to calculate the friction factor for section B. The values used to compute the friction factor, and the results of the calculation are shown in Table 3-9.

Table 3-9 Friction Factor Calculation for Section B

Average Velocity	1.42 m/s
D_h	0.0028735 m
Re based on Hydraulic Diameter (D_h)	34661
$\Delta P/L$	4800 Pa/m
f_{fluent}	0.0202
f_{blasius}	0.0231

The difference between the Fluent and theoretical (Blasius) friction factor is 12.5%. In both of the sections, the difference between the theoretical and the Fluent friction factor is within a reasonable percentage. These results give us a better understanding that the mesh resolution and k- ϵ model are appropriate to model the flow within the protection tube.

3.6.6 Calculation of Heat Transfer Coefficients for Guide Tube (Annular Duct)

As mentioned in section 3.6.4 the inner wall of the guide tube and the outer wall of the protection tube form an annulus (Figure 3-12) with $r_o = 0.225''$ and $r_i = 0.197''$.

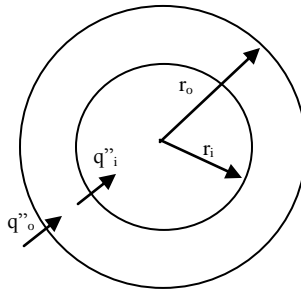


Figure 3-12 Annulus Dimensions

The goal of this section is to calculate the heat transfer coefficient of the inner and outer wall of the annulus and compare the calculated values to the ones reported by Fluent. The heat transfer coefficient (h) for the case of a fluid flowing in a circular-tube annulus does not depend only on the flow characteristics, but also on the heat flux ratio of

the outer and inner walls. For an annulus, the heat transfer coefficient is not the same for the inner and outer walls; therefore they have to be computed separately. The heat transfer coefficients for the inner and outer surfaces are defined as:

$$h_i = \frac{Nu_i \cdot k}{D_h} \quad (3.6.11) \quad [8]$$

$$h_o = \frac{Nu_o \cdot k}{D_h} \quad (3.6.12) \quad [8]$$

where $D_h = D_o - D_i$ for an annulus.

The Nusselt numbers on the inner and outer tubes can be evaluated from the following equations:

$$Nu_i = \frac{Nu_{ii}}{1 - (q_o''/q_i'')\theta_i^*} \quad (3.6.13) \quad [8]$$

$$Nu_o = \frac{Nu_{oo}}{1 - (q_i''/q_o'')\theta_o^*} \quad (3.6.14) \quad [8]$$

Nu_{ii} is the Nusselt number for the case in which the outer tube is insulated. Nu_{oo} is the Nusselt number for the case in which the inner tube is insulated. The variables θ_o^* and θ_i^* are influence coefficients [8].

It is important to mention that equations 3.6.13 and 3.6.14 are valid only for fully developed flow and for a constant heat flux condition. Since the heat flux varies axially along the height of the SPND system, only a small section of the annulus was considered in order to be able to assume a constant heat flux. The section considered extends from 146'' to 156''. Flow is turbulent ($Re = 35050$) and fully developed in this region. The average values for the heat flux in both walls (q_i'' and q_o'') were obtained from Fluent and are shown in Table 3-10.

Table 3-10 Average Heat Flux Values

q_o''	90367 W/m ²
q_i''	52953 W/m ²

Kays and Leung carried out extensive calculations over a wide range of Reynolds and Prandtl numbers for the case of one surface heated and the other insulated. Some of their results are presented in tabular form in the *Handbook of Heat Transfer* [2]. The tables are given for several values of r^* which is defined as:

$$r^* = \frac{r_i}{r_o} \quad (3.6.15) [2]$$

For the case of the SPND annulus, the value of r^* is equal to 0.87. There is no data provided for the value of $r^*=0.87$. The data used for the calculation, was interpolated using the values of $r^*=0.8$ and $r^*=1$. The interpolated values for the parameters in equations 3.6.13 and 3.6.14 are shown in Table 3-11.

Table 3-11 Interpolated Heat Flux Calculation Parameters

Nu_{ii}	86.5
θ_i^*	0.173
Nu_{oo}	85.2
θ_o^*	0.147

Plugging these values into 3.6.13 and 3.6.14 and solving for the heat transfer coefficient h_i and h_o , the following results were obtained: $h_o = 30830 \text{ W/m}^2$ and $h_i = 39231 \text{ W/m}^2$.

The heat transfer coefficient for the walls may also be obtained directly from Fluent. The values reported by Fluent and the percent difference from the calculated values are presented in Table 3-12.

Table 3-12 Comparison of Heat Transfer Coefficients

	Calculated [W/m ²]	Fluent [W/m ²]	% Difference
h _o	28640	29801	4 %
h _i	24383	24877	2 %

The difference between the values is within a reasonable percentage. This gives a better understanding that the results obtained for the temperature of the SPND system are correct. The same study was performed for other sections of the annulus, and the results are shown in Table 3-13.

Table 3-13 Heat Transfer Coefficients

Region	Calculated		Fluent		% Difference	
	h _o [W/m ²]	h _i [W/m ²]	h _o [W/m ²]	h _i [W/m ²]	h _o	h _i
128" to 138"	29325.8	22260.9	30552.1	22658.5	4.2 %	1.8 %
109" to 119"	29860.5	19625.6	31318.7	20108.7	4.8 %	2.4 %
70" to 79"	30816.88	8532.625	32547.02	8789.654	5.6 %	3.0 %

The error percentages between the Fluent and calculated values are all below 5.6 %.

3.7 Results

In the first part of this section velocity and temperature contours are shown at different heights of the SPND assembly. In the second part, the temperature is probed at several locations to obtain the maximum and average temperatures of the components in the assembly.

3.7.1 Velocity Contours

Velocity contours and vectors are shown in Figure 3-13. Slices in the yz and xy plane are shown. The slice in the xy plane is located near GT inlets 2-5 at a height of 34". The slice in the yz plane runs exactly through the center of the SPND assembly ($x=0$). Velocity vectors are shown in black, and color contours indicate the velocity in the z direction.

The flow within the protection tube is flowing upwards or in the positive z direction. It is interesting to see that the water in the guide tube channel flows in two directions.

Approximately 60% of the water entering the guide tube at 34" flows upward. The remaining 40% flows in a reverse direction from a height of 34" down to 4". As the fluid reaches a height of 4" it is sucked into the protection tube at PT inlets 1 and 2. The reverse flow is due to the fact that the pressure in the guide tube transition region (~34") is higher than the pressure at the bottom of the tube.

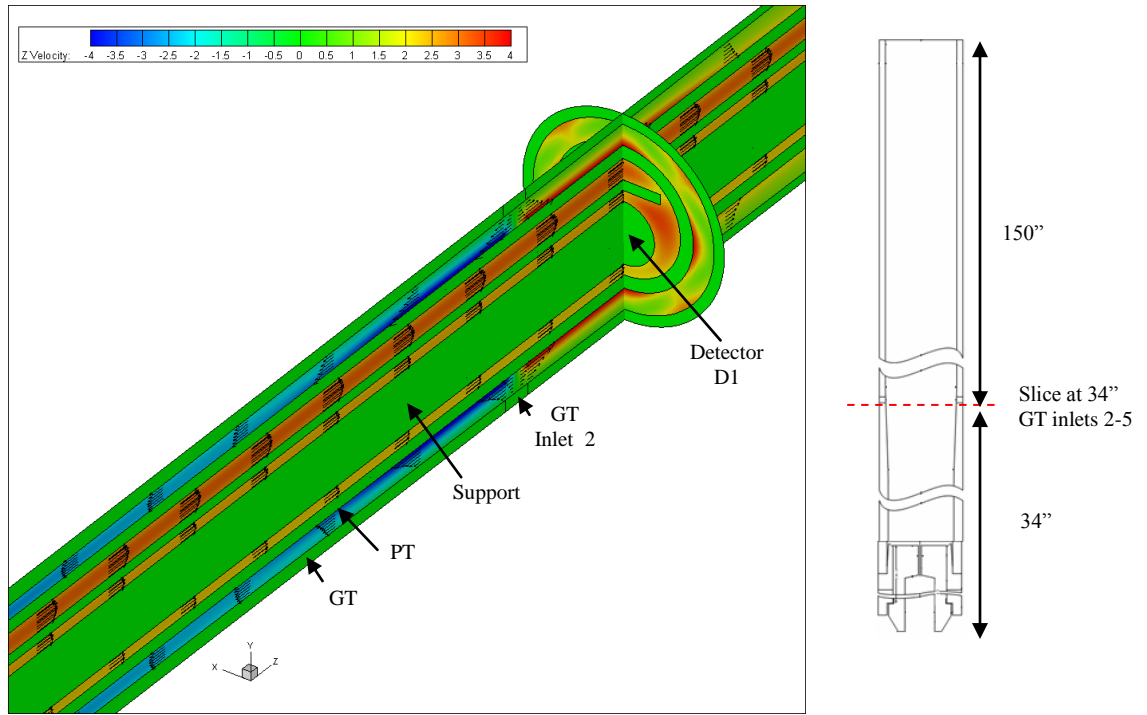


Figure 3-13 Velocity Field through Guide Tube and Protection Tube at 34"

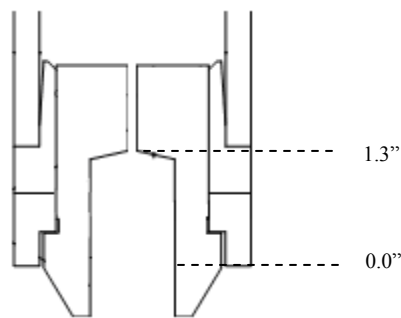


Figure 3-14 Guide Tube Bottom Insert

Figure 3-14 shows the bottom insert of the guide tube. A sudden contraction occurs at a height of 1.3", causing a pressure drop as seen in Figure 3-15. As mentioned earlier, reverse flow occurs as a result of this low pressure region at the bottom of the guide tube.

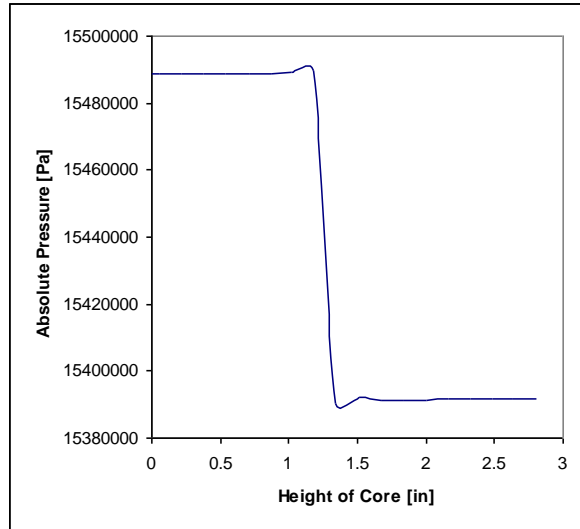


Figure 3-15 Pressure Variation at Inlet Region

Velocity profiles for the GT and PT channels were graphed and are shown in Figure 3-16. The color contours indicate the velocity in the z direction (along the height), and velocity vectors are shown in black. The figure shows slices in the xy and xz planes. The cross-section in the xy plane is located at a height of 123". As seen from the velocity profile, the velocity for the water within the guide tube channel ranges from 0 at the wall to 3.1 m/s at the center of the annulus. The velocity for water in the channel formed by the protection tube and the support ranges from 0 at the wall to 1.75 m/s at the center of this channel. At the height of the cross-section shown in Figure 3-16 (123 in.) the flow in the GT and PT channels is fully developed and turbulent. ($Re = 35000$ for GT channel, and $Re = 37900$ for PT).

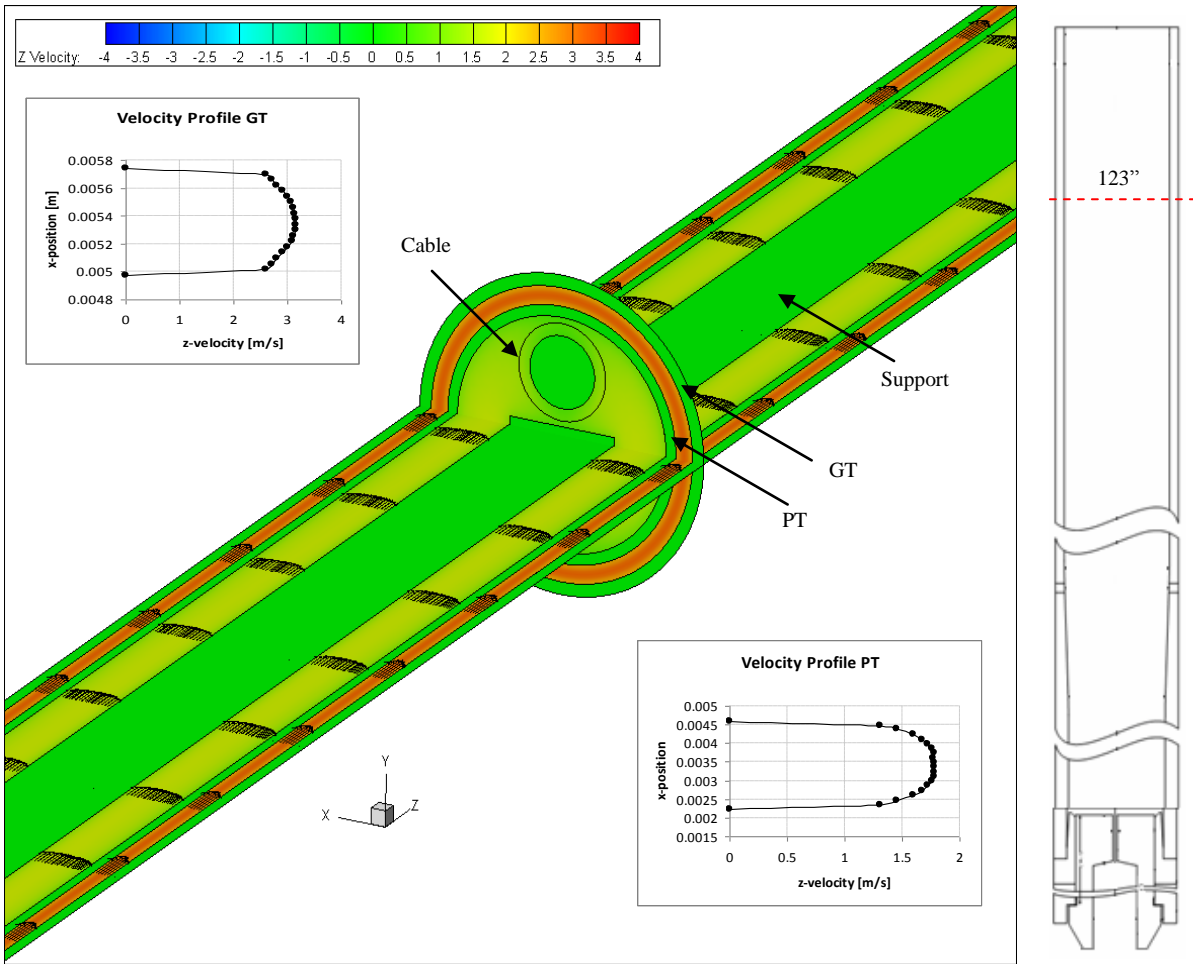


Figure 3-16 Velocity Profiles for Guide Tube and Protection Tube at 123”

3.7.2 Temperature Contours

The neutron flux in the fuel rod section acts on the SPND assembly from a height of 6” to 172”, producing internal heat in all of the components. The peak heat generation rates are found at a height of 89”.

Figure 3-17 shows the axial variation of temperature along the height of the guide tube. Four cross-sections are shown at different heights of the assembly. The average temperatures of the SPND detectors are also shown in the figures. The highest SPND temperature is seen in (a) and corresponds to detector in the highest position (D6). From

Figure 3-17 it can be concluded that the temperature of the SPND detectors increases as we move further along the height of the core.

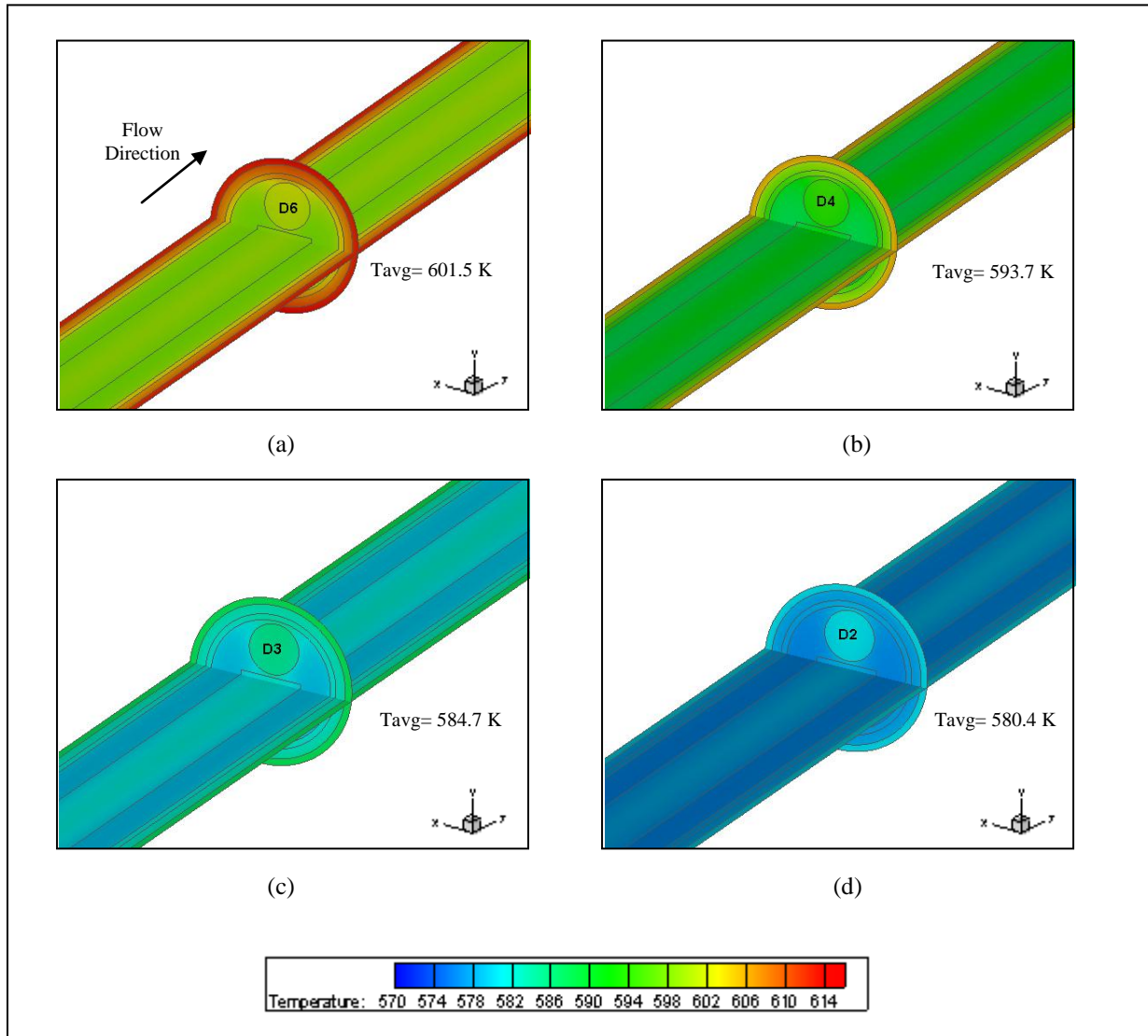


**Figure 3-17 Temperature Contours at Different Heights along the Core
(a) at 150", (b) at 114", (c) at 74" (d) at 54"**

Figure 3-18 presents a comparison of the GT outer surface temperature and the core free stream temperature along the height of the assembly. For a distance of 0" to 40" the temperature of the guide tube surface is higher than the temperature of the free stream. Therefore the heat transfer in this region is from the surface to the free stream.

For the remaining length of the guide tube, the temperature of the free stream is higher than that of the surface, indicating heat flow from the free stream into the guide tube. Figure 3-18 also shows that the temperature of the GT surface approaches the free stream temperature as the distance along the height of the core increases. From a height of 126" to 184" the temperature of the free stream is 618 K, which is right at the saturation temperature of water at 2250 psi (618.05 K). Again, from Figure 3-18 we see that the GT wall temperature approaches, but does not exceed, the maximum free stream temperature, and therefore the temperature of the GT will always remain under 618 K. As it was seen from the plots in Figure 3-17 the guide tube is the component of the SPND assembly that reaches the highest temperature. Consequently none of the other regions (either solid or fluid) in the assembly will exceed 618 K, the boiling temperature of water. With this in mind, it may be concluded that the temperature of the SPND system is limited by the temperature of the free stream, and that no boiling occurs in the SPND system.

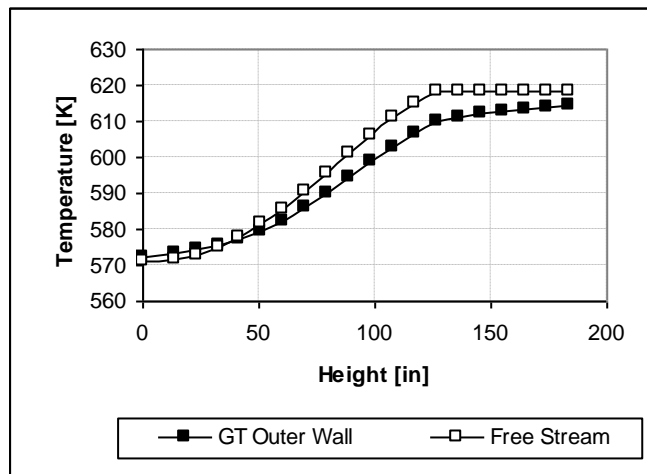


Figure 3-18 GT Outer Wall Temperature and Free Stream Temperature vs Height

The radial temperature distribution at different cross-sections along the height of the core is shown in Figure 3-19. The cross-sections correspond to the ones shown in Figure 3-17. When the radius r is between 0" and 0.09" the temperatures are measured at the support zone. The region for r between 0.09" and 0.177" corresponds to the water in PT. From 0.177" to 0.197" is the PT wall. The region for r between 0.177" and 0.225" corresponds to the guide tube channel. Finally, from 0.225" to 0.245" the temperature was measured at the GT wall. From Figure 3-19 it is seen that the temperature within the support and PT water region remains fairly constant when measured along the radius of the cross-sections, but the temperature tends to increase in the PT wall, GT water, and GT wall regions.

Also it is seen that due to the internal heat generation, temperature for the components increases along the height of the core.

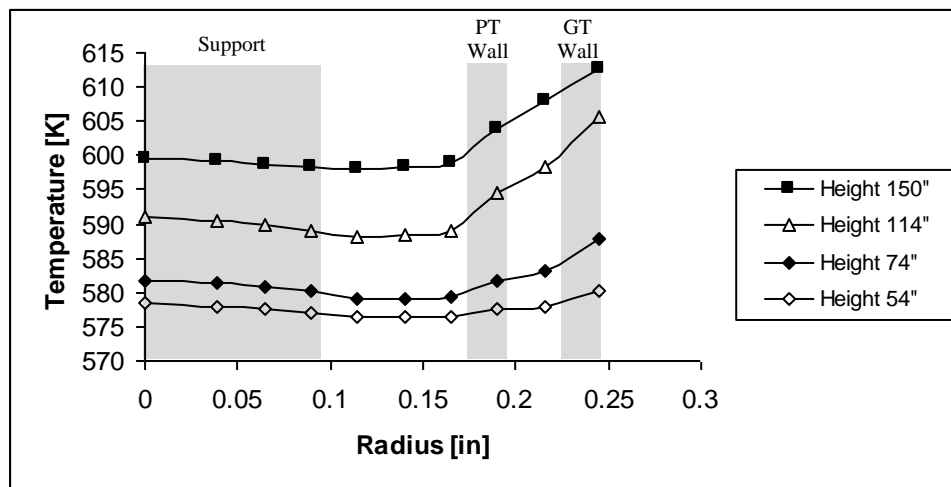


Figure 3-19 Radial Temperature Distribution at Different Heights

3.7.3 SPND Temperatures

It was of special interest to determine the maximum temperatures of the SPND detectors because the detectors generate a current that is proportional to the neutron flux, but after a limiting temperature this relationship will no longer be valid. The information provided by the detectors is key for proper reactor operation and control. The maximum permissible temperature for a detector is 622 K. Tables 3-14 and 3-15 show the average and maximum temperatures in each of the detectors.

Table 3-14 Average Temperature SPND Detectors

D1	D2	D3	D4	D5	D6
576.12 K	580.37 K	584.67 K	593.74 K	598.86 K	601.48 K

Table 3-15 Maximum Temperatures SPND Detectors

D1	D2	D3	D4	D5	D6
576.51 K	582.11 K	587.03 K	596.71 K	601.22 K	603.38 K

The maximum temperature for the SPND detectors is found at SPND D6 and is equal to 603.38 K.

3.7.4 Location of Maximum SPND Temperatures

Figure 3-20a shows temperature contours for the hottest SPND detector (D6). The region where the highest temperature is attained is where the detector is close to the protection tube (left side of detector). Figure 3-20b shows temperature contours for detector D5. The location of the maximum temperature is also where the detector is closest to the interior PT wall.

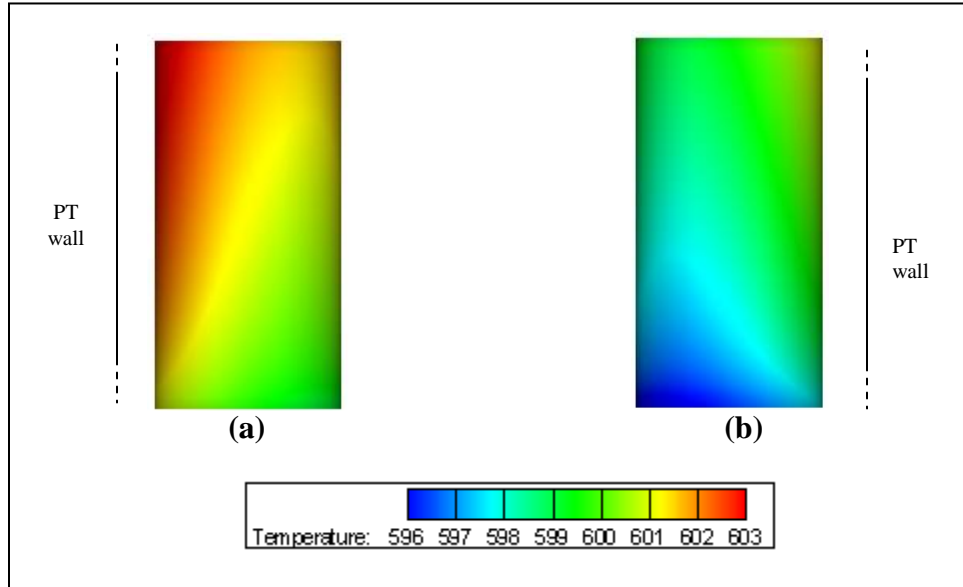


Figure 3-20 Temperature Contours (a) D6 (b) D5

3.7.5 Fluid Temperatures

The maximum temperature of the fluid in the guide tube and protection tube channels was determined in order to ascertain that no boiling occurs. Figure 3-21 shows temperature contours at a section of the assembly near the GT exit (184"). The maximum fluid temperature for the GT is located at this height.

The values for temperatures of the guide tube, protection tube, and the fluid zones are summarized in Table 3-16. The maximum temperature attained by the water in the GT channel is 613.7 K. For the water inside the protection tube the maximum temperature reached is 610.1 K. At a pressure of 2250 psi water boils at 618 K, therefore no boiling occurs within the assembly.

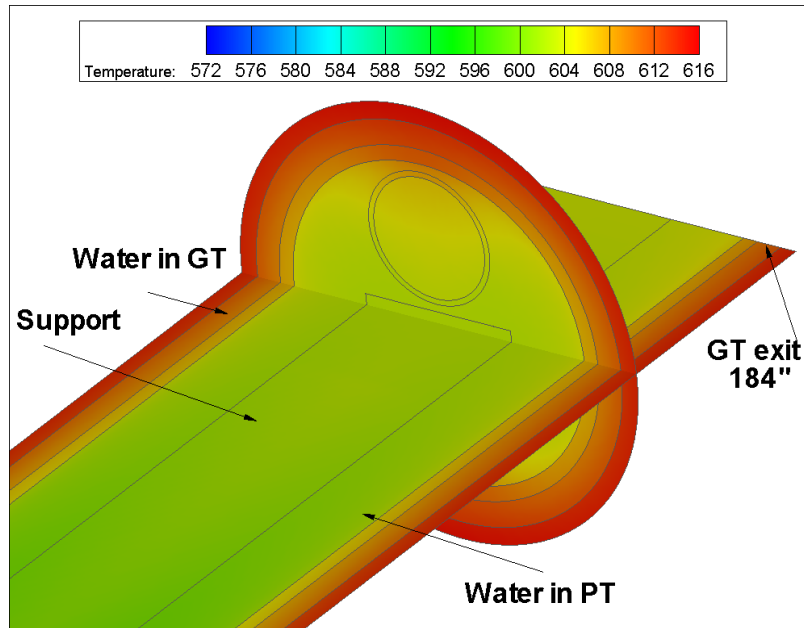


Figure 3-21 Temperature Contours at 184”

Table 3-16 Maximum and Average Temperatures for Components of Assembly

Component	Max. Temperature [K]	Avg. Temperature [K]
Guide Tube	615.6	591.70
Protection Tube	612.0	588.68
Water in GT channel	613.7	591.23
Water in PT channel	610.1	587.65

3.8 Summary and Conclusion

Using the data provided by Areva, a steady state solution of the temperature distribution of the SPND assembly was obtained. Several tests were performed in order to verify certain aspects of the calculation procedure. The maximum temperature in the SPND detectors is 603.4 K, at detector D6. This value is well below the maximum allowable value of 622 K, thus the relationship between the neutron flux and SPND temperature is valid during steady, normal operation conditions. The maximum temperature of the fluid within the assembly was determined to be 613.7 K. Water at 2250 psi boils at 618 K, therefore no boiling occurs.

Chapter 4 Overpower Transient Case

In Chapter 3, a steady-state solution for the flow and the heat transfer of the SPND assembly under normal reactor operation was presented. In Chapter 4, the response of the SPND assembly to the overpower transient scenario is investigated. The chapter starts with a description of the overpower transient scenario and its boundary conditions. After that, the verification studies and results obtained for this transient case are presented.

4.1 Description of Overpower Transient

The transient case presented in this chapter is referred to as overpower transient. The overpower transient results from either a failure in the Rod Cluster Control Assembly (RCCA) position control system, or an operator error that results in an uncontrolled withdrawal of a group of RCCA banks or sub-banks [5]. This transient scenario causes an increase in the core's power. In the specific case modeled in this chapter, the data provided by Areva indicated an increase of 17% in the reactor's power over a period of 30 seconds.

As described in the introduction, RCCAs are partially inserted in the core and are used to help control the average coolant temperature and to shut down the reactor. The RCCAs may be removed from the reactor core by means of control drive mechanisms located on the top part of the reactor pressure vessel. Removing the RCCAs from the reactor core sets off a reactivity imbalance such that the neutron population, and hence the power level, increases. The removal of this rods is the main factor causing the overpower transient.

As a result of the 17% increase in the core's power, the internal heat generation rates of the SPND components will also increase by 17 %. The increase in the power of the reactor occurs over a 30 second period at the rate shown in Figure 4-1.

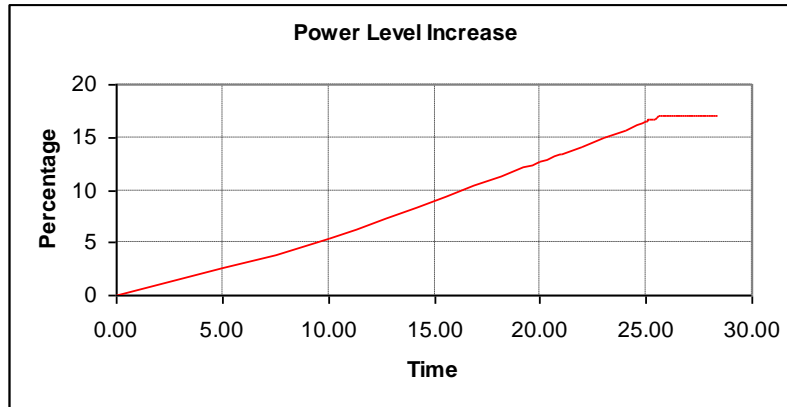


Figure 4-1 Increase in Power with Respect to Time

The initial power of the reactor core (at time=0 sec) is the same as the one for the SPND system under normal reactor operation. The power level then increases at an almost linear rate until it has increased by 17 % at a time of 25.6 seconds. The power then remains at a constant level from 25.6 to 30 seconds. In section 2.1.2 it was shown that the heat generation rates have a cosine-shaped distribution along the height of the SPND system. The shape of this distribution will continue to be the same over the 30 second period, but the heat generation values will increase as illustrated in Figure 4-2. A curve fit was performed for the power level curve (Figure 4-1), and the resulting equation was used to create a UDF that was utilized in Fluent to account for the increase in the volumetric heat generation terms. In the overpower transient, the flow rate through the SPND assembly is expected to remain constant throughout the 30 second period. Therefore the flow rates through the GT and PT should remain close to the values

obtained from the steady state calculation (GT flow rate = 0.04714 kg/s and PT flow rate = 0.04302 kg/s).

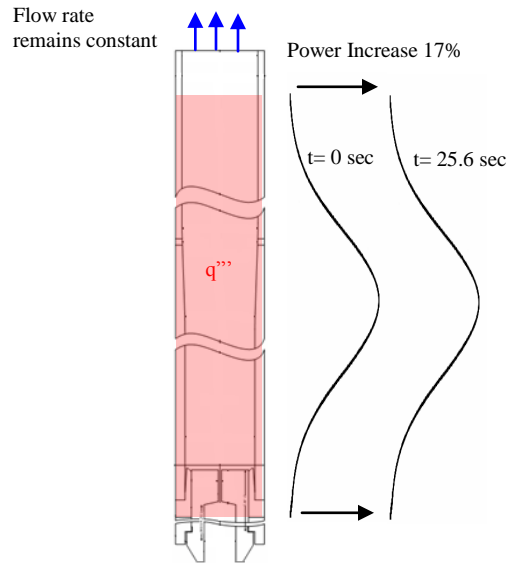


Figure 4-2 Overpower Transient Schematic

In the overpower transient, the conditions surrounding the guide tube vary with both time and space. Data for the pressures and temperatures along the height of the reactor core was provided by Areva and is shown in Appendix E. Figure 4-3a shows the static pressures at the three heights where the inlets and outlets of the SPND system are located. GT inlet 1 is located at 0", GT inlets 2-5 are located at 34", GT exit 1 and PT exits 1-3 are located at 184" (Figure 3-1). From Figure 4-3a it is seen that the pressure increases in an almost linear fashion until the time reaches 25.6 seconds. After that period of time, the pressure at these locations remains constant. It is important to note that the rate of change of the pressure is almost the same for the three heights, therefore it is not expected that the flow rate will change.

Figure 4-3b shows profiles of the free stream temperature of the fluid surrounding the guide tube. From the figure it is seen that the free stream temperature increases as time progresses, but the shape of the profile remains essentially the same.

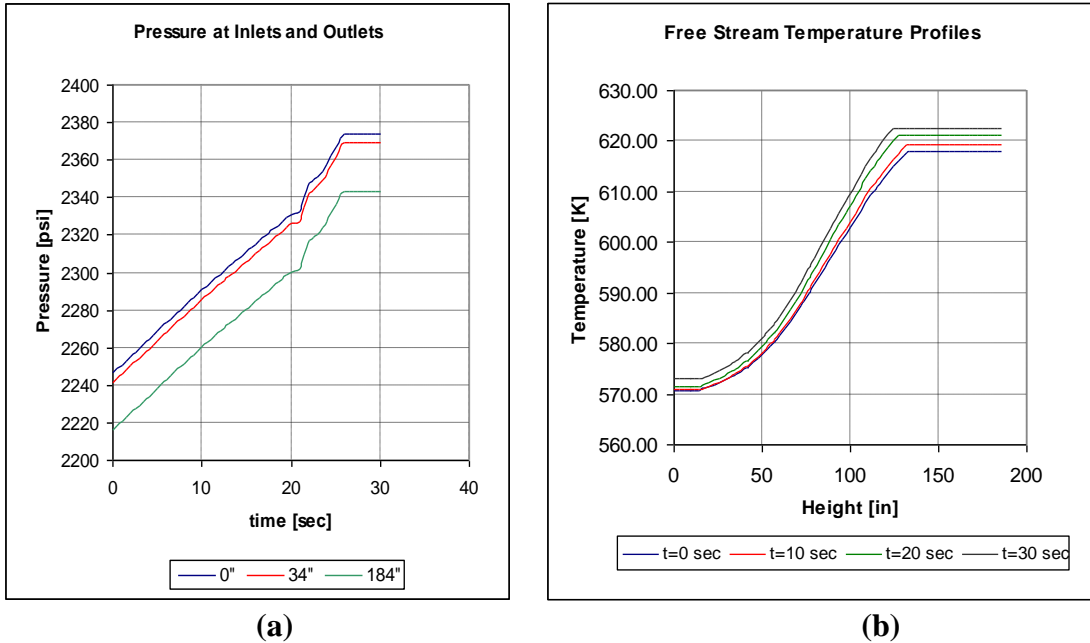


Figure 4-3 (a) SPND Pressure Boundary Conditions ; (b) Free Stream Temperature Profiles

In order to represent the previously described boundary conditions in Fluent, two UDFs were generated. Curve fits were done on the data provided by Areva (Tables E1 and E2) in order to obtain equations that would properly represent the behavior of pressure and temperature at the inlets and outlets of the SPND assembly. These equations were implemented in the UDF code. A detailed description of the UDFs that were used is given in Appendix B.

Since in the overpower transient the flow rate does not change and the heat generation rates increase over time, it is expected that the temperature of the detectors will increase during the 30 second period.

Finally, it is important to mention that the operating pressure of the reactor core changes with time as shown in Figure 4-4. It is important to know the operating pressure of the reactor in order to determine the temperature (T_{sat}) at which water boils for that operating pressure.

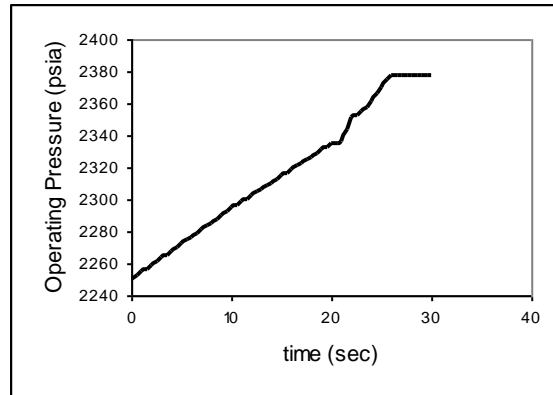


Figure 4-4 Core's Operating Pressure with Respect to Time

The overpower transient scenario that was previously described is one of the many safety related transient events analyzed by Areva. Additional information on the overpower transient and other events can be found in the NRC website [5].

4.2 Objective

The main objective of the second part of the project is to verify that the temperature of the SPND detectors does not exceed a maximum value of 622 K during a 30 second period. During this period of time, the power of the SPND assembly increases by 17 %, causing an increase in the temperature of the SPND components. The SPND detectors produce a current proportional to the neutron flux. Based on that signal, proper reactor operation is verified. Therefore, it is of utmost importance to verify that the detectors do

not exceed the maximum allowed temperature in order to ensure that the information they provide is reliable.

4.3 Solver Settings

The k- ϵ model was selected in the solver for the turbulence model. The mass, momentum, and energy conservation equations along with the transport equations for turbulent kinetic energy (k) and dissipation rate (ϵ), were solved for turbulent flow. A second order implicit scheme was used for the time discretization, and a time step of 0.2 seconds was used for the computation. For the pressure velocity coupling the SIMPLE algorithm was enabled, and the convection terms were differentiated by using a second order upwind scheme. The steady state calculation for the system under normal operation was used as the initial state for the overpower transient simulation.

In the previous section it was shown how the pressure at the inlets (GT inlets 1-5) and outlets (GT exit and PT exits 1-3) of the SPND system varies with time. Also it was shown that in the overpower transient the heat generation rates increase by 17% in a 30 second period. In order to be able to define the time varying pressure boundary conditions and the increasing heat generation rates in Fluent, curve fits were done on the data provided by Areva shown in Figures 4-1 and 4-3. The equations obtained from the curve fits were used to create UDFs that were used in Fluent to account for the time varying conditions. A detailed description of how the UDFs were programmed is given in Appendix B.

4.4 Establishing Validity of Results

The next sections will present a series of checks that were performed in order to ascertain the validity of the obtained results. First the correct implementation of the boundary condition UDFs was checked. Then a sensitivity analysis was conducted in order to make sure that the obtained results are independent of the time step. Lastly, a steady state analysis with the conditions corresponding to 30 seconds was performed, and the results were compared to the transient solution.

4.4.1 Revision of Boundary Conditions

In order to verify that the applied UDFs were working as expected, the actual boundary conditions were compared to the boundary conditions reported by Fluent. Figure 4-5 shows a comparison for the pressure at the heights of 184'' (Figure 4-5a) and 0'' (Figure 4-5b). From the figures it is seen that the values for the pressure at the boundaries of the domain that are reported by Fluent are in close proximity to the actual values given by Areva. Therefore, the equations used to write the UDFs are working as expected.

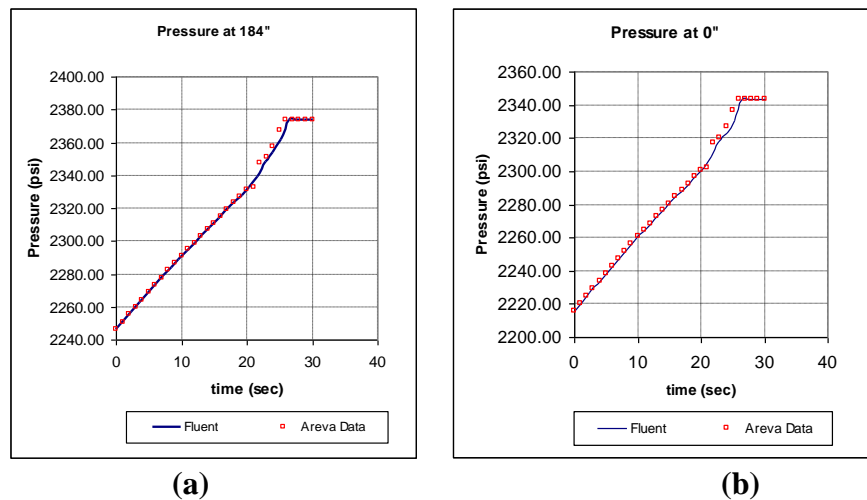


Figure 4-5 Comparison of Pressures Reported by Fluent and Pressures Specified by Areva

4.4.2 Sensitivity of Results based on Time Step (Δt)

Initially, in Fluent, the time step size was set to 0.2 seconds. The flow and energy simulations were conducted with this time step for the entire thirty second period. The flow rate through the guide tube, and the maximum temperatures attained by the SPNDs were monitored and recorded. Next, a sensitivity test was performed in order to ascertain that the results obtained did not vary significantly as the time step was reduced. The time step was then reduced to values of 0.1 and 0.05. The simulations for these two new cases were conducted for a 15 second period. The flow rates and temperatures obtained using the different time steps are compared in Tables 4-1, 4-2, and 4-3. As seen from the tables there is only a minimal variation in the values of the temperature and flow rate when using the different time steps. This confirmed that the results obtained using the 0.2 time step are independent of the time step.

Table 4-1 SPND Maximum Temperature after t=7 sec.

Δt (sec)	D6 [K]	D5 [K]	D4 [K]	D3 [K]	D2 [K]	D1 [K]
0.2	603.85	601.75	597.26	587.54	582.55	576.85
0.1	603.84	601.75	597.26	587.54	582.56	576.84
0.05	603.84	601.74	597.25	587.53	582.56	576.84

Table 4-2 SPND Maximum Temperature after t=15 sec

Δt (sec)	D6 [K]	D5 [K]	D4 [K]	D3 [K]	D2 [K]	D1 [K]
0.2	604.68	602.64	598.16	588.34	583.23	577.37
0.1	604.68	602.64	598.16	588.34	583.22	577.37
0.05	604.67	602.63	598.15	588.33	583.23	577.36

Table 4-3 Guide Tube Flow Rates after t= 15 sec

Δt [sec]	GT Flow Rate [kg/s]
0.2	0.04719735
0.1	0.04719402
0.05	0.04719601

4.4.3 Steady State Calculation

As mentioned in section 4.1, the boundary conditions remain constant in the time period from 25.6 seconds to 30 seconds. Using the boundary conditions of the system at 30 seconds, a steady simulation was conducted in order to compare to the results obtained by the unsteady simulation. Table 4-4 shows a comparison of the temperature for the SPND detectors for both cases. The fact that the results are similar serves as a sanity check for the results obtained during the transient simulation.

Table 4-4 Comparison for Detector Temperature between Transient and Steady Fluent simulations

	D6	D5	D4	D3	D2	D1
Transient	608.5 K	606.6 K	602.1 K	592.1 K	586.6 K	580.4 K
Steady	609.1 K	607.1 K	602.7 K	592.4 K	586.9 K	580.7 K
Difference %	0.09	0.08	0.1	0.05	0.05	0.05

4.5 Results

The Results section is composed of three main parts. In the first and second sections temperature contours and profiles will be shown at several cross-sections along the height of the SPND assembly in order to determine if the temperature of any of the detectors exceeded 622 K. In the third section, the maximum temperature for the fluid will be studied in order to ascertain if boiling has occurred during the 30 second time period.

4.5.1 Temperature Profiles

As a result of the increase in power by 17%, the temperature of the SPND detectors increased during the 30 second time period.

Figure 4-6 shows the increase in temperature of each detector with respect to time. The rate of change of temperature is almost the same for the six detectors. During the first 10 second period, the temperature varies at a rate of about 0.1 K/sec. From there on, the temperature of the detectors increases at almost a linear rate of 0.2 K/sec. From the steady state calculation conducted in Chapter 3, it was seen that the detector located at the highest point in the assembly, D6, is the one that reached the highest temperature during normal operation (603.4 K). During the 30 second period of time, detector D6 continues to have the highest temperature of the six detectors. The maximum temperature reached by D6 is 608.5 K at a time of 30 seconds. This value is still well below the maximum permitted value of 622 K, therefore there should be no problem in the SPND operation during the overpower transient.

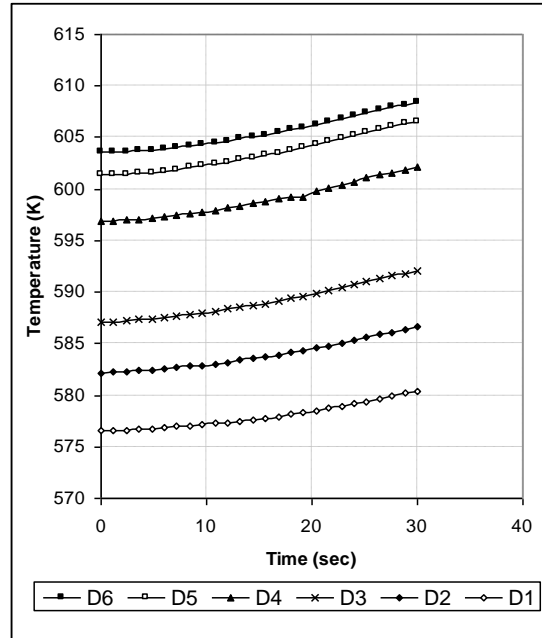


Figure 4-6 Maximum Temperature History for SPND Detectors

Figure 4-7a shows how the temperature profiles for the GT wall vary with time. The shape of the profile remains basically the same over time with a total increase in temperature of about 5 K at every point along the GT wall.

Figure 4-7b presents a comparison of the GT outer surface temperature and the free stream temperature along the height of the core at a time of 30 seconds. For a distance of 0” to 77” the temperature of the guide tube surface is higher than the temperature of the free stream. Therefore the heat transfer in this region is from the surface to the free stream. For the remaining length of the guide tube, the temperature of the free stream is higher than that of the surface, indicating heat flow from the free stream into the guide tube. Figure 4-7b also shows that the temperature of the GT surface approaches the free stream temperature as the distance along the height of the core increases.

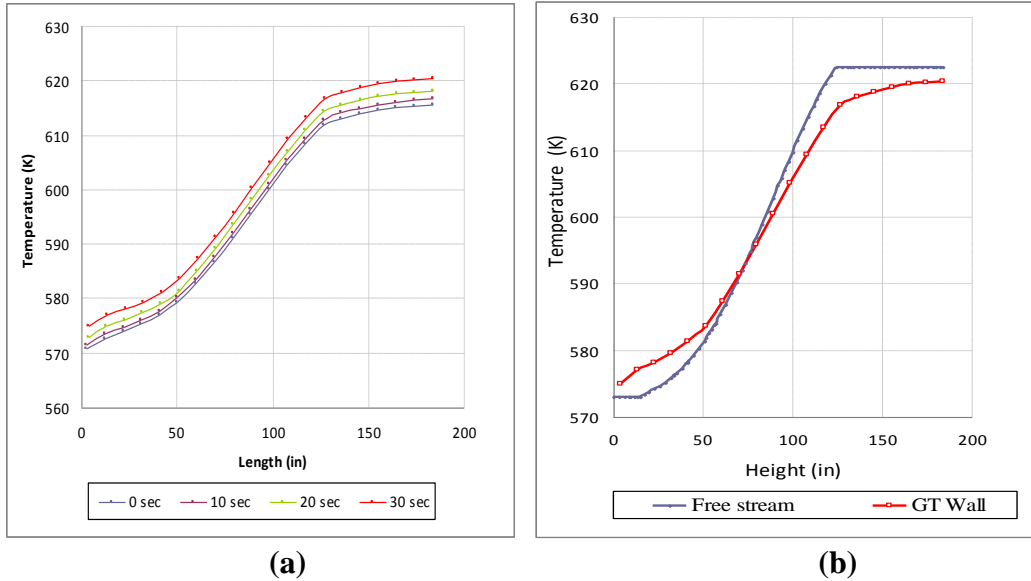


Figure 4-7 (a) Guide Tube Wall Temperature Profiles with Respect to Time; (b) Temperature Profiles at the GT Outer Wall and Free Stream

4.5.2 Temperature Contours

As seen from Figure 4-6, the SPND detector that reaches the highest temperature is detector D6. Figure 4-8 shows temperature contours obtained from Fluent at a cross-section intersecting D6. From the contours it is seen that the temperature of the detector increases with time from a value of 603.4 K to a value of 608.5 K. All the contours were taken at a height of 151". The times at which the contours were taken are as follows: (a) zero seconds, (b) 10 seconds, (c) 20 seconds, (d) 30 seconds.

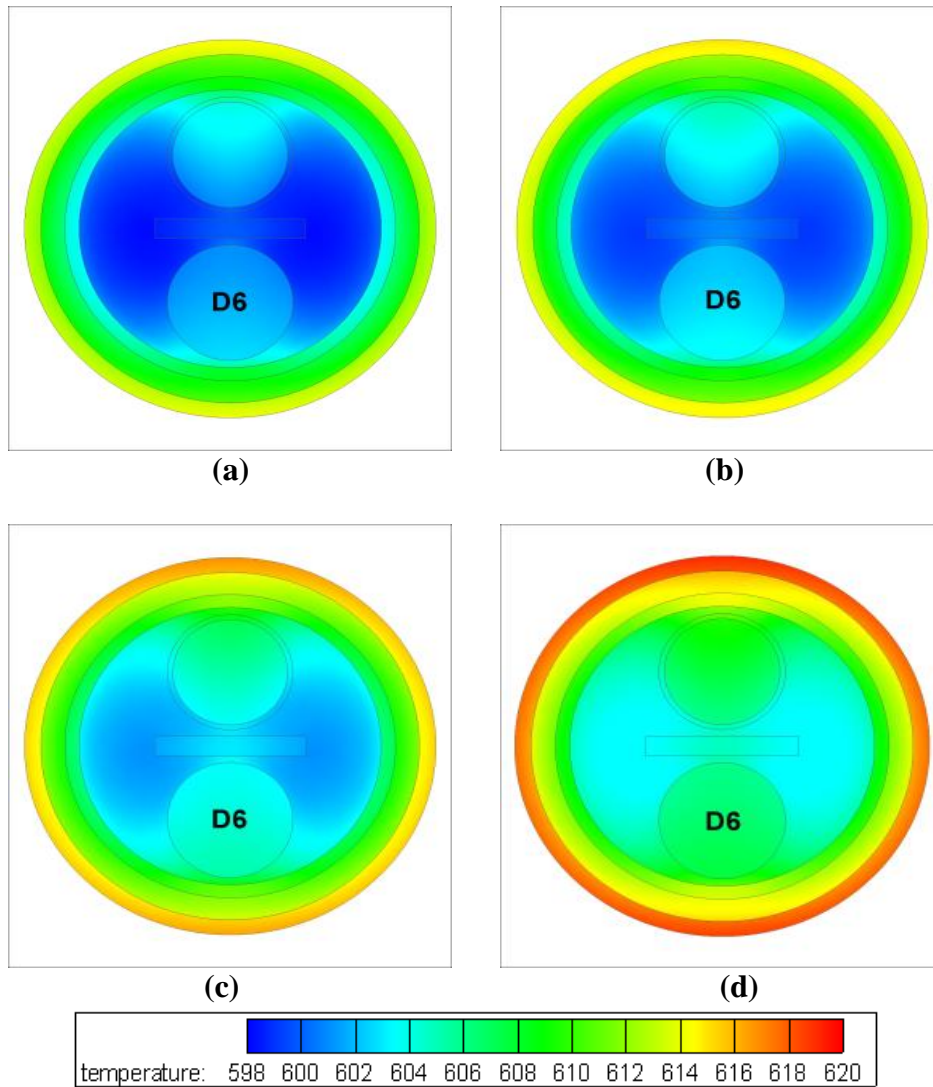


Figure 4-8 Temperature Contours at 151''
(a) 0sec ; (b) 10 sec; (c) 20 sec; (d) 30 sec

It is seen that the highest temperatures for D6 are reached where the detector is closest to the protection tube wall. In reality, the location of this maximum temperature will not be at that same point since the original position of the SPND detectors was modified as described in the geometry section in Chapter 2.

4.5.3 Final Maximum Temperatures

It is important to know the temperatures of each of the SPND components, especially the temperature of the fluid zones in order to ascertain that no boiling occurs inside the guide or protection tube. The maximum temperatures of the different zones at the end of the 30 second period are shown in Table 4-5.

The maximum temperature reached by the water within the SPND assembly is 618.55 K at 30 seconds. The operating pressure of the reactor at a time of 30 seconds is 2377 psia. The saturation temperature for water at this pressure is 622.5 K, therefore no boiling occurs in the SPND system during the overpower transient.

Table 4-5 Maximum Temperatures for SPND Components at 30 seconds

Zone	Maximum Temperature
GT	620.36 K
GT water	618.55 K
PT	616.79 K
PT water	614.78 K

4.5.4 SPND Detector Final Maximum Temperatures

This section presents a summary of the maximum temperatures reached by each of the SPND detectors in tabular form (Table 4-6). None of the temperatures of the detectors exceeds the maximum allowable temperature of 622 K. Therefore it is concluded that the SPND system will continue to operate in a reliable fashion during the entire 30 second period of the overpower transient.

Table 4-6 Maximum SPND temperatures after 30 seconds with $\Delta t=0.2$ sec

D6	D5	D4	D3	D2	D1
608.5 K	606.6 K	602.1 K	592.1 K	586.6 K	580.4 K

4.6 Conclusion

In this chapter, the overpower transient scenario was simulated. In this scenario, the power of the core increases by 17% in a 30 second period. The boundary conditions for this scenario were provided by Areva and implemented in Fluent using UDFs. The unsteady calculation was performed in Fluent using a time step of 0.2 seconds. Tests were conducted in order to prove that the results were independent of the time step. The results indicated that none of the detectors exceeded 622 K. In fact, the maximum detector temperature of 608.5 K is still well below the permitted value. Also, the temperature of the water in the SPND system remains below the saturation temperature of water, therefore no boiling occurs during the overpower scenario. Due to the lack of experimental or analytical data for the SPND system, no thorough validation of the results was possible, but the different checks for consistency discussed in this chapter give confidence in the validity of the obtained results.

Chapter 5 Partial Loss of Flow Transient

Chapter 5 presents the second transient scenario for the SPND system, which is referred to as the partial loss of flow transient. The chapter starts with a description of the partial loss of flow transient scenario and its boundary conditions. After that, the results obtained for this transient case are presented.

5.1 Description of Partial Loss of Flow Transient

The partial loss of flow transient simulates a reduction in the flow of coolant through the reactor core. Partial loss of forced reactor coolant flow may be caused by a mechanical or electrical failure in a pump motor or a fault in the power supply to the pump motor [6].

The pump failure causes a gradual reduction in the flow rate through the core and consequently through the SPND assembly. In the partial loss of flow transient, the flow rate through the SPND assembly reduces by 12.7% in relation to the flow rate during normal operating conditions. The flow rate percent reduction occurs over a 12 second period as shown in Figure 5-1.

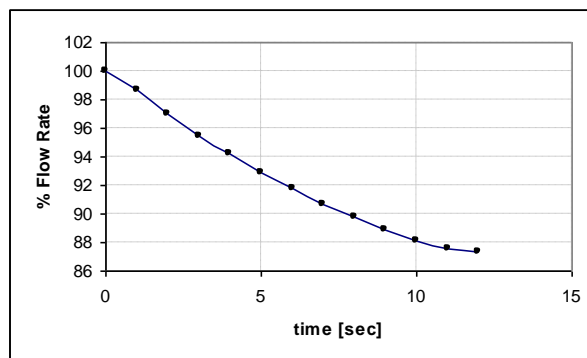


Figure 5-1 Reduction in Flow Rate through SPND Assembly

During the partial loss of flow transient, the power of the reactor core will remain constant during the first nine seconds after the loss of coolant flow begins. After that, the power reduces dramatically by 30 % in a period of three seconds due to a reactor scram (shut down). The change in power in the reactor core with respect to time is shown in Figure 5-2. The power reduction will cause the internal heat generation rates to also reduce by 30% in the period from 9 to 12 seconds. A curve fit was done on the curve shown in Figure 5-2 and the resulting equation was used to program a UDF in order to account for the internal heat generation reduction.

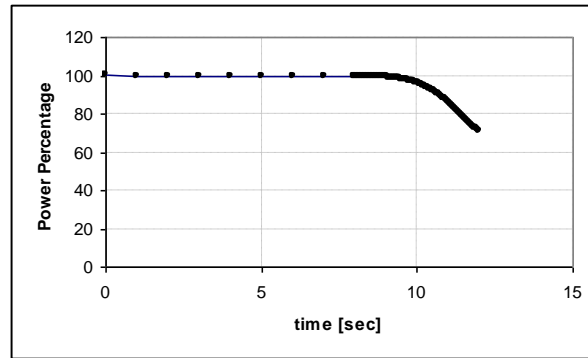


Figure 5-2 Core Power vs Time

The temperature of the SPND detectors is expected to increase as a result of the loss in coolant flow. The main goal of this section will be to determine the change in temperature in the detectors due to this reduction in flow rate.

Finally it is important to mention that the operating pressure of the reactor core changes with time as shown in Figure 5-3. It is important to know the operating pressure of the reactor in order to determine the temperature (T_{sat}) at which water boils for that operating pressure.

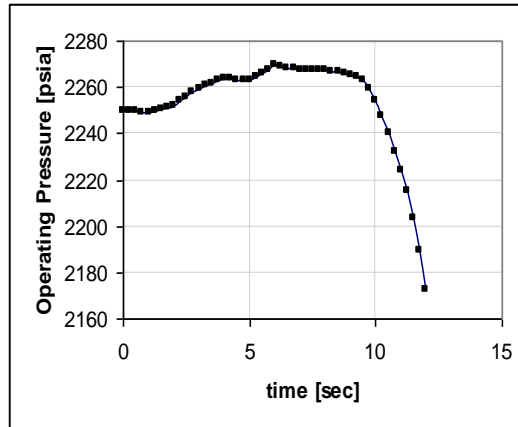


Figure 5-3 Operating Pressure with Respect to Time

The partial loss of flow transient scenario that was previously described is one of the many safety related transient events analyzed by Areva. Additional information on the partial loss of flow transient and other events can be found in the NRC website [6].

5.1.1 Inlet and Outlet Pressure and Temperature Conditions

This section continues with the description of the partial loss of flow scenario by explaining how the temperature and pressure vary with respect to time at the inlets and outlets of SPND assembly. The data presented in this section for the partial loss of flow transient was provided by Areva. The location of the inlets and outlets of the SPND is as follows: GT inlet 1 is located at 0", GT inlets 2-5 are located at 34", GT exit 1 and PT exits 1-3 are located at 184". (For a diagram containing the inlets and outlets refer to Figure 3-1). Figure 5-4 shows the pressure variation with respect to time for the three heights of interest, 0", 34", and 184".

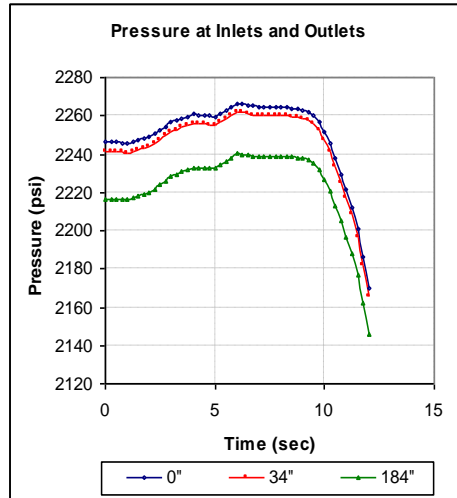


Figure 5-4 Pressure Boundary Conditions

The temperature at these three heights also varies with time as seen in Figure 5-5. The time varying pressure and temperature boundary conditions were incorporated into Fluent with the implementation of user defined functions.

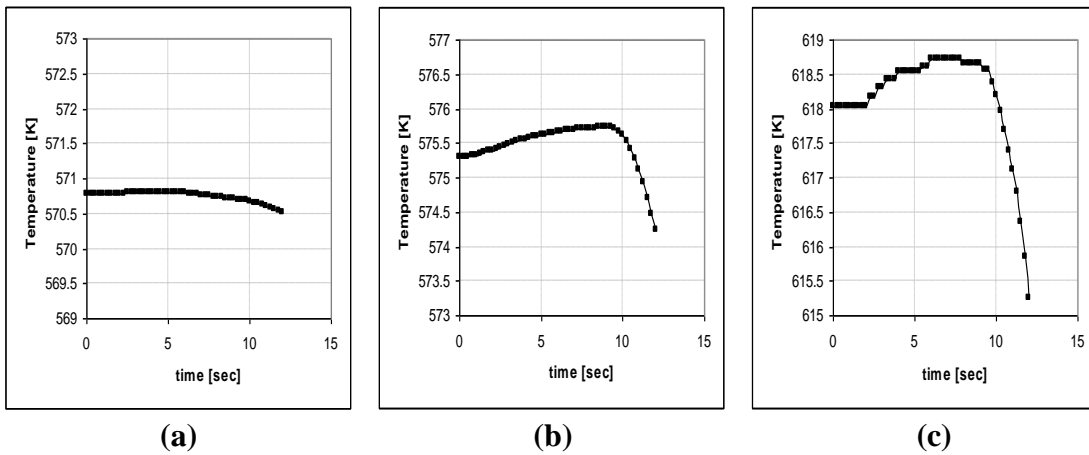


Figure 5-5 Temperature vs. Time at (a) 0", (b) 34", and (c) 184"

5.2 Objective

The main objective of the third transient scenario is to model what would occur if one of the coolant pumps failed, and verify that the temperature of the SPND detectors does not exceed a maximum value of 622 K during a 12 second period. During this period of time, the flow through the SPND assembly will decrease by 12.7 %, causing an increase in the temperature of the SPND components. As mentioned earlier, the SPND detectors produce a current proportional to the neutron flux. Based on that signal, proper reactor operation may be verified. Therefore, it is of utmost importance to verify that the detectors do not exceed the maximum allowable temperature in order to ensure that the information they provide is reliable.

5.3 Solver Settings

For the loss of flow transient, the k- ϵ model was selected in the solver for the turbulence model. The seven equations solved for turbulent flow were: continuity, momentum and energy conservation, turbulent kinetic energy (k), and dissipation rate (ϵ). The SIMPLE algorithm was enabled for the pressure velocity coupling and the convection terms were discretized by using a second order upwind scheme. For the discretization in time, a second order implicit scheme was used. The selected time step for the computation was 0.5 seconds. The steady state calculation for the system under normal operation was used as the initial state for the partial loss of flow transient simulation.

In section 5.1 it was shown how the pressure and temperature at the inlets (GT inlets 1-5) and outlets (GT exit and PT exits 1-3) of the SPND system vary with time. Also it was shown that in the partial loss of flow transient the heat generation rates

decrease by 30% in the period of 9 to 12 seconds. In order to be able to define the time varying pressure and temperature boundary conditions and the decreasing heat generation rates in Fluent, curve fits were done on the data provided by Areva shown in Figures 5-4 and 5-5. The equations obtained for the curve fits were used to create UDFs that were used in Fluent to account for the time varying conditions.

5.4 Sensitivity to Time Step

Initially, in Fluent, the time step size was set to 0.5 seconds. The flow and energy simulations were conducted with this time step for the entire twelve second period. The flow rate through the guide tube, and the maximum temperatures attained by the SPNDs were monitored and recorded. Next, a sensitivity test was performed in order to ascertain that the results obtained did not vary significantly as the time step was reduced. The time step was then reduced to values of 0.1 and 0.05. The simulations for these two new cases were conducted for a 6 second period. The flow rates and temperatures obtained using the different time steps are compared in Tables 5-1 and 5-2. As seen from the tables there is only a minimal variation in the values of the temperature and flow rate when using the different time steps. This confirmed that the results obtained using the 0.5 time step are independent of the time step.

Table 5-1 SPND Maximum Temperature after t=6 sec.

Δt (sec)	D6 [K]	D5 [K]	D4 [K]	D3 [K]	D2 [K]	D1 [K]
0.5	604.70	602.71	598.30	588.23	583.02	577.63
0.1	604.70	602.71	598.30	588.22	583.01	577.62
0.05	604.69	602.70	598.29	588.22	583.01	577.63

Table 5-2 Guide Tube Flow Rates after t= 6 sec

Δt [sec]	GT Flow Rate [kg/s]
0.5	0.04428922
0.1	0.04428702
0.05	0.04428598

5.5 Results

The next sections will present the flow and heat transfer results for the loss of flow transient.

5.5.1 Mass Flow Rate

According to the specifications provided by Areva for the partial loss of flow scenario, the flow rate through the guide and protection tube should reduce by 12.7% after a period of 12 seconds. In Fluent, there was no proper way to directly impose this flow rate reduction so another approach was followed. The pressure variation with respect to time at the inlets and outlets of the system was known from the data shown in Figure 5-4 in section 5.1.1. As described earlier, curve fits were done on the data shown in Figure 5-4 in order to obtain equations to implement them in the UDFs. Since the pressure conditions were used, rather than directly imposing the flow rate reduction, it was necessary to compare the flow rate reduction being reported by Fluent to the theoretical flow reduction provided by Areva. Figure 5-6 shows the flow rate through the guide tube as reported by Fluent. The graph also shows the theoretical value of the flow rate which was obtained by multiplying the flow rate reduction percentage (provided by Areva in Figure 5-1) by the initial flow rate. The value for the initial flow rate through the guide

tube was obtained from the results of the steady state simulation and is equal to 0.04714 kg/s.

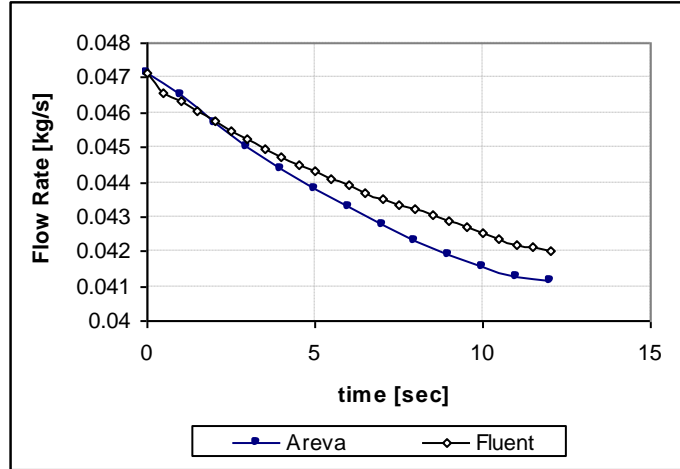


Figure 5-6 Comparison of Guide Tube Flow Rate

Although the flow rate reduction that was obtained during the Fluent simulation is not exactly the desired one, it is still within a reasonable range of error. The maximum difference between the theoretical (Areva) and Fluent flow rate is 2.4 % at ten seconds. The same comparison was done for the flow rate within the protection tube as seen in Figure 5-7. The maximum percent difference in this case is 2.94%.

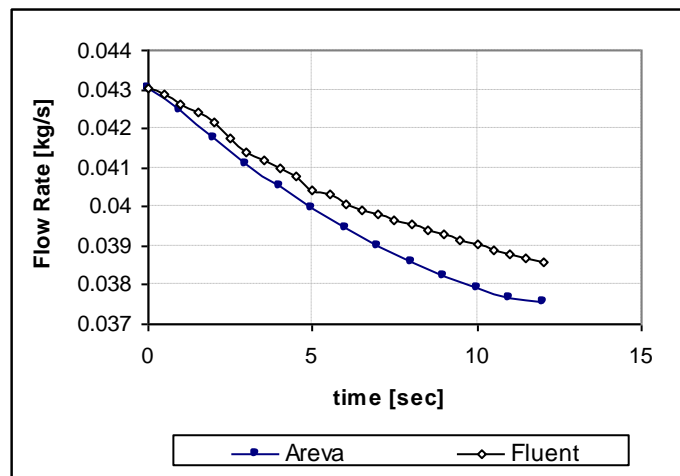


Figure 5-7 Comparison of Protection Tube Flow Rate

5.5.2 SPND Detector Temperature Profiles

The maximum temperature of each of the six SPND detectors was monitored during the 12 second period in order to determine if their temperature exceeded 622 K. This temperature marks the limit for proper operation of the SPND detectors.

As in the previous cases, the detector that has the highest temperature is D6. The maximum temperature for D6 is 619.6 K, which is below the allowable maximum. Towards the end of the calculation, detector D5 approaches the temperature of D6, reaching a value of 619.5 K.

Figure 5-8 shows the history of the maximum temperature of the detectors. It is seen that for the first five seconds of the simulation, the maximum temperature of all of the detectors remains constant even though the flow rate has already reduced by 6 % from the original. But after this period of time the temperature of the detectors increases at about 2.3 K/sec.

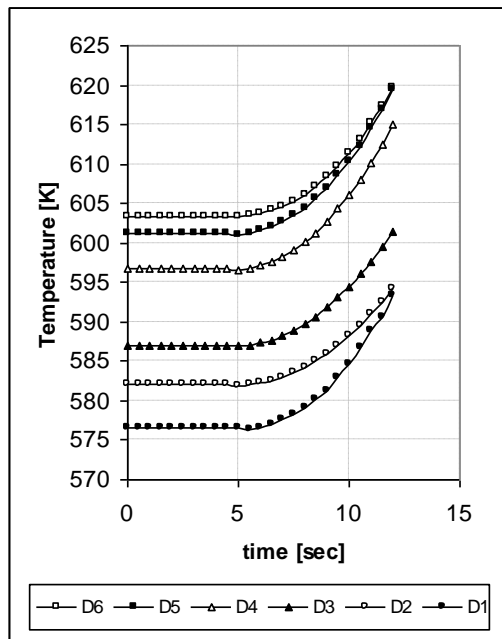


Figure 5-8 Maximum Temperature History for SPND Detectors

Temperature contours of the hottest detector (D6) are shown in Figure 5-9. All of the cross-sections shown were taken at a height of 151". The contours are at the following times: (a) 0 sec, (b) 4 sec, (c) 8 sec, (d) 12 sec. From the figures it is seen that the contour at (a) and the one at (b) are basically the same. This reflects the fact that the temperature does not change during the first four seconds.

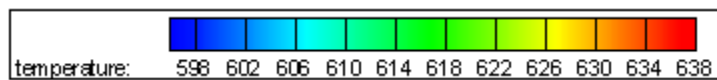
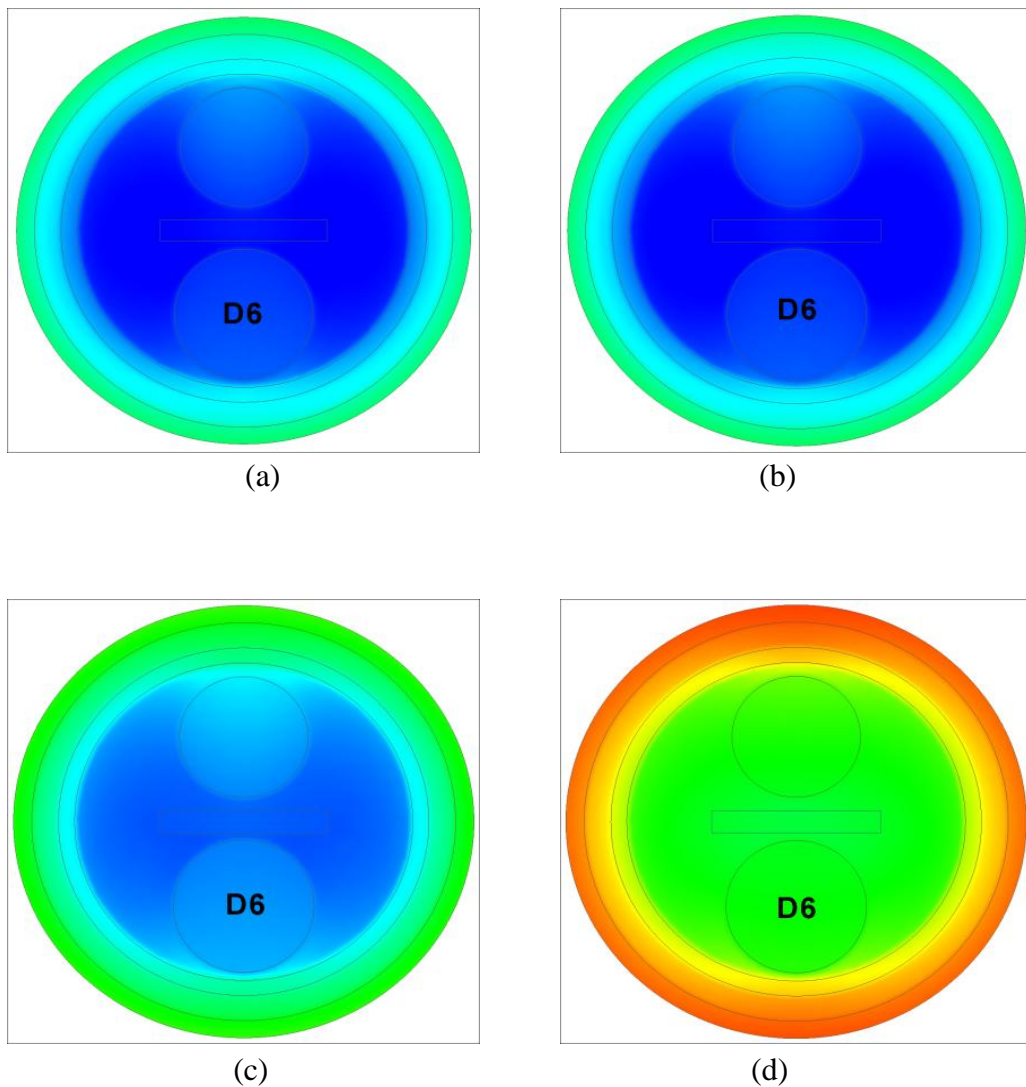


Figure 5-9 Temperature Contours at 151"
(a) 0 sec; (b) 4 sec; (c) 8 sec; (d) 12 sec

From the contour at (d) it is seen that the temperature of the water in the guide tube channel (second outermost ring) is well over the boiling temperature of water at a pressure of 2172 psi (615.2 K).

5.5.3 Maximum Temperature of SPND Components

A summary of the highest temperatures reached by the main SPND components is shown in Table 5-3. All of the components reach their maximum temperature at a time of 12 seconds. The values for both the PT and GT water are over 615.2 K (saturation temperature at a pressure of 2172 psi). The next section will give a closer examination to determine the regions in which boiling is occurring.

Table 5-3 Maximum Temperature for SPND Components at 12 seconds

Component	Maximum Temperature [K]
GT	655.8
GT Water	644.4
PT	635.9
PT Water	629.2

5.5.4 Boiling in the Guide Tube and Protection Tube Channels

The maximum temperature of the water in the guide tube channel was monitored in order to determine if boiling occurs within the SPND assembly. Figure 5-10 shows profiles for the maximum temperature of the water at four different times (0, 8, 10, 12 seconds).

Since the operating pressure of the reactor changes over time (Figure 5-3), the boiling temperature for the water in the system will also change with respect to time. Table 5-4 shows the operating pressure and saturation temperature at the four times shown in Figure 5-10.

Table 5-4 Boiling Temperatures with Respect to Time

Time	Operating Pressure (psi)	Boiling Temperature (K)
0	2250	618.05
8	2267	618.65
10	2254	618.20
12	2172	615.21

In Figure 5-10, the red line represents the boiling temperature of water at 0, 8, and 10 seconds (all of which are close to 618 K). The orange line represents the boiling temperature of water at 12 seconds (615.2 K). From Figure 5-10 it is seen that initially, none of the water in the guide tube is over the boiling temperature. As the time reaches 8 seconds, the temperature of the water in the guide tube exceeds 618.6 K in the region between 177” and 184”, therefore boiling occurs in this region. The region where boiling occurs continues to increase as time progresses. At 10 seconds, the region from 84” to 184” has a temperature over the boiling point (618.2K). Finally, at 12 seconds the region from 75” to 184” will have a temperature over the boiling point (615.2 K). From Figure 5-10 it is seen that at 10 and 12 seconds the fluid temperatures go well over the saturation temperatures. Two phase flow was not taken into consideration in Fluent, so even though the temperature exceeds the saturation temperature of water, the fluid continues to be treated as liquid water by Fluent. In reality the temperature of the water in the GT should remain at a fixed value of $T_{sat} = 618.2$ K at 10 seconds and $T_{sat} = 615.2$ K at 12 seconds, but the region in which boiling occurs would keep increasing.

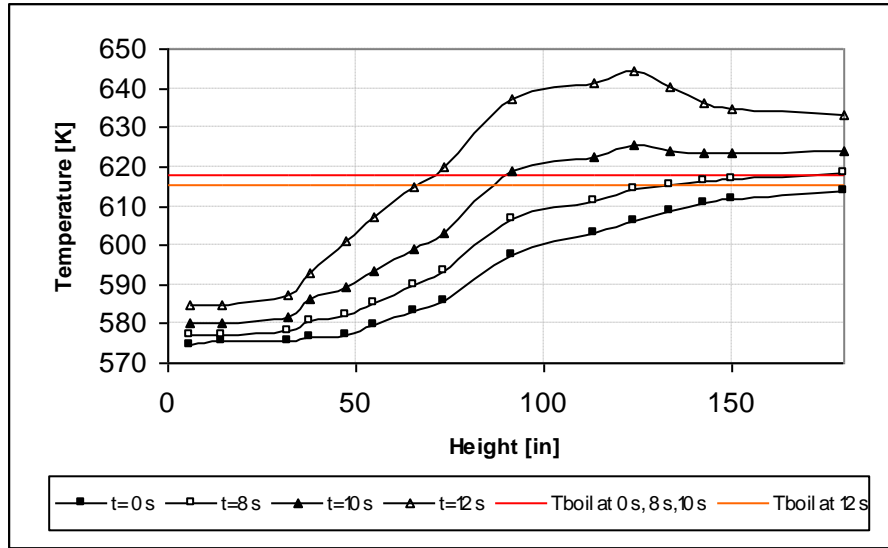


Figure 5-10 Maximum Temperature of the GT Water

The maximum temperature of the water inside the protection tube was also monitored and is shown in Figure 5-11. The temperature of the water at two times (11 and 12 seconds) is shown. Table 5-5 shows the operating pressure and saturation temperature at 11 and 12 seconds.

Table 5-5 Boiling temperatures for SPND

Time	Operating Pressure (psi)	Boiling Temperature (K)
11	2224	617.1
12	2172	615.21

In Figure 5-11 the red line represents the boiling temperature of water at 11 seconds. The orange line represents the boiling temperature of water at 12 seconds (615.2 K). As seen from the figure, the temperature of the water exceeds 617.1 K after 11 seconds have passed. The region in which boiling occurs is from 99” to 184”. After 12 seconds, boiling occurs in the region from 80” to 184”. SPND detectors D5 and D6 are located in this region.

It is important to remember that two phase flow was not taken into consideration in Fluent, so even though the temperature exceeds the saturation temperature of water, the fluid continues to be treated as liquid water by Fluent. Therefore the temperature of the fluid within the protection tube continues to increase (reaching a maximum value of 629.2 K). In reality though, the fluid temperature should not exceed $T_{\text{sat}} = 617.1$ K at 11 sec and $T_{\text{sat}} = 615.2$ K at 12 sec.

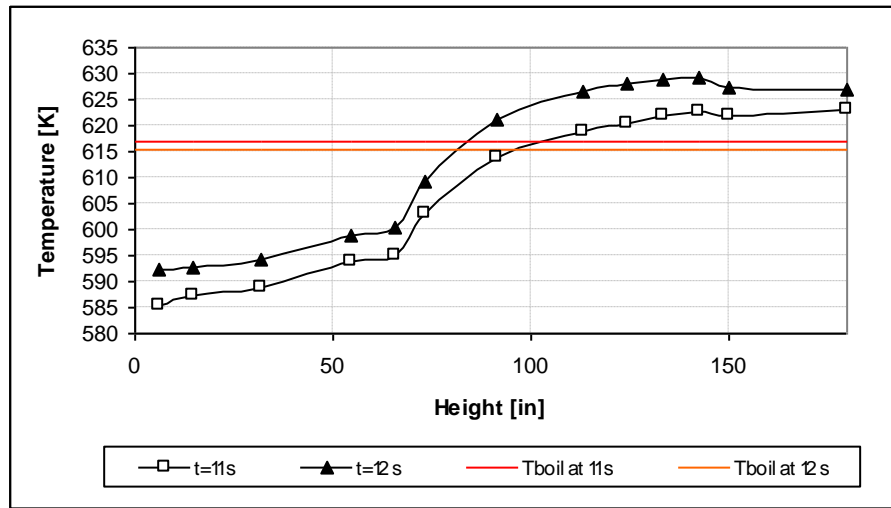


Figure 5-11 Maximum Temperature of the PT Water

Now that we have determined that boiling does occur within the guide tube and protection tube it is important to discuss the effect that boiling would have on the obtained results. There are two important factors that will affect the temperature of the system due to boiling. First, the temperature of the fluid within the SPND system will remain fixed at the saturation temperature rather than continue to increase. The second aspect that will change due to boiling is the heat transfer coefficient (h). As boiling starts to occur, the value of h will increase.

Figure 5-12 shows a temperature contour for detector D6 at a time of 12 seconds. From the figure it is seen that the temperature of the water in the PT surrounding D6 is

about 622 K. This temperature is above the saturation temperature, therefore in reality it should have remained at a fixed value of $T_{\text{sat}} = 615.2$ K. Also since boiling is occurring the value of h surrounding D6 will drastically increase, and therefore, in the absence of heat generation, the temperature of D6 would have approached the saturation temperature. But since detector D6 has internal heat generation, its temperature will be higher than the saturation temperature. However, the exact temperature would be difficult to evaluate. In order to evaluate the exact temperature, a two phase flow model would have to be used, but its implementation is outside the scope of this project.

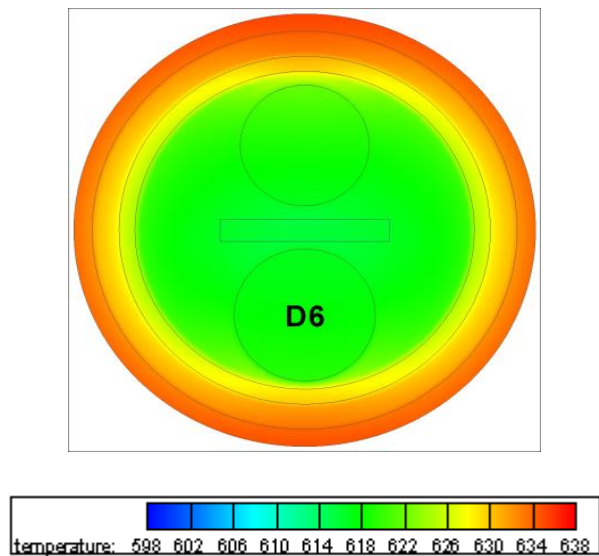


Figure 5-12 SPND D6 Cross-section at 151”

5.5.5 Temperature of Free Stream and GT Wall

An important conclusion that was reached in the steady state case presented in Chapter 3 is that the temperature of the SPND system under normal operation is limited by the temperature of the free steam flow. Therefore for the case of normal operation all of the components (fluid and solid) remain under 618 K and no boiling occurs. Figure 5-13

shows temperature profiles of the GT outer wall and free stream for the steady state case. As mentioned earlier, the steady state case was used as the initial state of the partial loss of flow transient.

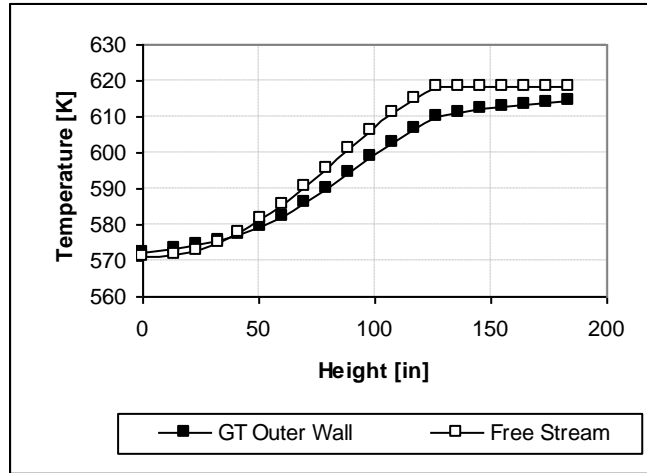
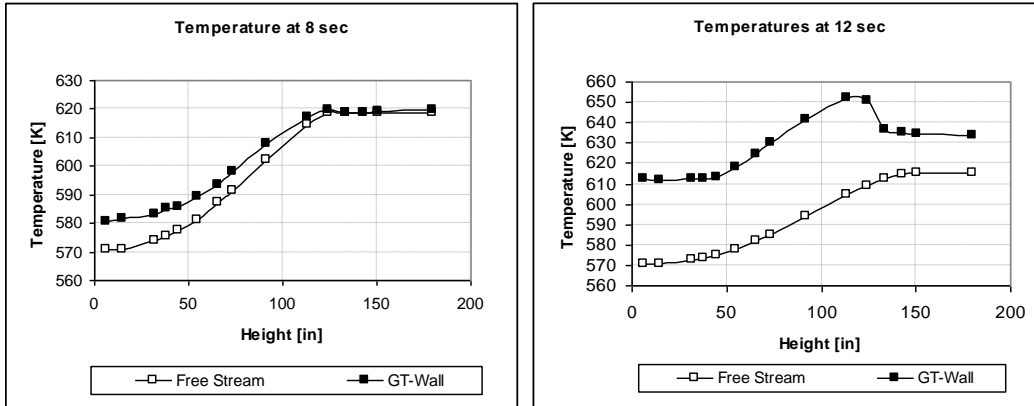


Figure 5-13 Temperature Profiles for the GT Wall and Free Stream at t=0 sec

As time progresses in the loss of flow transient simulation, the temperature of the GT wall increases in such a way that is no longer “limited” by the free stream temperature. Figure 5-14 shows the temperature profiles at t=8 sec and t=12 sec. After 8 seconds the temperature of the GT wall has already exceeded the free stream temperature along the entire height of the GT. After 12 seconds the temperature of the entire GT wall is well above the free stream temperature. It is important to note that the highest temperature reached by the free stream is right at the saturation temperature of water, 617.1 K (at 11 sec) and 615.2 K (at 12 sec). Since the temperature of the free stream no longer limits the temperature of the SPND system, then boiling occurs within the SPND system as was previously discussed in section 5.5.4.



(a) (b)
Figure 5-14 Temperature Profiles at (a) 8 sec; (b) 12 sec

5.5.6 Maximum Temperature of SPND detectors

Table 5-6 shows a summary of the maximum temperatures reached by the SPND detectors. None of the detectors surpassed the limit of 622 K.

Table 5-6 Maximum SPND temperatures after 30 seconds

D6	D5	D4	D3	D2	D1
619.6 K	619.5 K	614.9 K	601.4 K	594.3 K	593.3 K

Besides boiling, there is another factor that could affect the obtained results and that actually might cause the temperature of the detectors to increase. As shown in section 5.5.1, the flow rate through the guide and protection tube is higher than the values provided by Areva. If the flow rate had reduced to the exact value, then temperature of the detectors would have been higher than the values shown in Table 5-6.

5.6 Conclusion

The partial loss of flow transient case was modeled using the commercial software Fluent. In this scenario the flow rate through the SPND system reduces by 12.7 %. The boundary conditions for this scenario were provided by Areva and were implemented in Fluent using UDFs. The unsteady calculation was performed in Fluent using a time step of 0.5 seconds. Tests were conducted in order to prove that the results were independent of the time step. The flow rate reduction caused the temperature of the SPND detectors to increase. A maximum temperature of 619.6 K was reached by detector D6. However, if the flow rate had reached the exact 12.7% reduction, then the temperature of the detector would have been slightly higher. For the partial loss of flow scenario, boiling occurs in both the guide tube and protection tube.

References

1. "AREVA US EPR Brochure", AREVA NP, Inc., 2007.
2. Rohsenow, W., Hartnett, J., Cho, Y., "Handbook of Heat Transfer", McGraw-Hill, New York, NY, 1998.
3. "Fluent 6.3 Documentation", Fluent Inc., 2006.
4. Incropera, F., Dewitt, D., Bergman, T., Lavine, A., "Fundamentals of Heat and Mass Transfer", John Wiley and Sons, Inc., Hoboken, NJ, 2007.
5. "Section 15.4.2: Uncontrolled Control Rod Assembly Withdrawal at Power", AREVA NP, Inc., 2005 <<http://www.nrc.gov/reactors/new-reactors/design-cert/epr.html>>
6. "Section 15.3.1: Partial Loss of Forced Reactor Coolant Flow", AREVA NP, Inc., 2005 <<http://www.nrc.gov/reactors/new-reactors/design-cert/epr.html>>
7. Fox, R., McDonald, A., "Introduction to Fluid Mechanics", John Wiley and Sons, Inc., New York, NY, 1992.
8. Kays, W., Crawford, M., Bernhard, W., "Convective Heat and Mass Transfer", McGraw-Hill, New York, NY, 2005.
9. Wilcox, D., "Turbulence Modeling for CFD Third Edition", DCW Industries, Inc., California, 2006.
10. "MatWeb: Searchable Database of Material Properties", Automation Creations, Inc., 2008 <<http://www.matweb.com/>>.

Appendix A Governing Equations and Solver Settings

A.1 Governing Equations

The solver used for all of the computations in this project was the commercial software Fluent. These next sections will give more details about the equations solved by Fluent during flow and heat transfer simulations for the SPND assembly. Also the selected solver settings, the k-ε turbulence model, and the use of wall functions will be described.

A.1.1 Conservation of Mass

The mass conservation equation that is solved by Fluent is as follows:

$$\frac{\partial \rho}{\partial t} + \nabla \cdot (\rho \vec{v}) = 0 \quad (\text{A.1.1}) \quad [3]$$

For this project the flow was assumed to be incompressible with constant viscosity.

Therefore equation A.1.1 may be simplified to:

$$\nabla \cdot \vec{v} = 0 \quad (\text{A.1.2})$$

A.1.2 Momentum Equation

The momentum equation in the x, y, and z directions was solved. The momentum equation solved by Fluent is shown below:

$$\frac{\partial}{\partial t}(\rho \vec{v}) + \nabla \cdot (\rho \vec{v} \vec{v}) = -\nabla p + \nabla \cdot (\vec{\tau}) + \rho \vec{g} + \vec{F} \quad (\text{A.1.3}) \quad [3]$$

The stress tensor (τ) is defined as:

$$\vec{\tau} = \mu[(\nabla \vec{v} + \nabla \vec{v}^T) - \frac{2}{3} \nabla \cdot \vec{v} I] \quad (\text{A.1.4}) \quad [3]$$

In equation A.1.3, F represents the external body forces and ρg is the gravitational force. No external body forces were acting on the SPND assembly therefore $F=0$. The momentum equation may be simplified further for the case of incompressible flow with constant viscosity. Applying equation A.1.2, the momentum equation reduces to:

$$\rho \left[\frac{\partial \vec{v}}{\partial t} + (\vec{v} \cdot \nabla \vec{v}) \right] = -\nabla p + \mu \nabla^2 \vec{v} \quad (\text{A.1.5})$$

Finally, for the steady state case there is no variation of the solution with respect to time, thus the unsteady term $\frac{\partial}{\partial t}(\rho \vec{v})$ reduces to zero.

The second term on the left hand side of equation A.1.5 (referred to as the convective term) is of special importance. Due to its non-linear nature, it introduces difficulty into the process of solving the momentum equation. For the simulations conducted in this project, the convective term in the momentum equation was discretized using a second order upwind scheme which is described in section A.2.

A.1.3 Energy Equation

The energy equation that is solved by Fluent is as follows:

$$\frac{\partial}{\partial t}(\rho E) + \nabla \cdot (\vec{v}(\rho E + p)) = \nabla \cdot \left(k \nabla T - \sum_j h_j \vec{J}_j + (\vec{\tau}_{eff} \cdot \vec{v}) \right) + S \quad (\text{A.1.6}) \quad [3]$$

where $E = e + \frac{v^2}{2}$ and e is the internal energy.

The first term on the right hand side of A.1.6 accounts for the transfer of energy due to conduction. The second term on the right hand side accounts for the effect of

species diffusion [3]. This term may be set to zero, since only water flows through the SPND assembly. The third term accounts for the effects of viscous dissipation. This term is also set to zero for the SPND case since it is negligible for incompressible, low-Prandtl-number flows. Finally, the last term, S_h , includes the volumetric heat sources. The volumetric heat sources for each element in the SPND assembly were provided by Areva and are shown in Appendix D in Table D2. A UDF was used to account for this term in the energy equation.

For incompressible flows, Fluent neglects the pressure work ($\nabla \cdot (\vec{v}p)$) and kinetic energy terms $\left(\frac{v^2}{2}\right)$ [3]. After the simplifications described above, and assuming constant properties, the energy equation that Fluent solves reduces to:

$$\rho \frac{De}{Dt} = \frac{\partial}{\partial t}(\rho e) + \nabla \cdot (\rho \vec{v}e) = k(\nabla^2 T) + S_{UDF} \quad (\text{A.1.7})$$

A.2 Second Order Upwind (SOU)

The convective term in the momentum equation was discretized using a Second Order Upwind Scheme (SOU). The concept of upwinding is based on utilizing values of the solutions at previously encountered nodes (with respect to the flow direction) in order to approximate the solution at a new node. As an example, the one dimensional (x-component) SOU discretization of the convective term $\left(\rho u \frac{\partial u}{\partial x}\right)$ will be described.

Figure A-1 shows a 1-D discretization of the domain.

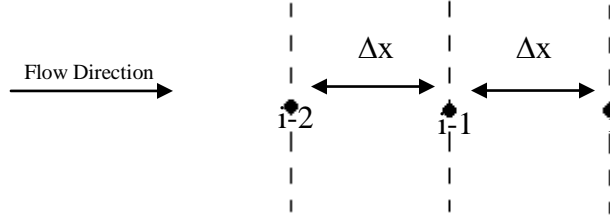


Figure A-1 Domain Discretization

The SOU scheme provides second order accuracy by utilizing the values of the velocity at (i-1) and (i-2). Taylor series expansions (equations A.2.1 and A.2.2) for the solution at the points (i-1) and (i-2) were obtained in order to approximate the derivative $\left(\rho u \frac{\partial u}{\partial x}\right)$.

$$u_{i-1} = u_i - \Delta \frac{\partial u}{\partial x} \Big|_i + \Delta^2 \frac{\partial^2 u}{\partial x^2} \quad (\text{A.2.1})$$

$$u_{i-2} = u_i - 2\Delta \frac{\partial u}{\partial x} \Big|_i + 2\Delta^2 \frac{\partial^2 u}{\partial x^2} \quad (\text{A.2.2})$$

Using equations A.2.1 and A.2.2 the SOU discretization for the convective term is as follows:

$$\frac{\partial u_i}{\partial x} = \frac{3u_i - 4u_{i-1} + u_{i-2}}{2\Delta x} \quad (\text{A.2.3})$$

Fluent also utilizes the SOU scheme to approximate the values of the solution at the cell faces. Figure A-2 shows a one dimensional sample discretization of a domain.

The cell centers are labeled W, P, E while the boundaries of each cell (cell faces) are labeled w_f and e_f . The distance between two cell centers is Δx .

The value of the solution ϕ (either velocity or temperature) is first computed by Fluent at the nodal locations (cell center), and the solution at the cell faces is then determined by using the known values.

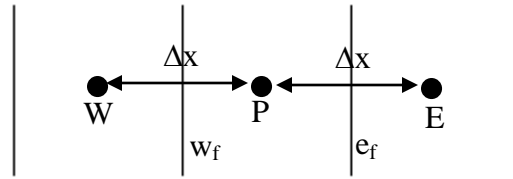


Figure A-2 Domain Discretization

When using second-order upwinding, Fluent expresses the solution at the cell faces as a Taylor series expansion as follows [3]:

$$\varphi_{w_f} = \varphi_P + \nabla \varphi_P \cdot \frac{\Delta x}{2} \quad (\text{A.2.4})$$

The subscripts in the expression A.2.4 refer to Figure A-2. Since P is a node at the center of the cell, the solution φ_P is known, and in order to find the gradient ($\nabla \varphi_P$), the Green-Gauss approach is used. This method will be described in the next section.

A.3 Green-Gauss Cell Based Gradient Evaluation

From equation A.2.4 it is seen that the gradient of the solution at point P ($\nabla \varphi_P$) has to be computed in order to be able to apply the second order upwind scheme. The gradient is calculated by using the Green-Gauss Cell based approach. This approach starts with the use of equation A.3.1.

$$\int \nabla \varphi dV = \int \varphi dA \quad (\text{A.3.1})$$

By using a simple midpoint approximation the volume integral may be approximated by:

$$\int \nabla \varphi dV = \nabla \varphi_P V \quad (\text{A.3.2})$$

Again using a midpoint approximation and performing a summation over the faces enclosing the volume, the surface integral may be approximated by:

$$\int \varphi dS = \sum \varphi_f A_f \quad (\text{A.3.3})$$

where A_f is the area of the face.

Finally, equating A.3.2 and A.3.3 and solving for the gradient we obtain the equation that Fluent uses to solve for $(\nabla \varphi_p)$.

$$(\nabla \varphi_p) = \frac{1}{V} \sum_f \varphi_f A_f \quad (\text{A.3.4}) [3]$$

A.4 Discretization in Time

Chapters 4 and 5 of the report presented two transient scenarios for the flow and energy conditions inside the SPND assembly. It is important to point out that for transient simulations the governing equations (sections A.1.1-A.1.3) have to be discretized in both time and space. A second order upwind scheme was used for the spatial discretizations as described in section A.2. A second order fully implicit scheme was used for the discretization in time.

The transient term in the governing equations may be expressed as:

$$\frac{\partial \varphi}{\partial t} = F(t, \varphi) \quad (\text{A.4.1}) [3]$$

where φ is the variable being solved for in the governing equation.

In order to obtain second order accuracy, Fluent discretizes the derivative in A.4.1 using backward differences as follows [3]:

$$\frac{\partial \varphi}{\partial t} = \frac{3\varphi^{n+1} - 4\varphi^n + \varphi^{n-1}}{2\Delta t} = F(t, \varphi) \quad (\text{A.4.2})$$

where n is the current time level t , and Δt is the size of the time step.

It still needed to be determined how to evaluate the function $F(t,\varphi)$. For the implicit scheme, $F(t,\varphi)$ is evaluated at the next time level $n+1$ (which corresponds to $t+\Delta t$). Using this fact, we arrive at the second order implicit scheme used by Fluent, shown in A.4.3.

$$\varphi^{n+1} = \frac{4}{3}\varphi^n - \frac{1}{3}\varphi^{n-1} + \frac{2}{3}F(t_{n+1},\varphi^{n+1})\Delta t \quad (\text{A.4.3})$$

A.5 Under - Relaxation Factors

Equations used for the SIMPLE algorithm allow for the specification of under-relaxation factors. These factors are especially helpful in order to attain convergence of the solution. Generally, the lower the value for the under-relaxation factor, the more time it will take for the solver to perform an iteration, but at the same time lower relaxation factors generally aid in convergence of solutions. For this simulation the under-relaxation factor for pressure was changed from its default 0.3 to a lower value of 0.1. The other under-relaxation factors were maintained at their default values. As the solution started to converge, the under-relaxation factor was increased in order to reduce the time per iteration.

A.6 Turbulence Modeling

A.6.1 Reynolds Averaged Equations

The continuity and momentum equations used to describe turbulent flow are similar to the ones presented in section A.1, but there are some relevant variations. The equations known as Reynolds-averaged equations can be used to describe turbulent flows. These equations are obtained by introducing the concept of Reynolds decompositions. The core of this idea is that the instantaneous velocity in turbulent flow may be decomposed into a fluctuating (u') and a steady component (\bar{u}) as expressed in equation A.6.1 [8].

$$u = \bar{u} + u' \quad (\text{A.6.1})$$

The Reynolds-averaged momentum transport equation is as follows:

$$\frac{\partial}{\partial x_j} (\rho \bar{u}_j \bar{u}_i) = -\frac{\partial P}{\partial x_i} + \frac{\partial}{\partial x_j} (\tau_{ij} - \rho \overline{u'_j u'_i}) \quad (\text{A.6.2}) \quad [8]$$

This equation is the same as equation A.1.3 expect for the new term $-\overline{u'_j u'_i}$ which is referred to as the Reynolds stress tensor (R_{ij}).

The Reynolds stress tensor (R_{ij}) is symmetric, and therefore it contains a total of six unknowns. Also, other unknowns to be solved are the pressure and the three velocity components from the momentum equation. Therefore, there are a total of ten unknowns, but only 4 equations to solve (the three components of the momentum equation and the continuity equation). In order to solve this problem, turbulence models introduce approximations in order to obtain the required number of equations [9]. The turbulence model used for this project is a two-equation model known as the k- ϵ model. This model will be described in section A.6.2.

A.6.2 K-Epsilon Model

The k-epsilon model was selected in the solver in order to model turbulent flow. This section describes the characteristics and equations of this model. The k- ϵ model was an appropriate choice for the SPND simulation because, according to the Fluent User Guide [3], this model provides robustness and economy, while still maintaining a reasonable accuracy for the purposes of this project. Robustness and economy are two important factors since the SPND geometry being modeled is very complex, and the size of the mesh is 4.5 million cells.

The k- ϵ model is referred to as a two equation model because it requires the simultaneous solution of the equation for the turbulent kinetic energy (k) and the equation for the dissipation rate (ϵ), in addition to the momentum and continuity equations.

Equation A.6.3 is the turbulent kinetic energy equation solved by Fluent.

$$\frac{\partial}{\partial t}(k) + \frac{\partial}{\partial x_j}(k u_j) = R_{ij} \frac{\partial u_i}{\partial x_j} - \epsilon + \frac{\partial}{\partial x_j} \left[\left(\nu + \frac{\nu_T}{\sigma_k} \right) \frac{\partial k}{\partial x_j} \right] \quad (\text{A.6.3}) [3]$$

The two terms on the left hand side of A.6.3 form the material derivative, which indicates the rate of change of k of a fluid particle [9]. The first term on the right hand side is known as the production term, and it accounts for the generation of turbulent kinetic energy [9]. The second term (ϵ), the dissipation per unit mass, is defined as:

$$\epsilon = \nu \frac{\overline{\partial u'_i \partial u'_i}}{\partial x_k \partial x_k} \quad (\text{A.6.4}) [9]$$

where ν is the kinematic viscosity of the fluid. The dissipation term indicates the rate at which k is converted into thermal internal energy [9].

One of the differing aspects between turbulence models is the way in which the dissipation is determined. The equation used by Fluent with the k- ϵ model for the dissipation rate (ϵ) is as follows:

$$\frac{\partial}{\partial t}(\epsilon) + \frac{\partial}{\partial x_i}(\epsilon u_i) = \frac{\partial}{\partial x_j} \left[\left(\nu + \frac{\nu_T}{\sigma_\epsilon} \right) \frac{\partial \epsilon}{\partial x_j} \right] + C_{1\epsilon} \frac{\epsilon}{k} \left(R_{ij} \frac{\partial u_i}{\partial x_j} \right) - C_{2\epsilon} \frac{\epsilon^2}{k} \quad (\text{A.6.5}) \quad [3]$$

The values that are assigned by Fluent to the constants ($C_{1\epsilon}$, $C_{2\epsilon}$, C_μ , σ_k , and σ_ϵ), which have been determined experimentally, are as follows [3]:

$$C_{1\epsilon} = 1.44, \quad C_{2\epsilon} = 1.92, \quad C_\mu = 0.09, \quad \sigma_k = 1.0, \quad \sigma_\epsilon = 1.3$$

It is important to highlight the fact that the equations for the k- ϵ model are only valid outside of the viscous sublayer [3]. Therefore the near wall region needs to be treated differently. The method followed was to use a wall function for the near wall region. This will be described in detail in the following section.

A.6.3 Wall Functions

If an accurate solution is desired when simulating turbulent flows, it is important to pay special consideration to the near wall region. As it was previously mentioned, the k- ϵ model is valid only for core turbulent flows, therefore it cannot be applied in the near wall region.

Before going into further details about how to treat the region near the walls, it is important to define non-dimensional parameters that are based on quantities that are significant in this region. First, the non-dimensional length y^+ is defined as:

$$y^+ = \frac{yu_\tau}{\nu} \quad (\text{A.6.6})$$

where y is the distance from the wall to the mid-point of the first cell, and ν is the kinematic viscosity of the fluid. The shear velocity u_τ is defined as:

$$u_\tau = \sqrt{\frac{\tau_w}{\rho}} \quad (\text{A.6.7})$$

The near wall region may be divided into three subsections: the viscous sublayer, buffer layer, and the fully-turbulent layer. Fluent classifies the three regions based on y^+ values. The region for $y^+ < 5$ is considered the viscous sublayer. The buffer layer is the region for $5 < y^+ < 60$. Finally, the turbulent layer is for $y^+ > 60$ [3].

Fluent allows the user to select between two options that may be used to model the near-wall region. The two options are referred to as Wall Function Approach and Near Wall Model Approach. In the wall function approach, rather than solving the viscous sublayer and the buffer layer, algebraic equations are utilized to tie the solution from the wall to the fully turbulent region [3].

Fluent selects the algebraic equation that will be applied to compute the solution depending on the value of y^+ . For values within the range $30 < y^+ < 300$ the “law of the wall” is used [3]. The Fluent definition for the law of the wall is as follows:

$$\frac{u}{u_\tau} = 2.5 \ln \left(u_\tau \frac{y}{\nu} \right) + 5.45 \quad (\text{A.6.8}) [3]$$

For the near-wall approach, the viscous sublayer and the buffer region are resolved. Therefore, the mesh near the wall has to be very fine. Fluent requires that y^+ be approximately equal to 1 in order to successfully apply this approach [3].

The wall function approach is the cheaper of the two in the sense that it allows the mesh near the walls to be coarser. Consequently the number of elements used to mesh the geometry is less and computational time is reduced. The wall function method was the one selected for the SPND calculation. For the purposes of this project, the details of the flow near the wall region were not of utmost importance, therefore using the wall function approach was adequate for the SPND simulation. During the meshing process, careful consideration was taken in order to maintain the y^+ value within the desired range for the wall function approach ($30 < y^+ < 300$).

Appendix B User Defined Functions

A user-defined function (UDF) is a function used to expand the default capabilities of the code [3]. The specific purpose of utilizing UDFs in this project was to be able to incorporate boundary conditions that vary in space and time.

Different types of macros and functions are provided by Fluent and can be used to program the UDF. The most important type of macro used to define a UDF is the DEFINE macro. A wide variety of DEFINE macros are provided by Fluent.

This section presents an explanation of the purpose and operation of the User-Defined Functions that were generated in order to be able to model the different scenarios applied to the SPND assembly. Much of the information presented in this section was obtained from the Fluent UDF Manual [3]. All of the UDFs were generated by utilizing thermal-hydraulic data provided by Areva for each of the different cases that were analyzed. The data is shown in Appendices D, E, and F.

Before moving on into the details of the UDFs used in this project, a few concepts of the grid terminology will be presented. These concepts will be useful when describing the UDF code. The computational domain is divided into cells which are assigned to a particular zone. In section 2.2.2 the different zones defined for the SPND geometry were described. In order to establish connectivity between adjacent cells Fluent utilizes internal data structures [3].

A summary of the Fluent data structures (obtained from the Fluent User Manual [3]) used when programming UDFs to access data from the solver is shown below:

- `face_t`: is an integer data type that identifies a particular face within a thread.
- `cell_t`: is an integer data type that identifies a particular cell within a cell thread.
- `Thread`: is a structure data type that stores data that is common to the group of cells or faces that it represents.

Throughout the SPND project, two different types of DEFINE macros were implemented. The two macros used were `DEFINE_SOURCE` and `DEFINE_PROFILE`. For the SPND scenario modeled in Chapter 3 (steady state under normal operation), the free stream temperature and the system heat generation rates varied with respect to position. The functions written to accomplish these variations will be described in sections B.1 and B.2. For the transient scenarios of chapters 4 and 5, the pressure and temperature in the reactor core varied with time. The functions written for these cases will be presented in section B.3.

B.1 UDF for Steady State Case (DEFINE_SOURCE)

For the SPND system under normal operation, a `DEFINE_SOURCE` macro was used to define the variable heat rates. The data provided by Areva for the heat generation rates is shown in Appendix D in Table D2. The data was plotted and a curve fit was done for each component of the SPND assembly as described in section 2.1.2. As an example, the UDF used for the guide tube source term will be described.

```

DEFINE_SOURCE(source_guide_tube, c, t)
{
  real x[ND_ND];
  real source;

  C_CENTROID(x,c,t);
  source = 0.;
  if (x[2] <= -0.168529 && x[2] >= -4.3712384)
  source=((0.0011*pow(x[2],5))+(0.1879*pow(x[2],4))+(1.7675*pow(x[2],3))+(4.3913*pow(x[2],2))+(1.549
2*(x[2]))+0.8268)*(10000000);

  else
  source = 0.;
  return source;
}

```

As seen from the code there are three arguments to DEFINE_SOURCE which are described in Table B-1.

Table B-1 DEFINE_SOURCE Arguments (Fluent UDF Manual)

Argument Type	Description
symbol source_guide_tube	UDF name
cell_t c	Index that identifies cell on which the source term is to be applied
thread t	Pointer to cell thread

The equation obtained for the curve fit was used to program the UDF by being assigned to the variable *source*. When the UDF is applied to a particular volume (in this case the guide tube) Fluent computes the proper source term for each individual cell in the thread depending on the location of the centroid of each cell. An important characteristic of the UDFs that implement the DEFINE_SOURCE macro is that they are called by Fluent from within a loop. This fact makes the programming process easier because it is not necessary to include a looping macro in the UDF code [3].

B.2 UDF for Steady State Case (DEFINE PROFILE)

A DEFINE_PROFILE macro was used to define the variation in temperature for the water flowing outside of the guide tube (free stream). The temperature of the free stream varies with respect to the length of the guide tube as discussed in Chapter 3. Again, a curve fit was done on the temperature data, and the equation was used in the UDF in a similar way as for the source terms. The UDF for the free stream temperatures is shown below.

```
DEFINE_PROFILE(free_stream_profile,t,i)
{
  real x[ND_ND];
  real y;
  face_t f;

  begin_f_loop(f,t)
  {
    F_CENTROID(x,f,t);
    y=x[2];
    if (y <= 0.2 && y > -0.18)
      F_PROFILE(f,t,i) = 570.79;

    else if (y <= -0.18 && y > -3.2)
      F_PROFILE(f,t,i) = ((-0.3946*pow(y,5))-3.9465*pow(y,4)-(12.2157*pow(y,3))-
      (9.3960*pow(y,2))-(8.1108*y)+569.5699);

    else if (y <= -3.2 && y >=-4.86)
      F_PROFILE(f,t,i) = 618.12;

    else
      F_PROFILE(f,t,i) = 300;
  }
  end_f_loop(f,t)
}
```

As seen from the code there are three arguments to DEFINE_PROFILE which are described in Table B-2.

Table B-2 DEFINE_PROFILE Arguments (Fluent UDF Manual)

Argument Type	Description
symbol free_stream_profile	UDF name
thread t	Pointer to thread to which boundary condition is applied
Index i	Index that identifies the variable that is to be defined

The UDF code for the free stream temperature needed to be able to compute the value for the temperature in each face, and loop over all of the faces. In order to accomplish this task, the pre-defined face looping macro *begin_f_loop(f,t)* is used. The equation for the free stream temperature is assigned to the corresponding face by using *F_PROFILE*. The macro *F_PROFILE* is placed within the face loop (*begin_f_loop(f,t)*). The loop will continue to iterate until it has gone through all the faces in the given cell thread [3].

B.3 UDFs for Transient Cases

The UDFs programmed for the transient cases had to account for variations in the pressure and temperature at the inlets and outlets of the SPND, and also the variation of the heat generation rates. The UDFs for the transient case are similar to the ones presented in sections B.1 and B.2, with the only difference being that the change in boundary conditions in these cases is with both time and space. Again, the *DEFINE_PROFILE* and the *DEFINE_SOURCE* macros were used. As an example, the UDF used to account for the variation in pressure at the GT inlet in the overpower transient (Chapter 4) will be described.

```

DEFINE_PROFILE(pressure1, t, i)
{
    face_t f ;

    real flow_time = RP_Get_Real("flow-time");

    begin_f_loop(f,t)
    {
        F_PROFILE(f,t,i) = ((-137.13*pow(flow_time,2))+(31955*flow_time)-25791)+44;
    }
    end_f_loop(f,t)
}

```

This UDF has the same basic concept as the one described in B.2 with the use of the *begin_f_loop* macro to loop over all of the faces that compose the GT inlet. Also, *F_PROFILE* is used to assign the corresponding pressure based on the current time of the simulation. The current physical flow time is accessed in Fluent by means of the RP variable macro *RP_Get_Real("flow-time")*.

The remaining UDFs for the pressures, source terms, and temperature for the transient cases also work using the same concepts and macros that have been described so far. The procedure remains the same for all cases:

1. Find the proper equation from the provided data and the curve fit.
2. Use macros to identify the variable of interest, and cells and faces to apply the UDF.
3. Use *RP_Get_Real("flow-time")* to identify the current physical flow time.
4. Compute the value for the variable of interest (temperature, pressure, or source) for the cell/face using *F_PROFILE* and the equation obtained in step 1.
5. Loop over the group of cells/faces.

Appendix C Material Properties

This appendix contains tables showing the properties for the materials used for each of the components. Thermal properties for water were chosen at the average free stream temperature of the water outside the guide tube ($T_{avg} = 594.15\text{K}$) and at the operating pressure of 2250 psi.

Table C-1 Properties for Water

Thermal conductivity	0.5286 W/m K
Density	677.87 kg/m ³
Viscosity	79.8 x 10 ⁻⁶ kg/ms
Specific Heat	6.203 kJ/kg K

Table C-2 Guide Tube (Zirconium alloy Zr-2.5Nb, Nuclear Grade) [10]

Thermal conductivity	17.1 W/m K
Density	6440 kg/m ³
Specific Heat	0.285 kJ/kg °C

Table C-3 Protection Tube (Austenitic Stainless Steel AISI 321) [10]

Thermal conductivity	16.1 W/m K
Density	9000 kg/m ³
Specific Heat	0.5 kJ/kg °C

Table C-4 Cables (Inconel 600) [10]

Thermal conductivity	14.9 W/m K
Density	8470 kg/m ³
Specific Heat	0.444 kJ/kg °C

The SPND detectors require special consideration since they are composed of three different parts: emitter, insulator, and collector. The cobalt emitter is surrounded by an insulator Al₂O₃, and the Inconel collector forms the outer sheath of the assembly. In order to simplify the geometry, and facilitate the mesh generation process, the three components were combined into a single solid. Since the computations do not

differentiate between emitter, insulator, and collector, it was necessary to derive equivalent properties for the combined solid. The equivalent properties found for the SPND detector are the following:

Table C-5 SPND (Cobalt, Al2O3, Inconel)

Thermal conductivity	50.2 W/m K
Density	6800 kg/m ³
Specific Heat	0.722 kJ/kg °C

The equivalent density was calculated by multiplying the density of each component times the volume fraction of the component as shown in equation C.1.

$$\frac{\rho_1 * V_1 + \rho_2 * V_2 + \rho_3 * V_3}{V_{Total}} \quad (C.1)$$

The same volume fraction procedure was followed to calculate the equivalent specific heat. The effective thermal conductivity, k_{eff} , was calculated by assuming that the SPND had a hollow thin cylinder at its center. The calculation is as follows:

$$\frac{\ln\left(\frac{r_2}{r_1}\right)}{2\pi * k_1 * L} + \frac{\ln\left(\frac{r_3}{r_2}\right)}{2\pi * k_2 * L} + \frac{\ln\left(\frac{r_4}{r_3}\right)}{2\pi * k_3 * L} = \frac{\ln\left(\frac{r_4}{r_1}\right)}{2\pi * k_{eff} * L} \quad (C.2)$$

The values for the radii and for the individual component thermal conductivity are shown in Table C-6 and Table C-7 respectively.

Table C-6 Radii for SPND Components

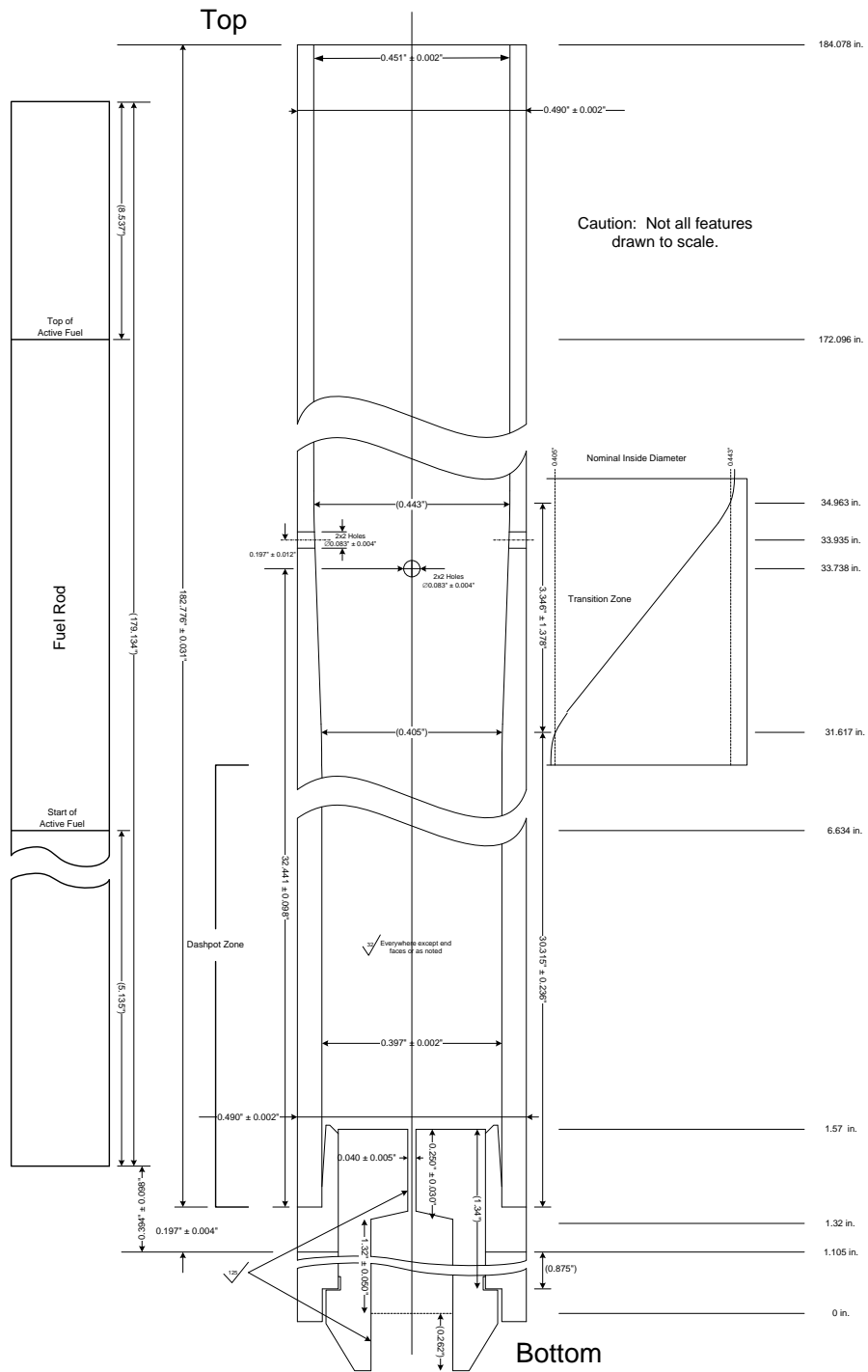
r1	Radius of hollow cylinder	0.00001 m
r2	Radius of emitter	0.0010 m
r3	Outer radius of insulator	0.0015 m
r4	Outer radius of collector	0.00185m

Table C-7 Thermal Conductivity for SPND Components

	Material	Thermal Conductivity [W/mK]
k1	Cobalt [4]	67.4
k2	Al ₂ O ₃ [4]	18.9
k3	Inconel 600 [10]	14.9

The value of the equivalent thermal conductivity was found to be: $k_{\text{eff}}=50.2$ W/mK

Appendix D Normal Operation Data



**Figure D1: Guide Tube in which the SPNDs are inserted in the fuel rod section.
(Figure Courtesy of Areva)**

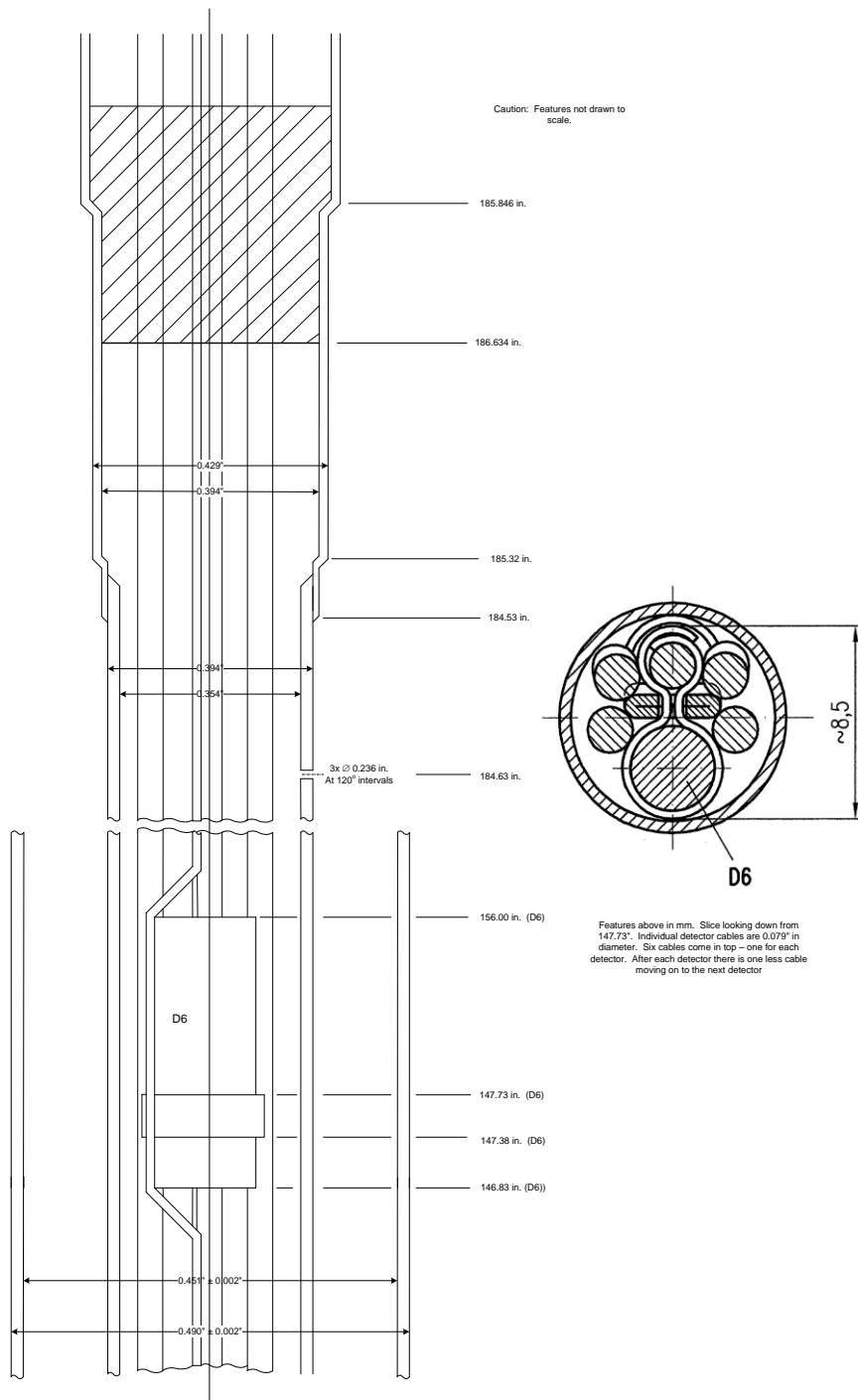


**Figure D2- Part 1- Protection Tube Detailed View
(Figure Courtesy of Areva)**

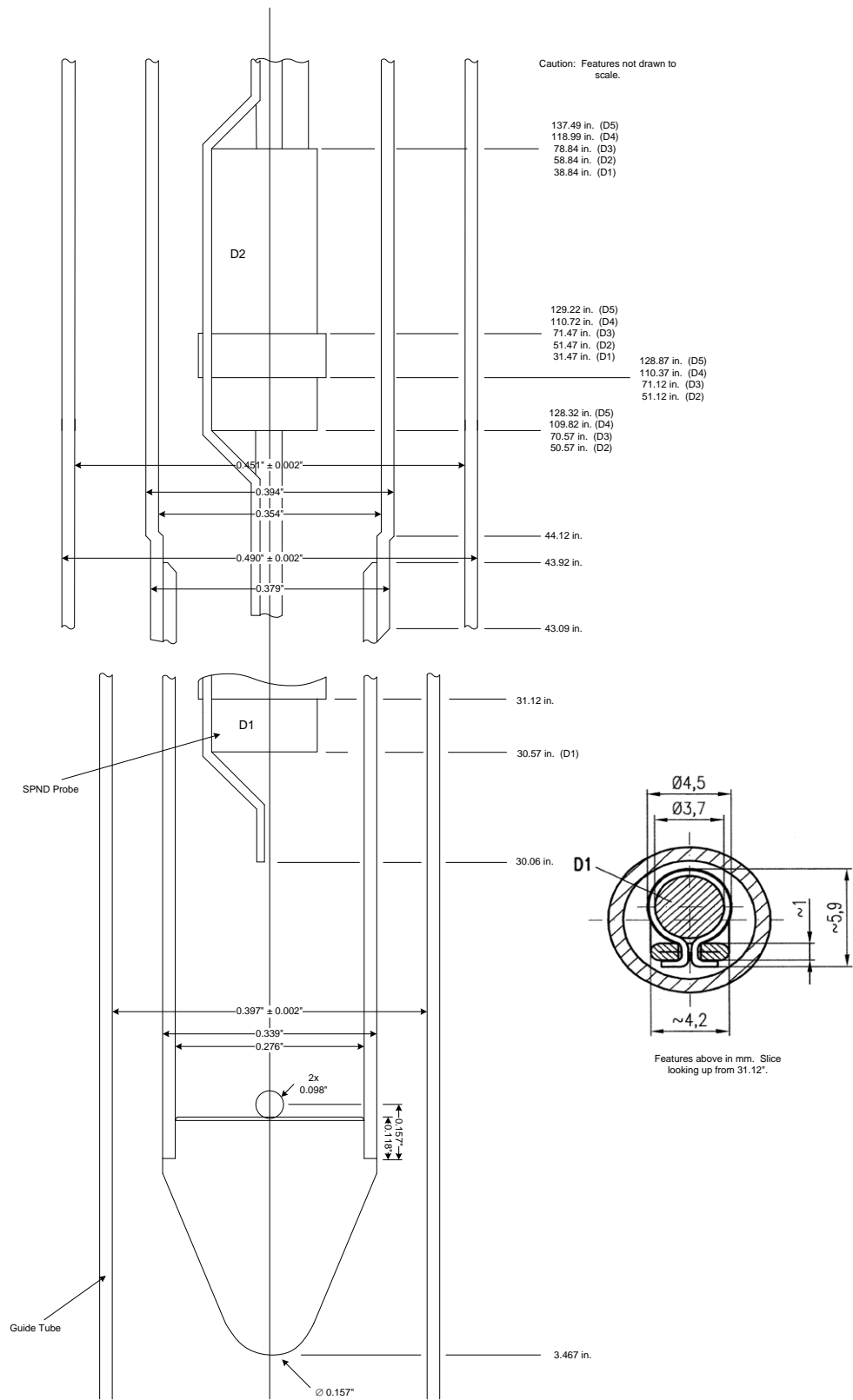


**Figure D2- Part 2- Protection Tube Detailed View
(Figure Courtesy of Areva)**

Table D-1: Thermal-Hydraulic Data Surrounding the Guide Tube

TIME =	0.000000	SECONDS	PRESSURE =	2250.000	PSIA	DATA FOR CHANNEL 4					
DISTANCE (IN.)	DELTA-P (PSI)	ENTHALPY (BTU/LB)	TEMPERATURE (DEG-F)	DENSITY (LB/CU-FT)	EQUIL. QUALITY	VOID FRACTION	FLOW (LB/HR)	MASS FLUX (MLB/HR-FT2)	VELOCITY (FT/SEC)	AREA (SQ-IN)	
-7.83	0.000	569.24	567.75	45.70	-0.318	0.000	2012.	2.4866	15.116	0.11650	
-4.83	0.197	569.24	567.75	45.70	-0.318	0.000	1975.	2.4406	14.836	0.11650	
-1.83	1.924	569.24	567.75	45.70	-0.318	0.000	2150.	2.6579	16.157	0.11650	
0.97	3.506	569.24	567.75	45.70	-0.318	0.000	2120.	2.6209	15.932	0.11650	
1.37	3.532	569.24	567.75	45.70	-0.318	0.000	2115.	2.6145	15.893	0.11650	
3.87	4.413	569.24	567.75	45.70	-0.318	0.000	2139.	2.6441	16.073	0.11650	
5.57	5.024	569.24	567.75	45.70	-0.318	0.000	2129.	2.6317	15.998	0.11650	
6.67	5.095	569.24	567.75	45.70	-0.318	0.000	2121.	2.6214	15.935	0.11650	
6.97	5.115	569.32	567.82	45.69	-0.318	0.000	2117.	2.6166	15.908	0.11650	
9.47	5.299	570.04	568.37	45.65	-0.316	0.000	2101.	2.5973	15.804	0.11650	
11.87	5.465	570.74	568.91	45.61	-0.314	0.000	2087.	2.5797	15.710	0.11650	
14.87	5.676	571.68	569.63	45.56	-0.312	0.000	2073.	2.5621	15.621	0.11650	
17.87	5.888	572.69	570.41	45.51	-0.310	0.000	2061.	2.5476	15.552	0.11650	
20.87	6.103	573.79	571.26	45.44	-0.307	0.000	2054.	2.5391	15.520	0.11650	
23.87	7.281	575.02	572.20	45.38	-0.304	0.000	2113.	2.6118	15.988	0.11650	
25.57	7.972	575.77	572.78	45.34	-0.302	0.000	2111.	2.6097	15.989	0.11650	
26.07	8.009	575.99	572.96	45.32	-0.302	0.000	2109.	2.6071	15.978	0.11650	
27.17	8.092	576.51	573.35	45.30	-0.301	0.000	2103.	2.5995	15.941	0.11650	
30.17	8.317	578.03	574.52	45.21	-0.297	0.000	2102.	2.5981	15.961	0.11650	
33.17	8.618	579.72	575.81	45.12	-0.293	0.000	2163.	2.6741	16.463	0.11650	
33.57	8.640	579.91	575.96	45.11	-0.292	0.000	2205.	2.7254	16.783	0.11650	
33.77	8.636	579.90	575.95	45.11	-0.292	0.000	2086.	2.5787	15.879	0.11650	
36.77	8.693	581.88	577.43	45.00	-0.288	0.000	2094.	2.5887	15.980	0.11650	
39.77	8.924	584.04	579.05	44.87	-0.282	0.000	2087.	2.5799	15.970	0.11650	
42.77	9.150	586.41	580.84	44.74	-0.277	0.000	2088.	2.5804	16.021	0.11650	
43.87	9.789	587.28	581.49	44.69	-0.275	0.000	2119.	2.6195	16.282	0.11650	
45.57	10.874	588.79	582.62	44.61	-0.271	0.000	2115.	2.6147	16.282	0.11650	
46.77	10.960	589.84	583.41	44.55	-0.268	0.000	2109.	2.6064	16.252	0.11650	
48.67	11.090	591.61	584.74	44.45	-0.264	0.000	2098.	2.5937	16.209	0.11650	
48.87	11.104	591.80	584.87	44.44	-0.264	0.000	2096.	2.5912	16.197	0.11650	
51.87	11.323	594.83	587.08	44.26	-0.256	0.000	2081.	2.5728	16.147	0.11650	
54.87	11.536	598.08	589.46	44.07	-0.249	0.000	2068.	2.5559	16.110	0.11650	
57.87	11.748	601.56	592.00	43.87	-0.240	0.000	2055.	2.5406	16.087	0.11650	
60.87	11.960	605.25	594.66	43.65	-0.231	0.000	2046.	2.5289	16.093	0.11650	
63.87	13.153	609.13	597.41	43.42	-0.222	0.000	2093.	2.5873	16.553	0.11650	
65.57	13.850	611.43	599.04	43.28	-0.216	0.000	2084.	2.5762	16.535	0.11650	
68.57	14.062	615.51	601.93	43.04	-0.207	0.000	2072.	2.5613	16.532	0.11650	
69.47	14.128	616.82	602.84	42.95	-0.203	0.000	2066.	2.5533	16.512	0.11650	
71.87	14.291	620.13	605.10	42.74	-0.195	0.000	2053.	2.5379	16.493	0.11650	
74.87	14.499	624.54	608.13	42.46	-0.185	0.000	2037.	2.5175	16.470	0.11650	
77.87	14.709	629.07	611.20	42.17	-0.174	0.001	2020.	2.4964	16.445	0.11650	
80.87	14.924	633.69	614.25	41.86	-0.163	0.001	2004.	2.4776	16.443	0.11650	
83.87	16.127	638.40	617.36	41.55	-0.151	0.001	2049.	2.5330	16.936	0.11650	
85.57	16.831	641.11	619.12	41.36	-0.145	0.002	2037.	2.5180	16.911	0.11650	
87.57	16.981	644.23	621.09	41.14	-0.137	0.002	2020.	2.4967	16.858	0.11650	
89.57	17.128	647.39	623.09	40.92	-0.130	0.002	2001.	2.4737	16.793	0.11650	
91.87	17.294	650.97	625.35	40.66	-0.121	0.003	1979.	2.4465	16.712	0.11650	
94.87	17.516	655.78	628.29	40.31	-0.109	0.004	1953.	2.4134	16.631	0.11650	
97.87	17.740	660.61	631.19	39.95	-0.098	0.004	1928.	2.3828	16.570	0.11650	
100.87	17.969	665.42	634.05	39.58	-0.086	0.006	1908.	2.3587	16.554	0.11650	
103.87	19.160	670.19	636.77	39.20	-0.075	0.007	1954.	2.4152	17.114	0.11650	
105.57	19.859	672.87	638.29	38.88	-0.068	0.011	1937.	2.3938	17.104	0.11650	
107.37	20.005	675.55	639.81	38.50	-0.062	0.016	1914.	2.3659	17.069	0.11650	
110.37	20.250	680.08	642.26	37.86	-0.051	0.026	1879.	2.3232	17.044	0.11650	
113.37	20.490	684.53	644.62	37.25	-0.040	0.035	1848.	2.2844	17.037	0.11650	
116.37	20.732	688.86	646.92	36.66	-0.030	0.043	1822.	2.2515	17.058	0.11650	
119.37	20.980	693.03	648.96	36.09	-0.020	0.051	1803.	2.2281	17.150	0.11650	
122.37	22.183	697.02	650.91	35.54	-0.010	0.059	1851.	2.2881	17.884	0.11650	
124.07	22.887	699.18	651.96	35.25	-0.005	0.064	1839.	2.2737	17.916	0.11650	
125.87	23.035	701.28	652.94	34.98	0.000	0.068	1823.	2.2539	17.898	0.11650	
128.87	23.275	704.74	652.94	34.78	0.009	0.074	1800.	2.2252	17.775	0.11650	
131.87	23.515	708.00	652.94	34.43	0.016	0.085	1767.	2.1844	17.622	0.11650	
134.87	23.763	711.05	652.94	33.38	0.024	0.120	1732.	2.1405	17.812	0.11650	
137.87	24.020	713.89	652.94	32.46	0.031	0.150	1711.	2.1153	18.102	0.11650	
140.87	25.239	716.48	652.94	31.65	0.037	0.176	1757.	2.1711	19.055	0.11650	
142.57	25.952	717.84	652.94	31.25	0.040	0.189	1748.	2.1606	19.206	0.11650	
145.57	26.213	719.99	652.94	30.63	0.045	0.209	1732.	2.1409	19.414	0.11650	
148.57	26.462	721.94	652.94	30.10	0.050	0.227	1716.	2.1213	19.580	0.11650	
151.57	26.703	723.69	652.94	29.63	0.054	0.242	1703.	2.1047	19.731	0.11650	
154.57	26.942	725.26	652.94	29.23	0.058	0.255	1694.	2.0935	19.899	0.11650	
156.77	27.117	726.30	652.94	28.96	0.061	0.264	1689.	2.0881	20.028	0.11650	
159.37	28.275	727.38	652.94	28.68	0.063	0.273	1734.	2.1431	20.754	0.11650	
161.07	29.073	728.04	652.94	28.52	0.065	0.278	1728.	2.1364	20.806	0.11650	
164.07	29.311	729.12	652.94	28.26	0.067	0.286	1721.	2.1275	20.909	0.11650	
167.07	29.546	730.13	652.94	28.03	0.070	0.294	1715.	2.1197	21.009	0.11650	
170.07	29.782	731.10	652.94	27.80	0.072	0.302	1712.	2.1160	21.143	0.11650	
171.97	29.928	731.70	652.94	27.66	0.074	0.306	1710.	2.1135	21.223	0.11650	
173.97	30.077	731.64	652.94	27.66	0.073	0.306	1709.	2.1122	21.211	0.11650	
175.77	30.202	731.58	652.94	27.66	0.073	0.306	1709.	2.1122	21.210	0.11650	
177.87	31.070	731.53	652.94	27.65	0.073	0.306	1750.	2.1635	21.733	0.11650	
179.57	31.800	731.46	652.94	27.65	0.073	0.306	1748.	2.1602	21.699	0.11650	
182.47	32.020	731.36	652.94	27.65	0.073	0.306	1759.	2.1746	21.846	0.11650	
182.97	32.770	731.34	652.94	27.65	0.073	0.307	1780.	2.1999	22.104	0.11650	
183.77	33.897	731.31	652.94	27.65	0.073	0.307	1780.	2.2005	22.110	0.11650	
187.37	34.143	731.17	652.94	27.65	0.072	0.307	1767.	2.1842	21.943	0.11650	
189.37	34.286	727.68	652.94	27.65	0.064	0.307	1772.	2.1898	22.001	0.11650	
191.37	34.432	727.42	652.94	27.65	0.063	0.307	1770.	2.1881	21.983	0.11650	

Table D-2 : Heat Generation Rates(W/cm³)

<u>Position</u>	<u>RPD</u>	Cobalt	Cobalt Insulator	Inconel Collector	Cable Insulation	Inconel Cables	Support Tube	Water in Lance	Instrument Lance	Water in GT	Guide Tube	Water Outside GT
172.096	0.3121	9.93	4.18	8.74	3.93	8.24	7.68	1.90	7.59	1.90	6.55	1.94
170.090	0.3142	9.99	4.21	8.80	3.96	8.29	7.73	1.92	7.63	1.92	6.60	1.95
167.091	0.3239	10.30	4.34	9.07	4.08	8.55	7.97	1.98	7.87	1.98	6.80	2.01
164.091	0.3420	12.31	5.20	10.88	4.86	10.23	9.54	2.39	9.41	2.36	8.14	2.39
161.092	0.3688	13.28	5.61	11.73	5.24	11.03	10.29	2.58	10.14	2.54	8.78	2.58
159.341	0.3884	13.98	5.90	12.35	5.51	11.61	10.84	2.72	10.68	2.68	9.24	2.72
156.799	0.4219	16.66	7.05	14.68	6.58	13.84	12.91	3.21	12.74	3.21	11.01	3.25
154.587	0.4558	18.00	7.61	15.86	7.11	14.95	13.95	3.46	13.77	3.46	11.90	3.51
151.587	0.5085	20.08	8.49	17.69	7.93	16.68	15.56	3.86	15.36	3.86	13.27	3.92
148.588	0.5681	22.44	9.49	19.77	8.86	18.63	17.38	4.32	17.16	4.32	14.83	4.37
145.588	0.6338	25.04	10.58	22.06	9.89	20.79	19.39	4.82	19.14	4.82	16.54	4.88
142.586	0.7047	27.84	11.77	24.52	10.99	23.12	21.57	5.36	21.28	5.36	18.39	5.43
140.838	0.7481	29.55	12.49	26.03	11.67	24.54	22.89	5.69	22.59	5.69	19.52	5.76
137.836	0.8249	32.59	13.78	28.71	12.87	27.06	25.24	6.27	24.91	6.27	21.53	6.35
134.837	0.9041	35.71	15.10	31.46	14.10	29.65	27.66	6.87	27.30	6.87	23.60	6.96
131.837	0.9842	38.87	16.44	34.25	15.35	32.28	30.12	7.48	29.72	7.48	25.69	7.58
128.838	1.0641	42.03	17.77	37.03	16.60	34.90	32.56	8.09	32.14	8.09	27.77	8.19
125.838	1.1426	45.13	19.08	39.76	17.82	37.48	34.96	8.68	34.51	8.68	29.82	8.80
124.083	1.1873	46.90	19.83	41.32	18.52	38.94	36.33	9.02	35.86	9.02	30.99	9.14
122.333	1.2308	48.62	20.55	42.83	19.20	40.37	37.66	9.35	37.17	9.35	32.12	9.48
119.333	1.3022	51.43	21.75	45.31	20.31	42.71	39.85	9.90	39.32	9.90	33.99	10.03
116.333	1.3685	54.06	22.85	47.62	21.35	44.89	41.88	10.40	41.33	10.40	35.72	10.54
113.334	1.4291	56.45	23.87	49.73	22.29	46.87	43.73	10.86	43.16	10.86	37.30	11.00
110.332	1.4829	58.58	24.76	51.61	23.13	48.64	45.38	11.27	44.78	11.27	38.70	11.42
107.333	1.5296	60.42	25.54	53.23	23.86	50.17	46.80	11.62	46.19	11.62	39.92	11.78
105.578	1.5533	61.35	25.94	54.05	24.23	50.95	47.53	11.80	46.91	11.80	40.54	11.96
103.829	1.5743	62.18	26.29	54.79	24.56	51.64	48.17	11.96	47.54	11.96	41.09	12.12
100.830	1.6041	63.36	26.79	55.82	25.02	52.61	49.08	12.19	48.44	12.19	41.87	12.35
97.828	1.6260	64.23	27.15	56.59	25.37	53.33	49.76	12.36	49.11	12.36	42.44	12.52
94.829	1.6405	64.80	27.40	57.09	25.59	53.81	50.20	12.47	49.54	12.47	42.82	12.63
91.829	1.6482	65.10	27.52	57.36	25.71	54.06	50.43	12.53	49.77	12.53	43.02	12.69
89.581	1.6500	65.17	27.55	57.42	25.74	54.12	50.49	12.54	49.83	12.54	43.06	12.70
87.581	1.6492	65.14	27.54	57.39	25.73	54.09	50.46	12.53	49.80	12.53	43.04	12.70
85.579	1.6458	65.01	27.49	57.27	25.67	53.98	50.36	12.51	49.70	12.51	42.96	12.67
83.830	1.6406	64.81	27.40	57.09	25.59	53.81	50.20	12.47	49.55	12.47	42.82	12.63
80.831	1.6262	64.24	27.16	56.59	25.37	53.34	49.76	12.36	49.11	12.36	42.44	12.52
77.829	1.6044	63.37	26.79	55.83	25.03	52.62	49.09	12.19	48.45	12.19	41.87	12.35
74.830	1.5747	62.20	26.30	54.80	24.57	51.65	48.19	11.97	47.56	11.97	41.10	12.13
71.830	1.5372	60.72	25.67	53.49	23.98	50.42	47.04	11.68	46.42	11.68	40.12	11.84
69.516	1.5029	59.36	25.10	52.30	23.45	49.30	45.99	11.42	45.39	11.42	39.23	11.57
68.580	1.4878	58.77	24.85	51.77	23.21	48.80	45.53	11.31	44.93	11.31	38.83	11.46
65.580	1.4346	56.67	23.96	49.92	22.38	47.05	43.90	10.90	43.32	10.90	37.44	11.05
63.829	1.4004	55.32	23.39	48.73	21.85	45.93	42.85	10.64	42.29	10.64	36.55	10.78
60.830	1.3369	52.81	22.33	46.53	20.86	43.85	40.91	10.16	40.38	10.16	34.89	10.29
57.830	1.2680	50.09	21.18	44.13	19.78	41.59	38.80	9.64	38.29	9.64	33.10	9.76
54.831	1.1946	47.19	19.95	41.57	18.64	39.18	36.56	9.08	36.08	9.08	31.18	9.20

51.829	1.1178	44.15	18.67	38.90	17.44	36.66	34.21	8.50	33.76	8.50	29.18	8.61
48.830	1.0388	41.03	17.35	36.15	16.20	34.07	31.79	7.89	31.37	7.89	27.11	8.00
48.635	1.0336	40.83	17.26	35.97	16.12	33.90	31.63	7.86	31.21	7.86	26.98	7.96
46.746	0.9832	38.83	16.42	34.21	15.34	32.25	30.08	7.47	29.69	7.47	25.66	7.57
45.579	0.9520	37.60	15.90	33.13	14.85	31.22	29.13	7.23	28.75	7.23	24.85	7.33
43.830	0.9053	35.76	15.12	31.50	14.12	29.69	27.70	6.88	27.34	6.88	23.63	6.97
42.803	0.8780	34.68	14.66	30.55	13.70	28.80	26.87	6.67	26.51	6.67	22.92	6.76
39.801	0.7995	31.58	13.35	27.82	12.47	26.22	24.46	6.08	24.14	6.08	20.87	6.16
36.802	0.7236	28.58	12.08	25.18	11.29	23.73	22.14	5.50	21.85	5.50	18.89	5.57
33.802	0.6515	25.73	10.88	22.67	10.16	21.37	19.94	4.95	19.68	4.95	17.00	5.02
33.521	0.6450	25.48	10.77	22.45	10.06	21.16	19.74	4.90	19.48	4.90	16.84	4.97
33.193	0.6375	25.18	10.65	22.18	9.94	20.91	19.51	4.84	19.25	4.84	16.64	4.91
30.193	0.5714	22.57	9.54	19.88	8.91	18.74	17.48	4.34	17.26	4.34	14.91	4.40
27.194	0.5114	20.20	8.54	17.80	7.98	16.77	15.65	3.89	15.45	3.89	13.35	3.94
26.078	0.4909	19.39	8.20	17.08	7.66	16.10	15.02	3.73	14.82	3.73	12.81	3.78
25.580	0.4820	19.04	8.05	16.77	7.52	15.81	14.75	3.66	14.56	3.66	12.58	3.71
23.830	0.4525	17.87	7.56	15.75	7.06	14.84	13.85	3.44	13.67	3.44	11.81	3.48
20.830	0.4081	16.12	6.82	14.20	6.37	13.39	12.49	3.10	12.32	3.10	10.65	3.14
17.830	0.3719	13.39	5.65	11.83	5.28	11.12	10.38	2.60	10.23	2.57	8.85	2.60
14.831	0.3443	12.40	5.23	10.95	4.89	10.30	9.61	2.41	9.47	2.38	8.19	2.41
11.829	0.3253	10.34	4.36	9.11	4.10	8.59	8.00	1.98	7.91	1.98	6.83	2.02
9.469	0.3163	10.06	4.24	8.86	3.99	8.35	7.78	1.93	7.69	1.93	6.64	1.96
6.930	0.3123	9.93	4.18	8.74	3.93	8.24	7.68	1.90	7.59	1.90	6.56	1.94
6.635	0.3121	9.93	4.18	8.74	3.93	8.24	7.68	1.90	7.59	1.90	6.55	1.94

Appendix E Overpower Transient Data

Table E-1 Delta-P Variation [psi]

Time (sec)	0 in	34 in	184 in
0	3.507	8.642	33.938
0.5	3.506	8.643	33.913
1	3.505	8.638	33.903
1.5	3.505	8.637	33.911
2	3.504	8.635	33.904
2.5	3.504	8.635	33.912
3	3.503	8.633	33.905
3.5	3.503	8.632	33.913
4	3.502	8.63	33.905
4.5	3.502	8.63	33.914
5	3.501	8.628	33.906
5.5	3.5	8.627	33.914
6	3.5	8.625	33.907
6.5	3.499	8.625	33.914
7	3.499	8.623	33.907
7.5	3.498	8.622	33.914
8	3.497	8.62	33.906
8.5	3.497	8.62	33.914
9	3.496	8.618	33.908
9.5	3.496	8.617	33.916
10	3.495	8.615	33.908
10.5	3.495	8.615	33.921
11	3.494	8.613	33.916
11.5	3.494	8.612	33.926
12	3.493	8.61	33.922
12.5	3.492	8.609	33.933
13	3.491	8.606	33.928
13.5	3.491	8.605	33.939
14	3.49	8.603	33.935
14.5	3.49	8.602	33.946
15	3.489	8.6	33.942
15.5	3.488	8.599	33.953
16	3.488	8.597	33.948
16.5	3.487	8.596	33.961
17	3.486	8.594	33.957
17.5	3.486	8.593	33.97
18	3.485	8.591	33.965
18.5	3.485	8.59	33.977
19	3.484	8.588	33.974
19.5	3.483	8.587	33.987
20	3.483	8.585	33.983
20.5	3.482	8.583	33.996
21	3.481	8.581	34.003
21.5	3.479	8.577	33.984
22	3.478	8.574	33.983
22.5	3.479	8.575	34.01
23	3.479	8.575	34.017
23.5	3.477	8.571	34.015

24	3.476	8.567	34.013
24.5	3.475	8.565	34.016
25	3.474	8.563	34.021
25.5	3.473	8.561	34.025
26	3.488	8.596	34.165
26.5	3.489	8.597	34.173
27	3.49	8.599	34.193
27.5	3.491	8.6	34.195
28	3.491	8.601	34.204
28.5	3.492	8.602	34.21
29	3.492	8.602	34.207
29.5	3.492	8.602	34.206
30	3.492	8.602	34.205

Table E-2 Free Steam Temperature Variation [K]

Position [in]	Time [sec]								
	t=0	t=4	t=8	t=12	t=16	t=20	t=24	t=28	
0	570.78	570.84	570.87	571.02	571.29	571.55	572.14	572.98	
3	570.78	570.84	570.87	571.02	571.29	571.55	572.13	572.98	
6	570.78	570.84	570.87	571.02	571.28	571.55	572.13	572.98	
8.8	570.78	570.84	570.87	571.02	571.28	571.55	572.13	572.97	
9.2	570.78	570.84	570.87	571.02	571.28	571.55	572.13	572.97	
11.7	570.78	570.84	570.87	571.02	571.28	571.54	572.13	572.97	
13.4	570.78	570.84	570.87	571.02	571.28	571.54	572.12	572.97	
14.5	570.78	570.84	570.87	571.02	571.28	571.54	572.12	572.97	
14.8	570.82	570.87	570.91	571.06	571.32	571.59	572.17	573.01	
17.3	571.13	571.19	571.23	571.38	571.66	571.94	572.52	573.37	
19.7	571.43	571.50	571.54	571.70	571.98	572.27	572.87	573.71	
22.7	571.83	571.91	571.96	572.13	572.42	572.72	573.32	574.17	
25.7	572.26	572.35	572.41	572.59	572.89	573.21	573.82	574.67	
28.7	572.73	572.83	572.90	573.09	573.41	573.73	574.36	575.22	
31.7	573.26	573.37	573.44	573.64	573.98	574.32	574.97	575.83	
33.4	573.58	573.70	573.78	573.99	574.33	574.68	575.33	576.20	
33.9	573.68	573.80	573.88	574.09	574.44	574.79	575.44	576.31	
35	573.90	574.03	574.11	574.32	574.68	575.04	575.70	576.57	
38	574.56	574.69	574.78	575.01	575.39	575.77	576.44	577.32	
41	575.28	575.43	575.53	575.78	576.18	576.58	577.28	578.16	
41.4	575.36	575.52	575.62	575.87	576.27	576.67	577.37	578.25	
41.6	575.36	575.51	575.62	575.87	576.27	576.67	577.37	578.26	
44.6	576.18	576.36	576.48	576.76	577.18	577.61	578.33	579.21	
47.6	577.09	577.28	577.42	577.72	578.17	578.62	579.37	580.26	
50.6	578.08	578.30	578.45	578.77	579.24	579.73	580.51	581.41	
51.7	578.44	578.67	578.82	579.15	579.64	580.13	580.92	581.82	
53.4	579.08	579.31	579.48	579.82	580.33	580.84	581.64	582.55	
54.6	579.52	579.76	579.93	580.28	580.81	581.33	582.15	583.06	
56.5	580.27	580.52	580.70	581.07	581.62	582.16	583.00	583.91	
56.7	580.34	580.60	580.78	581.16	581.70	582.25	583.09	583.99	
59.7	581.60	581.86	582.07	582.47	583.05	583.63	584.50	585.42	
62.7	582.95	583.21	583.44	583.88	584.49	585.11	586.02	586.95	
65.7	584.38	584.66	584.91	585.37	586.03	586.69	587.64	588.59	
68.7	585.87	586.17	586.45	586.95	587.64	588.34	589.33	590.27	
71.7	587.41	587.74	588.03	588.58	589.31	590.06	591.08	592.04	
73.4	588.32	588.66	588.97	589.53	590.30	591.07	592.12	593.09	
76.4	589.94	590.31	590.64	591.24	592.05	592.86	593.94	594.91	
77.3	590.45	590.83	591.17	591.78	592.59	593.41	594.51	595.49	
79.7	591.72	592.11	592.48	593.11	593.96	594.82	595.96	596.94	
82.7	593.42	593.83	594.22	594.89	595.79	596.71	597.89	598.88	
85.7	595.13	595.58	595.99	596.71	597.64	598.58	599.80	600.81	
88.7	596.84	597.31	597.75	598.50	599.48	600.48	601.75	602.78	
91.7	598.57	599.07	599.54	600.33	601.37	602.39	603.69	604.71	
93.4	599.55	600.07	600.55	601.36	602.39	603.46	604.78	605.81	
95.4	600.66	601.19	601.68	602.52	603.59	604.69	606.04	607.08	
97.4	601.78	602.32	602.83	603.69	604.80	605.93	607.31	608.33	
99.7	603.04	603.61	604.13	605.02	606.14	607.28	608.68	609.72	

102.7	604.67	605.27	605.81	606.72	607.89	609.08	610.52	611.58
105.7	606.30	606.91	607.48	608.42	609.64	610.86	612.32	613.36
108.7	607.89	608.52	609.11	610.07	611.31	612.56	614.06	615.12
111.7	609.41	610.06	610.66	611.66	612.94	614.24	615.74	616.77
113.4	610.26	610.92	611.53	612.56	613.85	615.12	616.64	617.68
115.2	611.11	611.77	612.41	613.42	614.70	615.99	617.53	618.58
118.2	612.46	613.14	613.78	614.82	616.14	617.48	619.02	620.02
121.2	613.78	614.47	615.13	616.19	617.53	618.83	620.36	621.37
124.2	615.03	615.74	616.40	617.46	618.78	620.11	621.67	622.51
127.2	616.17	616.89	617.56	618.63	619.98	621.07	622.02	622.51
130.2	617.25	617.98	618.66	619.76	620.49	621.07	622.02	622.51
131.9	617.84	618.57	619.26	619.92	620.49	621.07	622.02	622.51
133.7	618.03	618.83	619.31	619.92	620.49	621.07	622.02	622.51
136.7	618.03	618.83	619.31	619.92	620.49	621.07	622.02	622.51
139.7	618.03	618.83	619.31	619.92	620.49	621.07	622.02	622.51
142.7	618.03	618.83	619.31	619.92	620.49	621.07	622.02	622.51
145.7	618.03	618.83	619.31	619.92	620.49	621.07	622.02	622.51
148.7	618.03	618.83	619.31	619.92	620.49	621.07	622.02	622.51
150.4	618.03	618.83	619.31	619.92	620.49	621.07	622.02	622.51
153.4	618.03	618.83	619.31	619.92	620.49	621.07	622.02	622.51
156.4	618.03	618.83	619.31	619.92	620.49	621.07	622.02	622.51
159.4	618.03	618.83	619.31	619.92	620.49	621.07	622.02	622.51
162.4	618.03	618.83	619.31	619.92	620.49	621.07	622.02	622.51
164.6	618.03	618.83	619.31	619.92	620.49	621.07	622.02	622.51
167.2	618.03	618.83	619.31	619.92	620.49	621.07	622.02	622.51
168.9	618.03	618.83	619.31	619.92	620.49	621.07	622.02	622.51
171.9	618.03	618.83	619.31	619.92	620.49	621.07	622.02	622.51
174.9	618.03	618.83	619.31	619.92	620.49	621.07	622.02	622.51
177.9	618.03	618.83	619.31	619.92	620.49	621.07	622.02	622.51
179.8	618.03	618.83	619.31	619.92	620.49	621.07	622.02	622.51
181.8	618.03	618.83	619.31	619.92	620.49	621.07	622.02	622.51
183.6	618.03	618.83	619.31	619.92	620.49	621.07	622.02	622.51
185.7	618.03	618.83	619.31	619.92	620.49	621.07	622.02	622.51
187.4	618.03	618.83	619.31	619.92	620.49	621.07	622.02	622.51
190.3	618.03	618.83	619.31	619.92	620.49	621.07	622.02	622.51
190.8	618.03	618.83	619.31	619.92	620.49	621.07	622.02	622.51
191.6	618.03	618.83	619.31	619.92	620.49	621.07	622.02	622.51
195.2	618.03	618.83	619.31	619.92	620.49	621.07	622.02	622.51
197.2	618.03	618.83	619.31	619.92	620.49	621.07	622.02	622.51
199.2	618.03	618.83	619.31	619.92	620.49	621.07	622.02	622.51

Appendix F Partial Loss of Flow Transient Data

Table F-1 Delta-P Variation [psi]

Time (sec)	0 in	34 in	184 in
0	3.507	8.642	33.938
0.25	3.484	8.587	33.697
0.5	3.462	8.536	33.512
0.75	3.441	8.487	33.331
1	3.42	8.438	33.15
1.25	3.392	8.374	32.913
1.5	3.366	8.313	32.685
1.75	3.339	8.252	32.456
2	3.312	8.191	32.229
2.25	3.288	8.137	32.021
2.5	3.265	8.084	31.833
2.75	3.241	8.029	31.62
3	3.218	7.977	31.432
3.25	3.198	7.93	31.254
3.5	3.178	7.885	31.091
3.75	3.158	7.838	30.919
4	3.137	7.791	30.738
4.25	3.118	7.748	30.584
4.5	3.099	7.704	30.42
4.75	3.08	7.66	30.257
5	3.06	7.616	30.096
5.25	3.043	7.576	29.948
5.5	3.025	7.535	29.791
5.75	3.008	7.496	29.65
6	2.99	7.455	29.489
6.25	2.974	7.419	29.365
6.5	2.958	7.382	29.229
6.75	2.942	7.345	29.094
7	2.926	7.309	28.959
7.25	2.912	7.278	28.842
7.5	2.898	7.245	28.723
7.75	2.884	7.213	28.605
8	2.871	7.182	28.496
8.25	2.857	7.151	28.378
8.5	2.844	7.122	28.269
8.75	2.831	7.092	28.161
9	2.819	7.064	28.053
9.25	2.807	7.038	27.954
9.5	2.797	7.013	27.836
9.75	2.787	6.992	27.743
10	2.778	6.971	27.629
10.25	2.769	6.951	27.512
10.5	2.761	6.932	27.383
11	2.749	6.907	27.149
11.25	2.747	6.903	27.06
11.5	2.745	6.897	26.963
11.75	2.741	6.888	26.867
12	2.734	6.872	26.755

Table F-2 Free Stream Temperature Variation [K]

Position (in)	Time (sec)					
	t= 0 sec	t= 4 sec	t=6 sec	t= 8 sec	t=10 sec	t = 12 sec
0	570.79	570.81	570.79	570.73	570.67	570.51
3	570.79	570.81	570.79	570.73	570.67	570.51
6	570.79	570.81	570.79	570.73	570.67	570.51
8.8	571.04	570.81	570.79	570.73	570.67	570.51
9.2	571.10	570.81	570.79	570.73	570.67	570.51
11.7	571.45	570.81	570.79	570.73	570.68	570.51
13.4	571.68	570.81	570.79	570.73	570.68	570.51
14.5	571.83	570.81	570.79	570.77	570.68	570.51
14.8	571.87	570.85	570.83	571.12	570.72	570.54
17.3	572.22	571.18	571.17	571.45	571.06	570.79
19.7	572.58	571.49	571.49	571.89	571.38	571.04
22.7	573.07	571.91	571.92	572.37	571.82	571.38
25.7	573.60	572.37	572.39	572.89	572.29	571.73
28.7	574.21	572.87	572.90	573.47	572.81	572.13
31.7	574.88	573.42	573.47	573.83	573.38	572.57
33.4	575.30	573.76	573.82	573.93	573.74	572.84
33.9	575.43	573.86	573.92	574.18	573.84	572.92
35	575.72	574.09	574.16	574.89	574.09	573.11
38	576.57	574.78	574.86	575.68	574.79	573.63
41	577.51	575.53	575.64	575.77	575.58	574.23
41.4	577.64	575.62	575.72	575.77	575.67	574.29
41.6	577.70	575.62	575.72	576.68	575.66	574.27
44.6	578.75	576.48	576.61	577.68	576.57	574.97
47.6	579.88	577.43	577.58	578.77	577.56	575.73
50.6	581.09	578.48	578.66	579.17	578.64	576.57
51.7	581.56	578.86	579.04	579.87	579.04	576.87
53.4	582.30	579.52	579.72	580.35	579.73	577.41
54.6	582.83	579.98	580.19	581.15	580.22	577.77
56.5	583.71	580.75	580.98	581.23	581.01	578.39
56.7	583.80	580.83	581.07	582.59	581.09	578.46
59.7	585.25	582.13	582.39	584.04	582.44	579.49
62.7	586.75	583.52	583.82	585.61	583.89	580.62
65.7	588.32	585.00	585.34	587.21	585.43	581.82
68.7	589.93	586.54	586.92	588.89	587.03	583.08
71.7	591.58	588.15	588.57	589.89	588.72	584.38
73.4	592.53	589.10	589.54	591.62	589.71	585.16
76.4	594.22	590.78	591.25	592.18	591.43	586.53
77.3	594.74	591.31	591.79	593.57	591.98	586.97
79.7	596.11	592.63	593.14	595.41	593.37	588.07
82.7	597.82	594.39	594.96	597.26	595.21	589.52
85.7	599.53	596.16	596.76	599.14	597.04	591.00

88.7	601.23	597.95	598.59	600.99	598.93	592.49
91.7	602.90	599.76	600.43	602.04	600.78	593.98
93.4	603.84	600.76	601.46	603.27	601.84	594.84
95.4	604.92	601.91	602.64	604.47	603.06	595.83
97.4	605.99	603.08	603.84	605.81	604.26	596.81
99.7	607.19	604.37	605.15	607.60	605.60	597.90
102.7	608.71	606.07	606.89	609.33	607.41	599.37
105.7	610.17	607.77	608.61	611.03	609.13	600.83
108.7	611.58	609.38	610.27	612.67	610.85	602.24
111.7	612.91	610.97	611.91	613.56	612.48	603.64
113.4	613.63	611.86	612.77	614.44	613.38	604.43
115.2	614.38	612.69	613.63	615.89	614.27	605.18
118.2	615.56	614.09	615.08	617.23	615.72	606.45
121.2	616.67	615.46	616.42	618.54	617.08	607.71
124.2	617.72	616.69	617.68	618.65	618.20	608.89
127.2	618.12	617.88	618.73	618.65	618.20	610.01
130.2	618.12	618.53	618.73	618.65	618.20	611.08
131.9	618.12	618.53	618.73	618.65	618.20	611.67
133.7	618.12	618.53	618.73	618.65	618.20	612.23
136.7	618.12	618.53	618.73	618.65	618.20	613.11
139.7	618.12	618.53	618.73	618.65	618.20	613.95
142.7	618.12	618.53	618.73	618.65	618.20	614.74
145.7	618.12	618.53	618.73	618.65	618.20	615.24
148.7	618.12	618.53	618.73	618.65	618.20	615.24
150.4	618.12	618.53	618.73	618.65	618.20	615.24
153.4	618.12	618.53	618.73	618.65	618.20	615.24
156.4	618.12	618.53	618.73	618.65	618.20	615.24
159.4	618.12	618.53	618.73	618.65	618.20	615.24
162.4	618.12	618.53	618.73	618.65	618.20	615.24
164.6	618.12	618.53	618.73	618.65	618.20	615.24
167.2	618.12	618.53	618.73	618.65	618.20	615.24
168.9	618.12	618.53	618.73	618.65	618.20	615.24
171.9	618.12	618.53	618.73	618.65	618.20	615.24
174.9	618.12	618.53	618.73	618.65	618.20	615.24
177.9	618.12	618.53	618.73	618.65	618.20	615.24
179.8	618.12	618.53	618.73	618.65	618.20	615.24
181.8	618.12	618.53	618.73	618.65	618.20	615.24
183.6	618.12	618.53	618.73	618.65	618.20	615.24
185.7	618.12	618.53	618.73	618.65	618.20	615.24
187.4	618.12	618.53	618.73	618.65	618.20	615.24